AD-A053 271 NAVAL RESEARCH LAB WASHINGTON D C F/G 4/1
ATMOSPHERIC EXTINCTION MEASUREMENTS AT ND-YAG AND DF LASER WAVE--ETC(U)
FEB 78 J A DOWLING, K M HAUGHT, R F HORTON

UNCLASSIFIED NRL-8058 NL

1 OF 1
AD
A053271

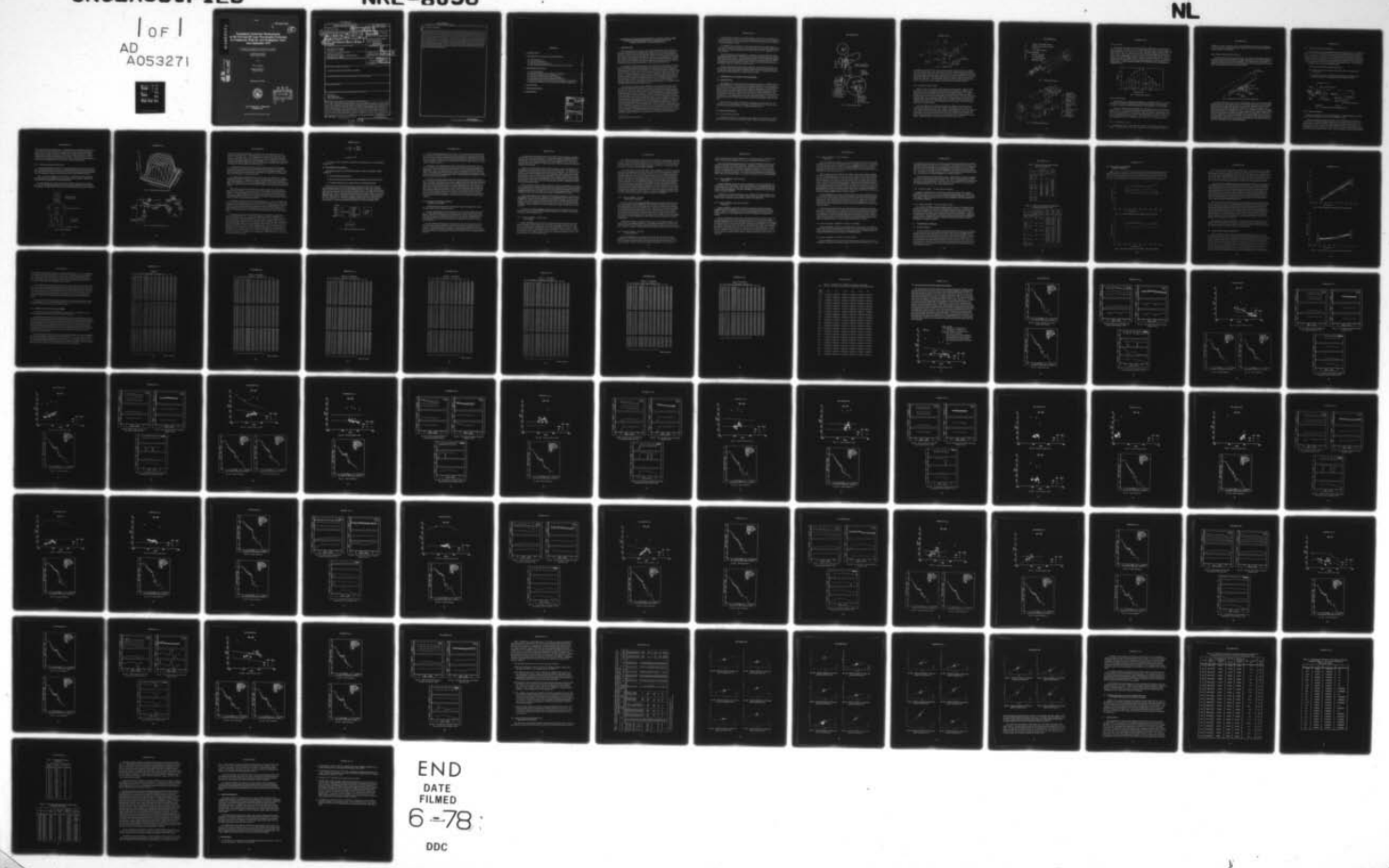

END
DATE
FILMED
6-78
DDC

NRL Report 8058

(12)

Atmospheric Extinction Measurements at Nd-YAG and DF Laser Wavelengths Performed in Conjunction With the JAN Propagation Tests, June-September 1975

J. A. DOWLING, K. M. HAUGHT, R. F. HORTON, G. L. TRUSTY, J.A. CURCIO, T.H. COSDEN, S. T. HANLEY, AND C.O. GOTT

Optical Radiation Branch
Optical Sciences Division

and

W. L. AGAMBAR

Potomac Research Inc.
McLean, Virginia

February 10, 1978

NAVAL RESEARCH LABORATORY
Washington, D.C.

UNCLASSIFIED

SECURITY CLASSIFICATION OF THIS PAGE (When Data Entered)

REPORT DOCUMENTATION PAGE	READ INSTRUCTIONS BEFORE COMPLETING FORM
1. REPORT NUMBER NRL Report 8058 (14) NRL-8058	2. GOVT ACCESSION NO. 3. RECIPIENT'S CATALOG NUMBER (9)
4. TITLE (and Subtitle) ATMOSPHERIC EXTINCTION MEASUREMENTS AT ND-YAG AND DF LASER WAVELENGTHS PERFORMED IN CONJUNCTION WITH THE JAN PROPAGATION TESTS, JUNE-SEPTEMBER 1975	5. TYPE OF REPORT & PERIOD COVERED Interim report on a continuing NRL Problem
	6. PERFORMING ORG. REPORT NUMBER
7. AUTHOR(s) J.A. Dowling, K.M. Haught, R.F. Horton, G.L. Trusty, J.A. Curcio, T.H. Cosden, S.T. Hanley, C.O. Gott and W.L. Agambar (10)	8. CONTRACT OR GRANT NUMBER(s) NRL Problem R05-31 Project 405-003-173-1 SRSL40AA76
9. PERFORMING ORGANIZATION NAME AND ADDRESS Naval Research Laboratory Washington, D.C. 20375	10. PROGRAM ELEMENT, PROJECT, TASK AREA & WORK UNIT NUMBERS (11)
11. CONTROLLING OFFICE NAME AND ADDRESS Department of the Navy Naval Sea Systems Command (PM-22/PMS-405) Washington, D.C. 20362	12. REPORT DATE February 10, 1978 (10 Feb 78) 13. NUMBER OF PAGES 85
14. MONITORING AGENCY NAME & ADDRESS(if different from Controlling Office)	15. SECURITY CLASS. (of this report) Unclassified (12) 86 p. 15a. DECLASSIFICATION/DOWNGRADING SCHEDULE

16. DISTRIBUTION STATEMENT (of this Report)

Approved for public release; distribution unlimited

17. DISTRIBUTION STATEMENT (of the abstract entered in Block 20, if different from Report)

18. SUPPLEMENTARY NOTES

19. KEY WORDS (Continue on reverse side if necessary and identify by block number)

Laser beams
Light transmission
Atmospheric attenuation

20. ABSTRACT (Continue on reverse side if necessary and identify by block number)

The NRL Infrared Mobile Optical Radiation Laboratory (IMORL) consisting of various infrared laser sources, large-aperture collimating optics, and precision calibrated infrared detectors and electronics was operated in conjunction with the JAN Baseline Demonstration Laser propagation tests during June-September 1975. The trailer-housed elements of the IMORL unit were deployed so as to use an atmospheric measurement path about 5 km long between the TRW Capistrano Test Site and Camp Pendleton Marine Base. Extensive measurements of atmospheric transmission at several DF laser wavelengths between 3.6 μm and 4.1 μm were obtained as well as measurements (Continued)

DD FORM 1 JAN 73 1473 EDITION OF 1 NOV 65 IS OBSOLETE
S/N 0102-014-6601

UNCLASSIFIED
SECURITY CLASSIFICATION OF THIS PAGE (When Data Entered)

251 950

20. Abstract (Continued)

at the Nd-YAG laser wavelength of 1.06 μm. The optical measurements were supported by meteorological observations near the IMORL transmitter and receiver sites. Atmospheric aerosol distributions were monitored during the experiments, and Mie scattering calculations were performed using the aerosol data and were compared to aerosol extinction values derived from the optical measurements obtained using the 5-km-long path. The water-vapor dependence of molecular absorption for each of the 22 DF laser lines studied was compared to values obtained during earlier experiments at the Cape Canaveral Air Force Station and to theoretical predictions based on a HI-TRAN calculation using a line atlas. The experimental apparatus used (IMORL facility) and the measurement procedures followed are briefly described. The measurement results obtained and their comparisons to theoretical predictions for molecular absorption and aerosol scattering at DF laser wavelengths are presented and discussed.

CONTENTS

ATMOSPHERIC EXTINCTION MEASUREMENTS AT ND-YAG AND DF LASER WAVELENGTHS PERFORMED IN CONJUNCTION WITH THE JAN PROPAGATION TESTS, JUNE-SEPTEMBER 1975

1. INTRODUCTION

This report describes the operation of the NRL Infrared Mobile Optical Radiation Laboratory (IMORL) and presents the results obtained for a series of measurements performed in conjunction with the JAN Baseline Demonstration Laser (BDL) propagation tests during the period June through September 1975. To effectively assess linear atmospheric effects and to provide in-situ molecular absorption values appropriate for the BDL laser during the Series B high-power tests, the NRL field measurements facility previously used for Nd-YAG and DF laser transmission studies at Cape Canaveral Air Force Station (CCAFS) was deployed and operated prior to and during the Series B tests.

A knowledge of molecular absorption and aerosol extinction values effective for the BDL laser during the high-power propagation tests is essential for interpretation of calorimetric data associated with the high-power runs. (Molecular scattering is negligible at the wavelengths of interest, that is, near 3.8 μm, and aerosol absorption is currently understood to be a minor component of the total aerosol extinction.) More importantly, comparisons of measured high-power focal-spot sizes to theoretical predictions must use representative values for atmospheric absorption which enter nonlinearly in contributing to the focal-spot-size budget of a thermally bloomed beam. The IMORL facility was used during the Series B tests to gain added confidence in values used for atmospheric molecular-absorption and aerosol-scattering coefficients appropriate to the TRW-Capistrano Test Site (CTS) location for the BDL shot times.

The extinction data taken for the 22 DF lines and for 1.06 μm 3 months prior to the JAN tests during the 1975 Florida experiment were available at the outset of the Series B tests; however the extent to which the data analysis and interpretation had progressed by the start of the JAN tests did not yield high confidence in having available a well-understood, high-accuracy predictive capability for atmospheric molecular absorption at DF wavelengths. Today, after nearly a year of continuing analysis, including refinement of data-processing techniques combined with the requisite comparisons of the field measurement results to predictive models, the situation has substantially improved. One can in fact predict molecular absorption at the DF frequencies contained in the BDL output spectrum with high reliability over a moderate temperature range for any value of absolute humidity likely to be encountered in the field. The latter knowledge resulted from a continuing crosscomparison of the field-measurement results to calculational models which have been upgraded by the inclusion of improved information derived from laboratory measurements. Experimental data for molecular absorption measured in the field during the Florida and Capistrano experiments are compared to current versions of such predictive models in Section 3 of this report and will be described in detail therein.

Manuscript submitted August 30, 1976.

The additional confidence in molecular absorption values and in the assessment of aerosol effects gained by carrying out actual measurements concurrent with the BDL tests is certainly justified in terms of the important role which these data have in the analysis of the JAN propagation results.

The IMORL facility is housed in several large instrumented van trailers which contain a variety of laser sources and large optics, including a combustion-driven CW DF laser, a precision 91-cm-diameter Cassegrainian transmitter telescope, and a comparable-size receiver telescope.

A detailed description of this facility is contained in a report describing the earlier experiments conducted at the CCAFS location in February and March 1974 and repeated during the following year [1]. An abbreviated description of the experimental apparatus with emphasis on the features added for the JAN tests is contained in Section 2. The experimental procedures used and a description of the routines and procedures used for analyzing the data are contained in Section 2 as well.

Section 3 describes the results obtained during the two measurement periods, one prior to Series B (30 July through 22 August 1975) and the second in conjunction with the high-power tests (10 through 23 September 1975). Section 4 enumerates the observations and conclusions which can be drawn from the results.

2. EXPERIMENTAL FACILITIES AND PROCEDURES

2.1 Experimental Site

The apparatus used in the low-power extinction measurements at the TRW Capistrano Test Site (TRW-CTS) can be grouped into two categories; that used for optical measurements and that devoted to supporting meteorological measurements. The equipment was housed in several van trailers whose positions during the experiment are shown in Fig. 1. The extinction-measurement equipment was contained in the laser transmitter and pump trailers (positions 10 and 11 in Fig. 1) and in the receiver trailer located either at the terminus of the 5-km path position (8) or at the "zero-path" position (9), which was used for calibration. Meteorology support was provided by instrumentation contained in the NRL meteorology van (7) and in the electronics trailer at the transmitter end of the path (12).

Station power was provided by TRW for the equipment at the receiver end. The transmitter site was self-sufficient, with storage of supplies provided by the supply trailer (13) and electrical power provided by a 75-kW diesel generator (14).

2.2 Optical Instrumentation

2.2.1 Laser Transmitter Facility

The transmitter facility is self-contained in the transmitter and pump trailers (Fig. 1). Figure 2 shows the layout of the transmitter trailer. Half of the interior is occupied by

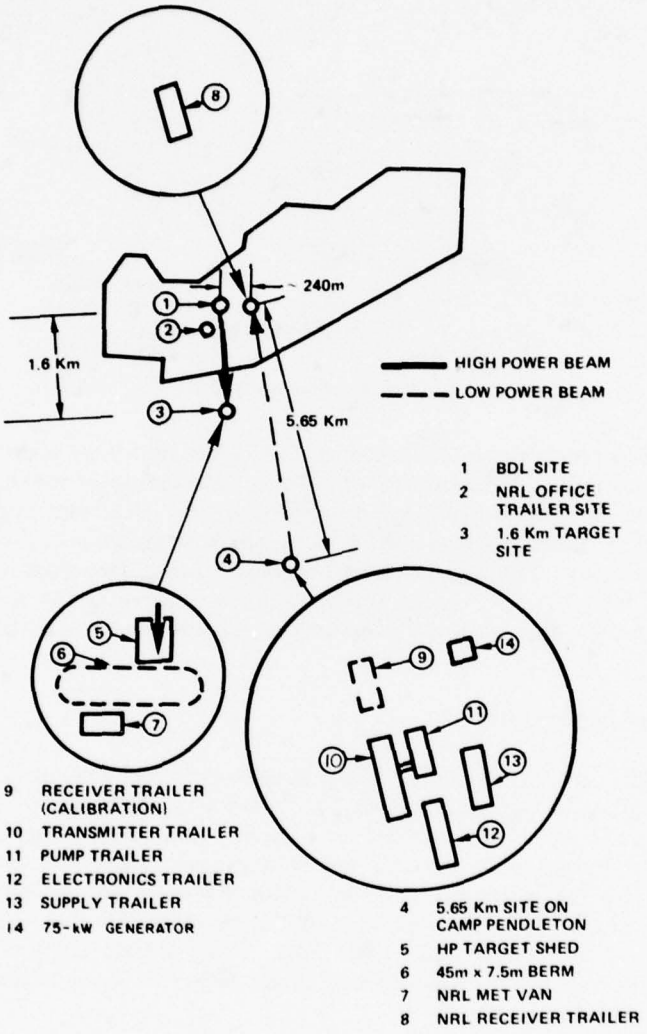

Fig. 1 — BDL propagation range

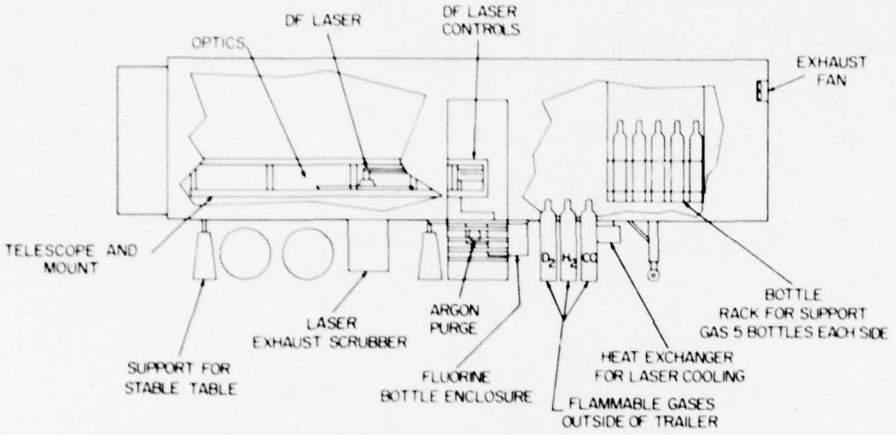

Fig. 2 — Transmitter trailer

the transmitter telescope and its mount; all of the optics and laser sources are contained within the telescope frame. The other half of the trailer contains measurement electronics, vacuum pumps, gas storage, tools, and working space. Heat exchangers for DF and Nd-YAG laser cooling, a fluorine-cylinder enclosure, and a chemical scrubber box are mounted beneath the trailer floor. The pump trailer houses the large, two-stage vacuum pump required by the DF laser. A 20-cm-diameter vacuum line connects the vacuum pump in its trailer to the DF laser exhaust scrubber mounted beneath the transmitter trailer.

2.2.2 Transmitter Optical System

Figures 3 and 4 are schematics of the transmitter optical systems. Figure 3 shows the layout of the 91-cm-aperture Cassegrainian telescope, which has an effective focal length of 32 m and is supported by the optical bench depicted in Fig. 2. This bench is supported by piers sitting on the ground and is vibrationally isolated from the trailer, providing support for the lasers and transfer optics shown in Fig. 4. Of note are the HeNe alignment laser (L1) and its beam expander (BE1), the Nd-YAG laser (L2) and its beam expander (BE2), and the DF chemical laser (L3). The DF laser beam is collimated and matched to the entrance pupil of the Cassegrainian telescope using a variety of flats and high-f-number spherical mirrors.

The HeNe alignment laser and Nd-YAG lasers are combined by a dichroic beam-combining plate (D1); this coaxial beam is added to the DF laser beam by another dichroic beam-combining plate (D2). The resulting colinear beams, which have been matched to the entrance pupil of the Cassegrainian telescope, are delimited by a pupil mask (M) and brought to the system focal point (f) by the off-axis parabolic mirror (OAP). The beam is then modulated by a chopper (C) and transmitted via the Cassegrainian telescope system. Additional details concerning this system can be found in Ref. 1.

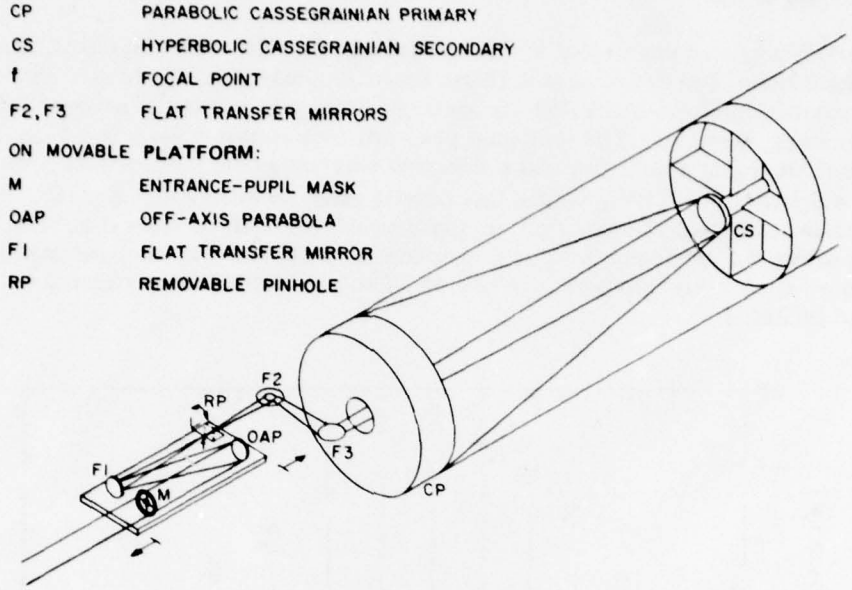

Fig. 3 — Cassegrainian telescope

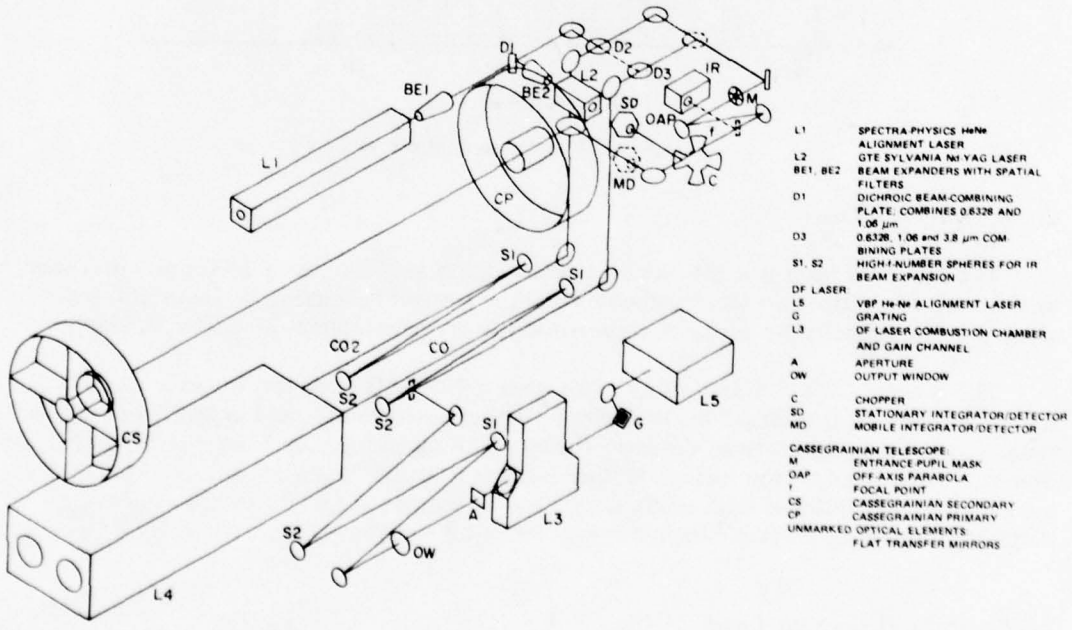

Fig. 4 — Transmitter optical system

2.2.3 *DF Laser*

The DF laser was engineered by Henry Bobitch of TRW Space Systems, Redondo Beach, California. The device uses a 15-cm linear supersonic nozzle to achieve a gain volume approximately 1 cm square by 15 cm long. This gain volume is situated between two CaF_2 Brewster windows. The long gain path provides approximately 2.5 W multiline TEM_{00} output, using a gold flat and a 2-m-radius-of-curvature, 95%-reflecting output window, or a 0.1-to-0.5-W TEM_{00} single line output using an intracavity grating. The gas consumption rates used allowed routine continuous operation of from 3 to 4 hours daily. Figure 5 shows the single-line output power spectrum for the various lines used in the measurements. A more complete description of the DF laser and its characteristics are contained in Ref. 1.

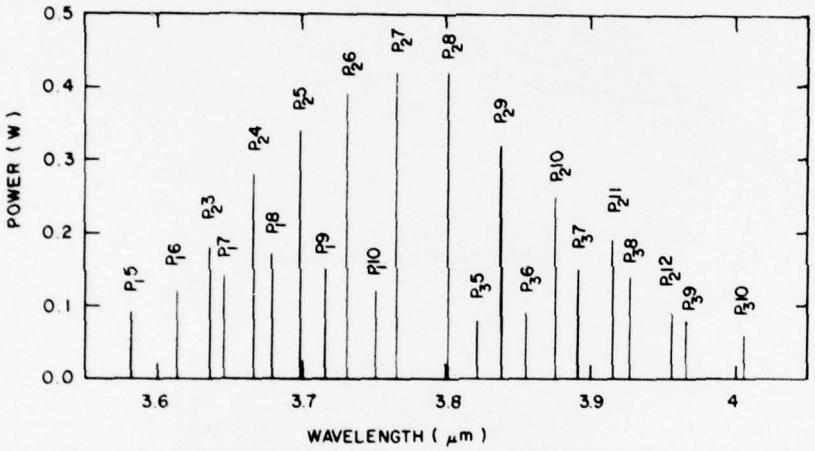

Fig. 5 — DF laser power spectrum

2.2.4 *Nd-YAG Laser*

The Nd-YAG laser is a CW device operating at a wavelength of 1.06 μm. It is used as a source for extinction measurements to allow aerosol extinction to be monitored, since there is virtually no molecular absorption in the atmosphere at this wavelength.

The laser, a GTE Sylvania Model 605, uses a Nd-YAG laser rod set in a "double elliptical" reflector, is pumped by two 500-W incandescent lamps, and is limited to a low order mode by an aperture in the laser cavity. The output power is approximtely 0.11 W. The mode structure of the laser is further improved during beam expansion through the use of a spatially filtered laser collimator. The output of the collimator is a smooth, Airy distribution of 2-cm e^{-2}diameter with an output power of approximately 80 mW.

2.2.5 *HeNe Alignment Laser*

The alignment laser, to which both the transmitter and ultimately the receiver are aligned, is a Spectra-Physics Model 125. This laser develops approximately 75 mW in a

"TEM_{00}-like" mode. Because the laser is used for collimation through the Cassegrainian system, the output is spatially filtered and collimated to a smooth "tophat" distribution of approximately 2.5-cm diameter.

2.2.6 Receiver Trailer and Optical System

The receiver is housed in another van trailer. The receiver optical system collects the transmitted beam after it has traversed the measurement path and the received intensity is accurately measured using the detector/integrator. The optical system is supported by a massive steel optical bench which, like the transmitter, rests on piers sitting on the ground and is thus independent of the receiver trailer motion.

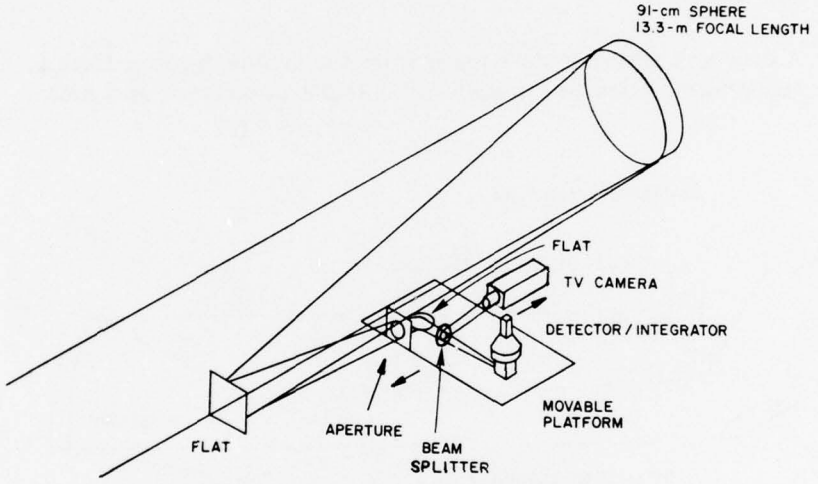

Fig. 6 — Optical receiver used in the extinction measurements

As shown in Fig. 6, the optics of the receiver system consist of a 13.3-m-focal-length spherical mirror and auxiliary flat mirrors used to fold the beam inside the receiver trailer. The entrance pupil of the collecting mirror is unoccluded. Operating the sphere off-axis results in minor problems with aberrations, which do not affect the operation of the detector/integrators, since the image size can be 1.3 cm in diameter and still be integrated. Only when the effects of scintillation and beam wander cause the incident beam to wander off the receiver mirror are problems encountered. For the measurements at TRW-CTS, a television camera was used with a beamsplitter in the receiver optical train such that the size and position of the 1.06-μm spot on the receiver mirror could be monitored from the transmitter trailer using a TV picture and microwave relay link. This allowed beam alignment to be monitored remotely during BDL firings.

2.2.7 *Extinction Measurement Apparatus*

The atmospheric extinction measurement scheme is depicted in Fig. 7. Initially the ratio of the stationary and mobile detector responses is determined with the mobile detector in position A. In position B the losses to the atmospheric path and optical elements are measured. The loss to the optical elements alone is measured by placing the transmitter and receiver adjacent to one another in the calibration location shown in Fig. 1. The optical reflectivity measured during calibration is factored out of the long-path ratio measurement to yield the loss due solely to atmospheric effects. Such a measurement technique makes use of the following features:

- Detectors which reliably measure total power;
- A ratiometer which accurately determines the ratio of the responses of two detectors;
- A data link which sends a signal from the mobile detector back to the ratiometer located in the transmitter trailer (a distance of 5 km).

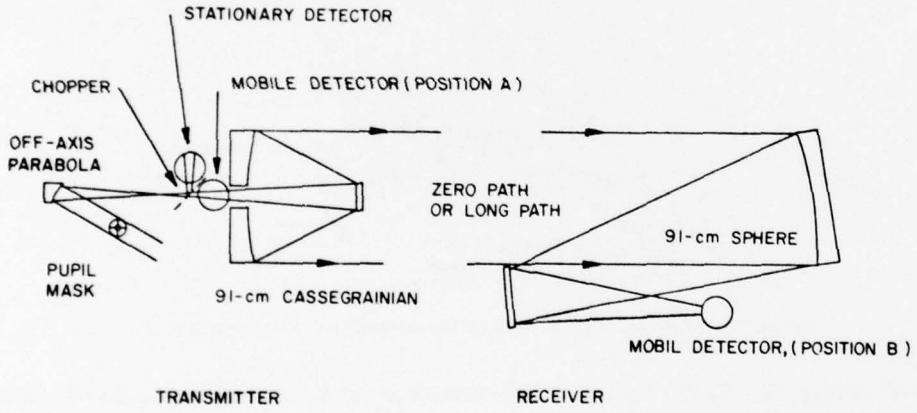

Fig. 7 — Atmospheric-extinction measurement scheme

2.2.8 *Detector/Integrators*

Figure 8 is a schematic of the detector/integrator. A liquid-nitgrogen-cooled InSb bottom-window detector views the top of the integrator interior.

The optical integrator assembly is designed so that the InSb detector response is proportional to the spatially integrated intensity in the incident beam and insensitive to small changes in location of the input beam within the integrator input aperture. Diffusely reflecting interior surfaces and baffles preventing directly reflected light from illuminating the detector element are used to achieve these results. The integrator collects all of the incident radiation which enters the device vertically after being folded from the

horizontal by a gold-coated flat mirror. A kinematic mount is employed to provide consistent positioning. The positions of the mobile and stationary detector/integrators are shown in Fig. 7. Figure 9 shows the integrator/detector spatial response to a narrow 1.06-μm beam incident on the detector. The response ideally would show a "tophat" distribution which would be independent of wavelength. The InSb detectors used are sensitive over a wavelength interval from about 1 to 6 μm, allowing the same detectors to be used for the 1.06-μm Nd-YAG and 3.8-μm DF extinction measurements.

2.2.9 Extinction-Measurement Electronics

As previously discussed, the ratio of the signals developed by the two InSb detectors must be reliably determined both for the zero-path calibration position and the long path. The electronics which have been developed were shown to work quite satisfactorily during the field measurement program conducted during 1975 at Cape Canaveral, Florida.

Figure 10 is a block diagram of the electronics. A 37-Hz 50% chopper alternately sends the radiation to be ratioed to each of the two detector/integrators. Signals from both detectors are amplified by identical preamplifiers.

The preamplifiers each contain a filter and an amplifier with switch-selected gain. The front ends provide stable biasing and stable, low-noise amplification for the InSb detector signals. The filter rejects as much noise as possible while preserving the squareness

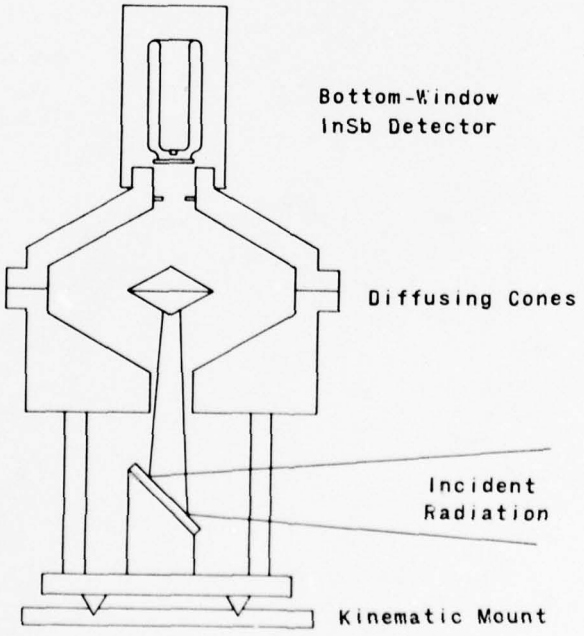

Fig. 8 — Detector/integrator

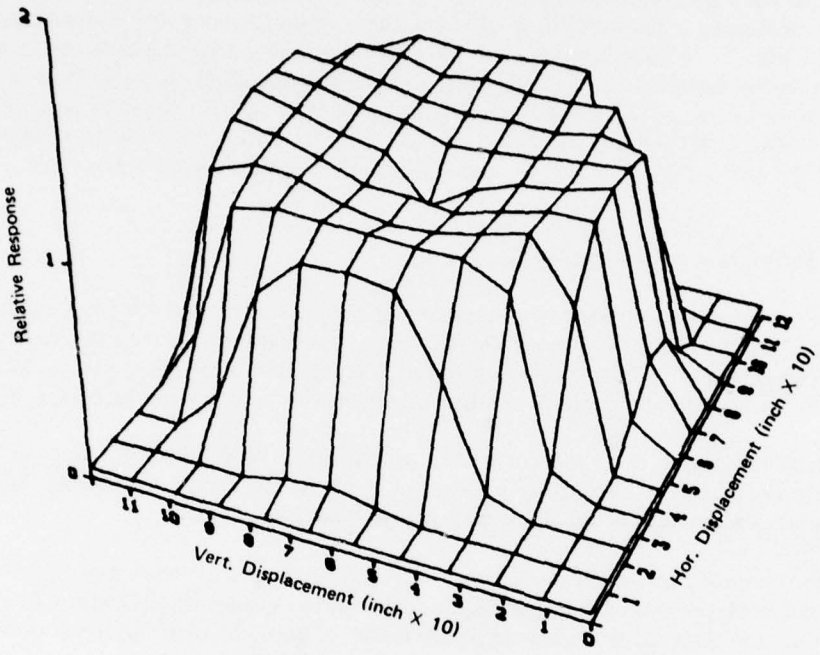

Fig. 9 — Detector/integrator spatial response

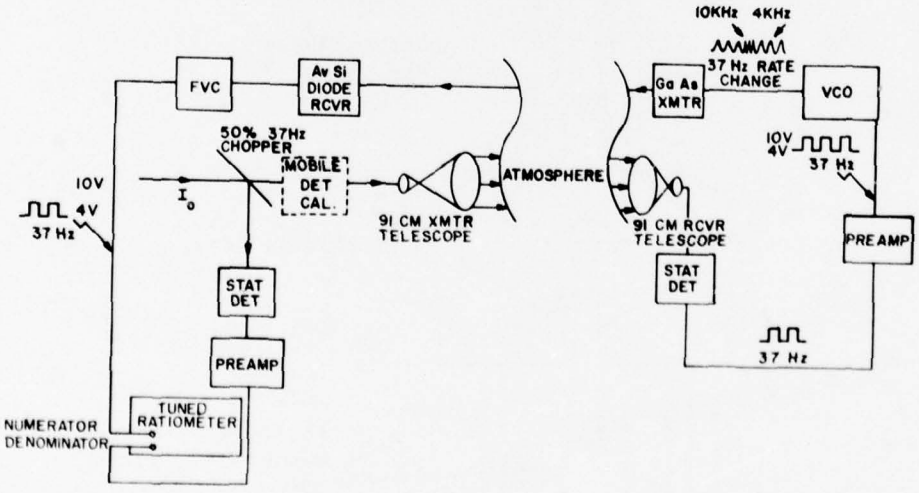

Fig. 10 — Extinction measurement system

of the 37-Hz waveforms, providing an indication to the users that the detectors are aligned and working properly. The frequency-response curve of the filter is such that 37 Hz is on the flattest part. The preamplifiers are provided with 12 selectable gain values in a logarithmic progression of four steps per decade of amplification. This feature allows the signals derived from the preamplifiers to be of a similar level for the tuned ratiometer and data link while covering both a wide range of incident power on the detectors and the detector response to 1.06 and 3.8 μm.

As shown in Fig. 10, the two 37-Hz electrical signals are fed into the ratiometer. The signal from the stationary detector preamplifier goes directly to the denominator input of the ratiometer, since both units are positioned in the transmitter trailer. At all times the signal from the mobile detector preamplifier is transmitted to the numerator input of the ratiometer via the GaAs data link.

A voltage-controlled oscillator (VCO) is used to encode the mobile-detector signal amplitude onto the GaAs laser beam so that the laser pulse repetition rate is proportional to the signal amplitude. A frequency-to-voltage converter (FVC) is used to decode the signal at the transmitter site to recover the original signal. The intensity of the GaAs laser beam is not important as long as it is adequate to trigger the silicon avalanche photodiode receiver.

The complete data link was included in the system whenever the mobile detector was used in the B position. In the A position the VCO and FVC were coupled directly together. Previous experiments had shown this to be an adequate procedure to avoid errors due to long-term variations in the VCO and FVC electronics. The GaAs transmitter and silicon avalanche diode detector combination posed no stability problems during either the Florida or the California experiments.

The ratiometer includes precision matched bandpass filters to select the fundamental frequency of the chopped inputs, precision rectifier circuits, a unique dc-ratio circuit, and a Bessel filter to average the output. The ratio circuit uses a single logarithmic transistor junction to perform all nonlinear signal operations. Errors that might otherwise arise from mismatches between several transistors are thus eliminated. The ratiometer also includes a self-calibration feature and automatic gain ranging to allow a large input dynamic range.

The ratiometer response is intentionally slow; it has an effective averaging time of 4.3 s and a settling time of 17 s. The noise bandwidth of 0.86 Hz is equivalent to a lock-in amplifier with the same averaging time. But, unlike a lock-in amplifier, the ratiometer is insensitive to chopping harmonics, requires no phase-reference input, and tolerates moderate drifts (about 5%) in the chopping frequency. Automatic gain control (AGC) copes with moderate changes in the laser intensity. This AGC does not cause transient errors in the ratiometer output, a feature required because of the long settling time. The ratiometer error is less than 0.2%, which is negligible with respect to other measurement uncertainties. The corrected ratio r of the mobile to stationary detector signals takes into account both the ratiometer output R as well as the preamplifier gain settings. Since an integer gain setting of g corresponds to an actual gain G of $10^{g/4}$, the ratio r of the mobile to stationary detector signals is

$$r = R\,\frac{G_s}{G_m} = R\,\frac{10^{g_s/4}}{10^{g_m/4}}$$

or

$$r = R10^{(g_s - g_m)/4} \quad .$$

So, in practice, three numbers are recorded for each separate extinction measurement: R, g_m, and g_s.

2.3 Meteorological Instrumentation

Meteorology support for the TRW BDL experiment, which was provided by NRL, consisted of:

- Two micrometeorology stations,
- An aerosol particle-size spectrometer and atmospheric CO_2 level monitor, and
- A data-processing system for rapid reduction of meteorological data.

Each of the two micrometeorology stations was situated near an end of the low-power propagation path. One micrometeorology system was housed in the electronics trailer and was located at the site on Camp Pendleton (Fig. 1). The other micrometeorology system was associated with the NRL meteorology van and was located near the 1.6-km BDL target site. The two micrometeorology stations are duplicates. Figure 11 is a block diagram of these stations. Measurements include wind speed, vertical and horizontal wind-direction components, air temperature, barometric pressure, dew point, and solar insolation. The sensors for each of these measurements are mounted on a portable tower approximately 5 m high and separated approximately 25 m from the station itself.

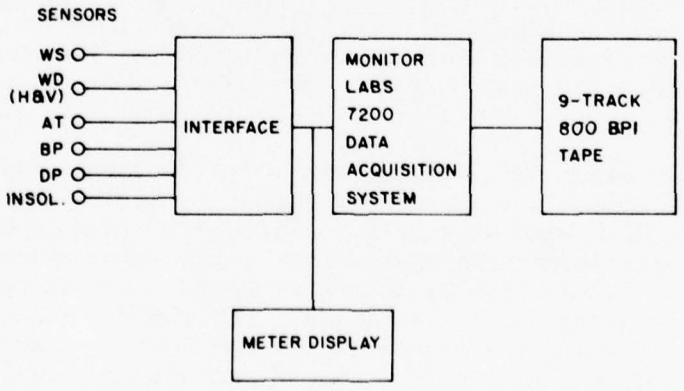

Fig. 11 — Meteorological measurement system

All meteorological parameters shown in Fig. 11 are recorded each second along with date and time on digital tape at each meteorology station by the data acquisition system. Most of the sensors used in the meteorological measurements are calibrated prior to fielding the experiment, primarily using factory-supplied calibrations. Exceptions are the dewpoint measurements. These units are calibrated periodically throughout a day by a simple switch to calibrate operation.

In addition to the instrumentation used for measurements shown in Fig. 11, the NRL meteorology van contains an atmospheric CO_2 monitor and an aerosol particle-size spectrometer. The aerosol particle-size spectrometer is a Particle Measuring Systems, Inc. (PMS) device capable of counting particles in four size ranges from 0.1 μm to 4.0 μm in radius. The sampling head for the aerosol particle-size spectrometer is mounted on a separate tower near the other meteorological sensors. All measurements are digitally recorded, and the data are processed off-line.

In addition to the meteorology station used at the transmitter end of the 5.65-km path, the electronics trailer houses an extensive, computer-based data acquisition/processing system, including a Nova 1220 computer with a 32K-word memory, three Link tape drives with a self-contained operating system, a keyboard CRT display with hard copy unit, a high-speed line printer/plotter, and two nine-track digital tape drives. The computer system is used to reduce, average, tabulate, and plot meteorological data off-line using data tapes produced during the experiments. These tapes are processed off-line at about an 8-to-1 reduction from real time to yield tabulated 1- and 10-minute average values of each of the meteorological parameters. In addition, time-history plots of any selected set of these variables, such as contained in the next section, can be produced using existing programs.

2.4 Procedures Used for Data Acquisition, Reduction, and Analysis

A particular sequence of laser line measurements was used throughout the experiment (see Table 2) for the following reasons:

- Initial optical alignment of the DF laser cavity and external transfer optics made use of a HeNe alignment laser beam reflected in the sixth order by the DF laser cavity grating, resulting in a cavity alignment for 2633.979 cm^{-1}. Only a minor grating adjustment was then required to produce oscillation on the $P_2 8$ DF line at 2631.067 cm^{-1}. Accordingly DF laser extinction measurements were performed in a sequence starting with the $P_2 8$ line.

- After additional laser lines were selected in the order of increasing wavenumber, the $P_2 8$ line was repeated, followed by a decreasing order, with each measurement set ending in a third measurement at the $P_2 8$ line. Three distinct measurement at this line provided an immediate estimate of experimental reproducibility and also served to indicate temporal variability of the atmosphere during the total time devoted to a long-path measurement run.

The measurement procedure involved two distinct modes of operation, depending on the location of the mobile detector. A typical day's operation usually began with a measurement of the detector relative response for each DF laser line with the mobile detector placed in the transmitter trailer. These runs, designated A runs, were made to provide a day-to-day measure of the relative response of the two detectors and associated measurement electronics.

After an A run the mobile detector would be moved to the receiver trailer, and the transmission ratios would again be measured for each DF laser line. For long-path measurements the receiver was located about 5 km from the transmitter. On some days however the receiver trailer was placed next to the transmitter trailer to make the zero-path measurements needed to calibrate the long-path data. When the mobile detector was located in the receiver, the run was designated a B run. Because data from the two distinct types of B runs must be processed differently, the B-run designations were later changed to B0 and B5. In this manner the processing programs were able to distinguish zero-path B runs from long-path B runs.

After the B run the mobile detector would be returned to the transmitter for another series of measurements. This final measurement series, designated the C run, was performed to determine whether the relative response of the two detectors and associated optics had changed appreciably since the earlier A run. The processing programs preserve the separate designation of the C runs but otherwise treat them as though they were A runs.

The experimental data were recorded in notebooks at the field site. These data were later punched onto cards and then transmitted to the KRONOS time-share system of the CYBERNET computer network operated by Control Data Corporation via a remote batch terminal. The raw data include the measured ratio of the two detector signals, the gain settings for the two preamplifiers, and an identification for each of the 22 DF laser lines investigated. Similar measurements were also made for the single 1.06-μm line of the Nd-YAG laser.

A series of 15 computer programs was developed for processing data from the transmission experiments. These FORTRAN-language programs were intended for interactive processing on the KRONOS system.

2.4.1 Program D02KMH: Zero-Path Ratio Curve Fitting

Program D02KMH processes all of the zero-path measurements (A, B0, and C runs). Each measurement is first matched with the spectral wavenumber of the laser line, and then the recorded ratio is appropriately scaled to the preamplifier gain settings. A least-squares-error polynomial is calculated for the wavenumber-ratio pairs in each run. Based on the significance of the improvement in the fit's coefficient of determination that could be obtained by using a higher order polynomial, the program automatically selects a curve-fit polynomial of not more than third order.

The resulting polynomial is evaluated at the wavenumbers corresponding to each measured line. The scaled ratio, its deviation from the calculated polynomial value, and that deviation relative to the standard deviation of the other points in the fit are all written to the printer output file. The polynomial coefficients are written to a separate file, from which they can later be read by program D03KMH.

A curve fit of the measured ratios offers several advantages. It allows the calibration points to be interpolated to cover lines which may have been missed during the zero-path calibration runs. The curve fit also tends to smooth some of the variation observed in the data. Finally, the curve fit and its related output provide an excellent method for examining the data for potential errors which may have occurred in the data-recording process. Past experience has generally uncovered a few lines (less than 1%) whose measurement parameters were not correctly transferred from the experimenter's notebook to the input data file. (A new automatic data-logging procedure will hopefully eliminate most of these problems during future experiments.) The most common of these errors occurs when an incorrect spectral-line identification causes the measured line to become associated with the wrong spectral wavenumber. Since a gross error for one line can adversely affect the final results obtained for all the other lines, errors of this type should be located and corrected as early as possible. In practice the D02KMH program is often run two or three times before all of these errors have been eliminated.

2.4.2 Program D03KMH: Zero-Path Transmission Calculations

For each zero-path run, program D03KMH reads the polynomial coefficients from the file generated by program D02KMH. The polynomial is evaluated at the wavenumbers corresponding to each of the 22 DF laser lines (even if a particular line may have been omitted from the zero-path calibration run). After all the zero-path runs occurring on a given day have been processed, the A run is averaged with the C run (if the latter run was made); the B0 runs are averaged if more than one of these runs were made For each line the ratio of the average of the B runs to the average of the A and C runs represents the actual transmission of the transmitter-receiver system at that corresponding wavenumber. It is this transmission coefficient that is used to normalize the long-path measurements.

Ideally there should be no difference between the A run performed prior to the B runs and the C run performed afterward. The program output must be examined to determine whether the system response changed appreciably between the A run and the C run. It may be necessary to discard data from days when a significant change was observed.

2.4.3 Program D04KMH: Zero-Path Correction Factors

Program D04KMH reads the transmissions from the file generated by program D03KMH. For each DF wavenumber, the program calculates the average of the zero-path transmissions obtained on those days prior to the long-path runs and then the average transmission obtained after the last long-path measurement. The "before" and

"after" transmissions are linearly interpolated on a day-by-day basis to yield the best estimate of the zero-path transmission for each of the long-path-measurement days.

By using this interpolated transmission, the long-path transmission data can be normalized to determine the absolute transmission. Recall that to calculate the long-path transmission the B-run ratio is divided by the A (and C) run ratio of that day. So the absolute transmission will be the long-path transmission divided by the zero-path transmission as interpolated for that day. The program combines the two latter quantities to produce (for each laser wavenumber and for each day) a multiplicative correction factor. These correction factors are written to an output file for later use by program D05KMH.

2.4.4 Program D05KMH: Laser Extinction Calculations

Program D05KMH calculates the absolute transmission for each line measured over the long path. The measured ratio is first scaled according to the preamplifier gain and is then normalized by the correction factor appropriate for that particular spectral wavenumber on that particular day. (This latter information is read from the output file generated by program D04KMH.)

In addition to the absolute transmission the coefficient of extinction (based on the known length of the path) is also calculated. These results and the date, time, line identification, and spectral wavenumber are then written to the output file.

2.4.5 Program D09KMH: Molecular Absorption Calculations

Program D09KMH compares the extinction coefficients produced by program D05KMH with those calculated by the best molecular absorption algorithms currently available. Each of the 22 DF laser lines has its own algorithm which expresses the molecular absorption as a polynomial function of both air temperature and water-vapor pressure.

For each measured line an input file of meteorological data is scanned to obtain the air temperature and the water-vapor pressure at the time of the optical measurement. (Program D15KMH produces the meteorological data file by combining the meteorological measurements made at each end of the path.) Once the molecular absorption is calculated, it is subtracted from the observed extinction. Depending on the quality of the algorithm, this difference represents the amount of extinction due to nonmolecular effects. These effects are generally attributed to aerosol extinction, and the latter difference is referred to as the "derived" aerosol extinction (DAE). Finally, the measured extinction, the calculated molecular absorption (CMA), and the derived aerosol extinction are written to an output file.

2.4.6 *Program D10KMH: Aerosol Extinction Calculations*

Since the wavenumber dependence of the aerosol extinction would not be expected to change appreciably over the wavenumber range of the DF laser lines, it is assumed that the derived aerosol extinctions produced by program D09KMH either will be constant or will vary slowly with time. For each run, program D10KMH performs a least-squares-polynomial fit of the derived aerosol extinction against time. The resulting function is a polynomial of order not more than two.

This polynomial then represents the best estimate of the aerosol extinction during the DF laser measurement runs. The function can be evaluated for the time corresponding to a given DF measurement to obtain a smoothed estimate of the aerosol extinction. The latter quantity can be termed an "adjusted" aerosol extinction (AAE). If the adjusted aerosol extinction is subtracted from the observed extinction, the resulting difference represents an "apparent" molecular absorption (AMA). Along with the information provided on the input file (generated by program D09KMH), the adjusted aerosol extinction and the apparent molecular absorption are written to the output file. The output file is used by program D08KMH to produce molecular-absorption graphs and by programs D11KMH and D14KMH to produce aerosol-extinction graphs. An example of the tabular output file generated by program D10KMH is given in the next section.

Program D10KMH also contains coding which allows data from specified DF laser lines to be excluded from the curve fit. Thus lines for which the molecular-absorption algorithm is suspect can be prevented from having an adverse effect on the nature of the least-squares-polynomial fit. After calculating the fit without these lines, the program then uses the resulting polynomial to estimate the aerosol extinction for the excluded lines. As for the other lines, the aerosol extinction thus obtained is then used to determine the apparent molecular absorption.

In this manner an estimate of the molecular absorption for a suspect line can be produced which is independent of the estimate provided by the molecular-absorption algorithm for that line. When the absorptions obtained by this technique agree with those predicted by the algorithm, the quality of the algorithm then can be established (at least to within an overall additive constant). Finally large discrepancies between the apparent molecular absorption and that predicted by the molecular-absorption algorithm readily enables the identification of those DF laser lines whose algorithms require further refinement.

2.4.7 *Graphics Programs: D08KMH, D11KMH, and D14KMH*

Programs D08KMH, D11KMH, and D14KMH produce graphs which are intended to provide a means for visually examining the results of the optical extinction measurements. At this stage the data are further refined by iteratively graphing the D10KMH results, adjusting the D10KMH input, and rerunning the D10KMH program.

2.4.8 *Program D08KMH: Molecular Absorption Graphics*

Program D08KMH plots the apparent molecular absorption (obtained from program D10KMH) as a function of water-vapor pressure for each of the 22 DF laser lines. A solid

line indicating a least-squares fit to these data and a dotted line representing the molecular-absorption calculation are also shown on these graphs. The graphs allow the quality of the molecular-absorption algorithm to be estimated by observing whether or not the algorithm agrees with the experimentally determined absorptions. Those lines for which the agreement is not good can be flagged in the D10KMH input file, removing them from the curve fits. The apparent molecular absorptions can then be recalculated for the remaining DF laser lines. Plots gererated by program D08KMH are included in Section 3.

The lines singled out by these graphs are given a high priority for further investigation in a series of independent laboratory measurements. These controlled laboratory measurements lead to newer algorithms for those lines. Then the new algorithms are compared with the long-path experimental results. This process is now being carried out jointly by NRL and Science Applications Inc., Ann Arbor, Michigan [2,3].

2.4.9 Program D11KMH: Aerosol Extinction Graphics

Program D11KHM plots the derived aerosol extinction (obtained from program D10KMH) as a function of time for each long-path-measurement day. The curve-fit estimates of the apparent aerosol extinction produced by program D10KMH are also included in the graphs. Data points which are seen to deviate significantly from the calculated fit can be further scrutinized.

2.4.10 Program D14KMH: Combined Aerosol Graphics

Like program D11KMH, program D14KMH produces a graph of the derived aerosol extinction as a function of time for each long-path-measurement day. In addition to the DF aerosol determinations at 3.8 μm, the Nd-YAG extinction measurements at 1.06 μm are included in these graphs. (Since there is negligible molecular absorption at 1.06 μm, the observed Nd-YAG extinctions are attributed to aerosol scattering effects.) Finally, the aerosol extinction calculated from independent measurements of particle-size distributions are presented for comparison purposes. Examples of the graphical output of program D14KMH are presented in Section 3.

3. EXPERIMENTAL RESULTS

3.1 General Comments

As stated in Section 1, two separate experimental measurement series were conducted in conjunction with the JAN propagation test series. Tables 1a and 1b summarize the measurement schedule during each series. Table 1a lists the times during which DF extinction measurements were made, including those runs done for the zero-path calibration configuration described earlier. Aerosol particle distributions measured with the PMS aerosol spectrometer system in the NRL meteorology van are shown in this section of the report for the times indicated in column 5 of Table 1a. Table 1b contains similar information but in addition includes a list of the BDL shot numbers and times and lists the corresponding times for which PMS data are shown.

Table 1a — Extinction Measurement Schedule Prior To Series B Tests

Day	Date	Extinction Measurement Time		PMS Data Record
		Start	Stop	
211	7/30	(zero path)	—	—
212	7/31	—	—	—
213	8/1	—	—	—
217	8/5	1645	1800	1700
				1800
218	8/6	1615	1745	1600
				1700
219	8/7	1420	1515	1500
220	8/8	1100	1145	1100
224	8/12	1700	1740	1700
225	8/13	1150	1230	1200
		1415	1500	1500
226	8/14	1350	1430	NA
		1545	1630	NA
227	8/15	1200	1230	1200
		1630	1715	1700
232	8/20	—	—	—
233	8/21	—	—	—
234	8/22	—	—	—

Table 1b — Extinction Measurement and BDL Shot Schedule During Series B Tests

Day	Date	Extinction Measurement Time		BDL Shot Number	BDL Shot Time	PMS Data Record
		Start	Stop			
253	9/10	(zero path)	—	—	—	—
255	9/12	1115	1215	VLI-165	1200	1200
		1345	1445	VLI-166	1420	1400
				VLI-167	1642	1700
				VLI-168	1825	1800
258	9/15	1200	1245	VLI-169	1259	1300
259				VLI-170	1233	1300
259	9/16	1500	1545			1600
				VLI-171	1820	1800
260	9/17			VLI-172	1133	1200
		1330	1430	VLI-173	1332	1400
		1430	1515	VLI-174	1447	1500
				VLI-175	1650	1700
				VLI-176	1916	1900
261	9/18	1030	1130	VLI-177	1048	1100
				VLI-179	1404	1400
				VLI-180	1542	1600
262	9/19	1045	1215	VLI-181	1226	1200
				VLI-182	1523	1500
				VLI-183	1807	1800
265	9/22	—	—	—	—	—
266	9/23	—	—	—	—	—

3.2 Measurement-System Optical-Efficiency Calibrations

Figures 12 and 13 are plots of the optical-system efficiency versus wavenumber as determined during the zero-path runs prior and subsequent to the 5-km-path measurements using the procedures outlined in Section 2.4.2. The transmission curves obtained for the various zero-path measurement days listed in Tables 1a and 1b are labeled as to day, with the solid curves obtained prior to and the dashed curves subsequent to the 5-km data.

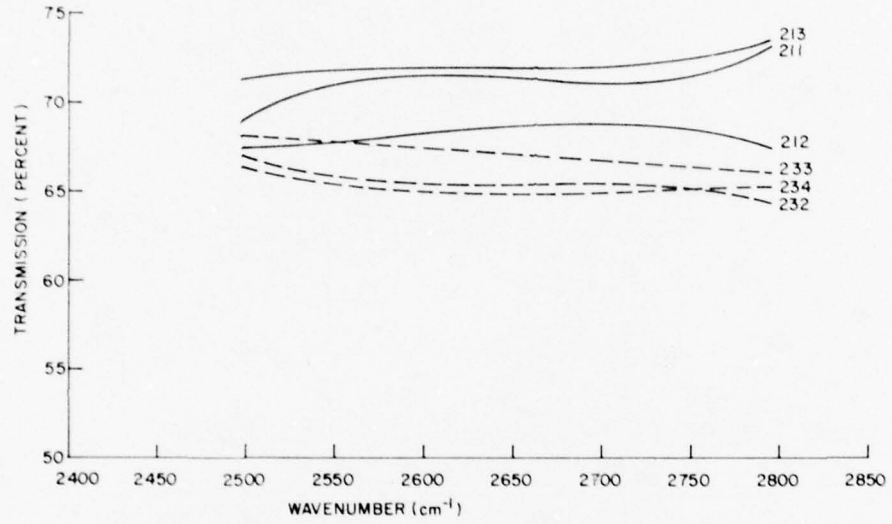

Fig. 12 — Zero-path transmissions vs wavenumber for the first test series

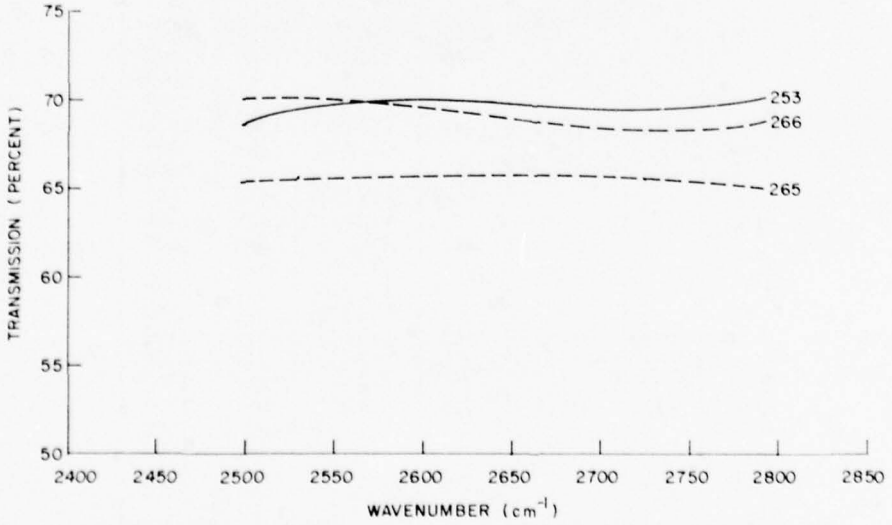

Fig. 13 — Zero-path transmissions vs wavenumber for the second test series

The curve for day 211, unlike the other curves, has a second derivative that is markedly nonzero. On day 211 the zero-path calibration data did not span the entire range of DF wavenumbers, and the ends of this curve represent an extrapolation of the least-squares curve fit performed by program D02KMH. That is, no data were obtained for the regions at the ends of the curve. Though the information provided at the center of the curve is as valid as that of any of the other curves, the day-211 curve was subsequently discarded because of the undesirable (and wholly artificial) effects introduced by extrapolating the curve fit.

As seen in Fig. 12, a maximum spread in measured efficiency of 67% to 73% for any one wavelength was observed. When the data for days 212 and 213 are averaged, the resulting curve (averaging about 71%) is smoother than any of the individual runs. The zero-path-day data taken at the end of the first experiment series are more closely clustered and yield an average transmission of about 66%. This 5% difference indicates a loss in the average combined efficiency of the ten optical surfaces between the focal point of the transmitter (Fig. 4) and the entrance to the detector/integrator (Fig. 6). That the individual runs taken on days 232 through 234 are more tightly grouped probably reflects the increased precision realized in the measurement procedure which the field team gained from repeated practice in data collection during the measurement period.

The zero-path data collected during the second measurement series associated with the BDL tests are shown in Fig.13. The average efficiency (initially about 66%) shows a smaller absolute decrease than observed during the first half of the two-part measurement series. The averaging and daily interpolation procedures described in Section 2.4.3 were used to model the zero-path transmission correction factors applied to each long-path measurement using the data shown in Figs. 12 and 13. If all of the runs shown in these two figures were averaged and used as a time-independent correction, then a maximum spread of efficiency values from 64% to 73% would be included in the average, about twice that observed for averages including only those runs performed in a 2-or 3-day period (before or after a 10-to-20-day period of long-path measurements).

The linerarly interpolated optical-efficiency feature included in the data-reduction procedure is a best guess under the circumstances. It is included because evidence in Figs. 12 and 13 points to a gradual systematic decrease in efficiency over the experimental period due to continued exposure of the optical surfaces to the environment.

3.3 Detector Relative-Response Calibrations

As previously described, an A run was performed with both detectors located in the transmitter trailer prior to a long-path run, which was usually followed later by a C run duplicating the A-run configuration. Figures 14 and 15 show the curves obtained for detector relative response as a function of wavenumber on each of the long-path-measurement days listed in Tables 1a and 1b. Figure 14 shows the A-and-C-run averages used to normalize the B-run data for the first measurement session; comparable data from the second session are shown in Fig. 15. In all cases the normalization curves shown are generated by (a) evaluating the polynomial fits to the A and C runs at each of the laser frequencies, (b) averaging the two values thus obtained (provided both an A and C run were made on a given day) and inverting this average normalization constant, and (c) interpolating between numerical values

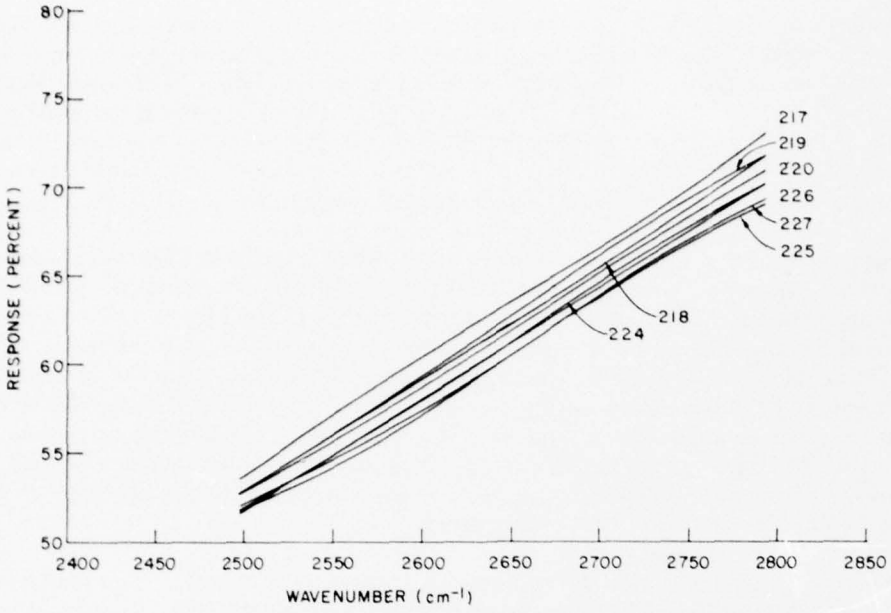

Fig. 14 — Detector response vs wavenumber for the first test series

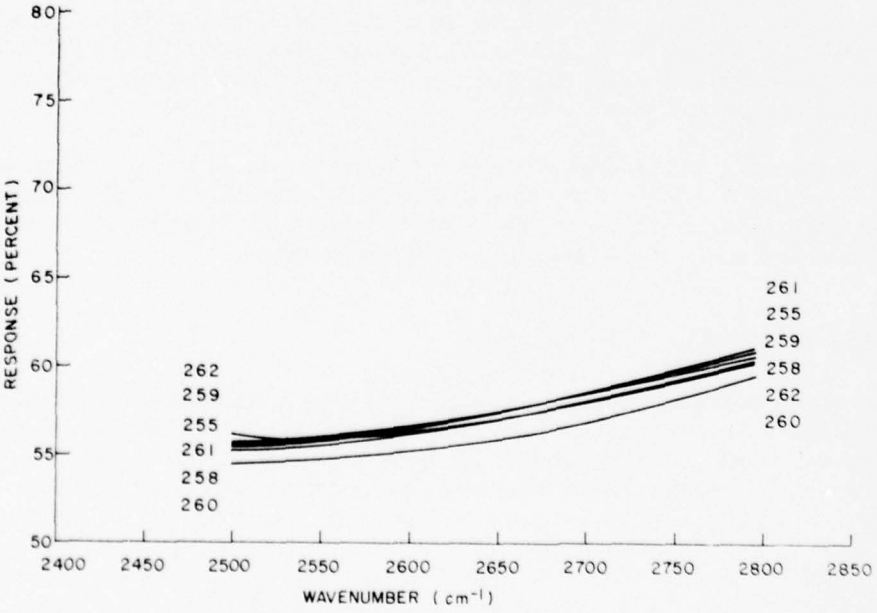

Fig. 15 — Detector response vs wavenumber for the second test series

thus obtained with straight-line segments. The data graphed in Fig. 14 show a consistently reproducible wavenumber dependence of the family of normalization curves accompanied by a gradual wavelength-independent decrease in response with increasing experimental day. This behavior can be attributed to a slight differential degradation in reflectivity between the chopper C and the flat folding mirror following it which folds the beam onto the mobile detector MD in the calibration position (Fig. 4).

The mobile detector was replaced prior to the start of the second series of measurements due to a loss of vacuum in the liquid-nitrogen dewar; hence the family of response curves shown in Fig. 15 is flatter. In both figures the maximum change in response observed at any one wavelength over the course of the experimental session is approximately 4% to 5%, with about 1% to 1.5% change observed for runs made on consecutive days. The latter figure is typical of the variations observed between values measured in A and C runs on the same day for a given line and represents the fundamental reproducibility inherent in the measurement procedure.

The systematic decrease in the wavelength-dependent response ratio from start to finish of an experimental session is not particularly significant, since the dectector relative response is normalized daily using the procedures described earlier.

3.4 Tabulation of Results from Program D10KMH

The final output from program D10KMH is presented in Table 2. This listing is the result of four iterative refinements of the type described in Section 2.

Initial difficulties with the $P_1 8$, $P_1 9$, and $P_1 10$ lines led to their exclusion from the curve fits calculated by the program. Subsequent refinement of the $P_1 9$ and $P_1 8$ algorithms (Table 3) by Woods et al.[2] resulted in their successful reinstatement in the curve fits. These improved algorithms enhanced the self-consistency of the data set to the point where similiar (but less severe) difficulties could be identified with the $P_1 6$ and $P_2 4$ lines. Thus, with the molecular-absorption algorithms now available, the best agreement between the observed long-path field measurements and the theoretical predictions (based on independent laboratory measurements) is achieved when the $P_1 6$, $P_1 10$, and $P_2 4$ lines are excluded from the curve fits used to estimate the aerosol extinction.

For each DF line measured over the long path, Table 2 lists the day, time, run (MODE), spectral line identification, wavenumber [4], air temperature T (°C), water vapor pressure P (torr), and the following coefficients of extinction (km^{-1}): the measured extinction (EXT), the calculated molecular absorption (CMA), the derived aerosol extinction (DAE), the adjusted aerosol extinction (AAE), and the apparent molecular absorption (AMA). The data tabulated here were used to produce the plots presented in the next two subsections.

Table 2

NRL OF LASER EXTINCTION MEASUREMENTS CAPISTRANO, 1975
DATA FILE: CREATED BY C10KMH1 INTENDED FOR C08KMH, D11KMH, AND D14KMH

DAY	TIME	MODE	LINE	WAVENUMBER	T	P	EXT	CMA	DAE	AAE	AMA
217	1647	AS	P2-8	2631.067	22.63	12.99	.0743	.0329	.0414	.0478	.0265
217	1650	AS	P2-7	2655.863	22.64	12.94	.1293	.0905	.0388	.0473	.0820
217	1658	AS	P2-6	2680.179	22.66	12.80	.1124	.0533	.0591	.0461	.0663
217	1702	AS	P1-9	2691.606	22.69	12.76	.0900	.0419	.0481	.0455	.0445
217	1706	AS	P2-5	2701.999	22.72	12.75	.0852	.0264	.0588	.0449	.0403
217	1722	AS	P1-8	2717.538	22.77	12.64	.1690	.1265	.0425	.0425	.1265
217	1726	AS	P1-7	2742.997	22.76	12.58	.0534	.0304	.0230	.0419	.0115
217	1728	AS	P2-3	2750.094	22.76	12.55	.0670	.0369	.0301	.0416	.0254
217	1730	AS	P1-5	2762.434	22.75	12.52	.0902	.0611	.0291	.0412	.0490
217	1733	AS	P2-8	2631.067	22.71	12.53	.0743	.0318	.0425	.0408	.0335
217	1737	AS	P1-5	2617.386	22.67	12.55	.0766	.0202	.0564	.0402	.0364
217	1739	AS	P2-9	2605.806	22.64	12.56	.0910	.0454	.0456	.0399	.0511
217	1741	AS	P1-6	2564.197	22.62	12.56	.0690	.0276	.0414	.0396	.0294
217	1743	AS	P2-10	2580.096	22.59	12.57	.1034	.0650	.0384	.0393	.0641
217	1745	AS	P1-7	2570.522	22.57	12.58	.1078	.0620	.0458	.0390	.0688
217	1747	AS	P2-11	2561.952	22.54	12.60	.0719	.0340	.0379	.0387	.0332
217	1752	AS	P1-8	2546.175	22.47	12.66	.0967	.0484	.0483	.0379	.0588
217	1754	AS	P2-12	2527.391	22.44	12.68	.0706	.0319	.0387	.0376	.0330
217	1756	AS	P1-9	2521.769	22.42	12.70	.0717	.0338	.0379	.0373	.0344
217	1758	AS	P1-10	2496.721	22.39	12.73	.0832	.0481	.0351	.0370	.0462
217	1759	AS	P2-8	2631.067	22.37	12.74	.0561	.0323	.0238	.0368	.0191
217	1654	AS	*P1-10	2665.219	22.65	12.87	.0916	.0343	.0573	.0467	.0449
217	1724	AS	*P2-4	2727.309	22.77	12.61	.0842	.0502	.0340	.0422	.0420
217	1730	AS	*P1-6	2767.968	22.75	12.52	.0977	.0765	.0212	.0412	.0565
218	1611	AS	P2-8	2631.067	26.83	12.89	.1200	.0326	.0874	.0915	.0385
218	1616	AS	P2-7	2655.863	26.89	12.97	.1568	.0904	.0663	.0891	.0675
218	1622	AS	P2-6	2680.179	27.10	13.12	.1562	.0538	.1024	.0843	.0719
218	1624	AS	P1-9	2691.606	27.17	13.17	.1187	.0421	.0766	.0827	.0360
218	1626	AS	P2-5	2701.999	27.25	13.22	.1165	.0264	.0901	.0811	.0354
218	1628	AS	P1-8	2717.538	27.32	13.27	.1992	.1355	.0637	.0795	.1197
218	1633	AS	P1-7	2742.997	27.34	13.37	.1097	.0306	.0791	.0755	.0342
218	1640	AS	P2-3	2750.094	27.21	13.48	.1150	.0381	.0769	.0698	.0452
218	1645	AS	P1-5	2762.434	27.12	13.56	.1447	.0647	.0800	.0658	.0789
218	1650	AS	P2-8	2631.067	27.27	13.60	.0998	.0343	.0655	.0618	.0380
218	1652	AS	P2-9	2605.806	27.33	13.61	.1126	.0482	.0644	.0602	.0524
218	1653	AS	P1-6	2564.197	27.37	13.62	.1147	.0292	.0855	.0594	.0553
218	1706	AS	P2-10	2580.096	27.76	13.65	.1088	.0655	.0433	.0589	.0599
218	1709	AS	P1-7	2570.522	27.86	13.65	.1000	.0623	.0377	.0665	.0535
218	1710	AS	P2-11	2561.952	27.89	13.64	.0819	.0361	.0458	.0657	.0382
218	1712	AS	P1-8	2546.175	27.95	13.64	.0871	.0484	.0387	.0641	.0430
218	1715	AS	P2-12	2527.391	28.04	13.63	.0727	.0320	.0407	.0617	.0310
218	1718	AS	P1-9	2521.769	28.12	13.60	.0675	.0337	.0338	.0593	.0282
218	1726	AS	P1-10	2496.721	28.32	13.51	.0760	.0477	.0283	.0528	.0432
218	1730	AS	P2-8	2631.067	28.42	13.46	.0630	.0339	.0291	.0506	.0334
218	1733	AS	P2-7	2655.863	28.46	13.46	.1218	.0939	.0279	.0572	.0946
218	1736	AS	P2-6	2680.179	28.51	13.46	.0884	.0549	.0335	.0548	.0536
218	1738	AS	P1-8	2717.538	28.54	13.45	.1618	.1381	.0237	.0532	.1386
218	1618	AS	*P1-10	2665.219	26.96	13.02	.1139	.0338	.0801	.0875	.0264
218	1630	AS	*P2-4	2727.309	27.39	13.32	.1189	.0528	.0661	.0779	.0410
218	1643	AS	*P1-6	2767.968	27.16	13.53	.1904	.0809	.0955	.0674	.1130
219	1426	AS	P2-8	2631.067	27.51	13.97	.0796	.0352	.0444	.0451	.0345
219	1428	AS	P2-7	2655.863	27.46	13.96	.1431	.0976	.0455	.0461	.0970
219	1431	AS	P2-6	2680.179	27.39	13.91	.0970	.0572	.0398	.0474	.0496
219	1433	AS	P1-9	2691.606	27.35	13.88	.0893	.0440	.0453	.0483	.0410
219	1435	AS	P2-5	2701.999	27.31	13.81	.0986	.0276	.0710	.0493	.0493
219	1437	AS	P1-8	2717.538	27.27	13.76	.1967	.1408	.0459	.0502	.1365
219	1442	AS	P1-7	2742.997	27.19	13.68	.0863	.0313	.0550	.0525	.0338
219	1444	AS	P2-3	2750.094	27.14	13.59	.0910	.0385	.0525	.0534	.0376
219	1447	AS	P1-5	2762.434	27.24	13.51	.1189	.0644	.0545	.0548	.0641
219	1448	AS	P2-8	2631.067	27.30	13.49	.0706	.0340	.0366	.0552	.0244
219	1450	AS	P1-5	2617.386	27.41	13.45	.0748	.0207	.0542	.0561	.0188
219	1452	AS	P2-9	2605.806	27.53	13.40	.1080	.0475	.0605	.0570	.0510
219	1457	AS	P1-6	2564.197	27.82	13.29	.0959	.0285	.0674	.0593	.0366
219	1458	AS	P2-10	2580.096	27.88	13.27	.1237	.0648	.0588	.0598	.0639
219	1500	AS	P1-7	2570.522	28.00	13.22	.1120	.0616	.0504	.0607	.0513
219	1502	AS	P2-11	2561.952	27.93	13.32	.0920	.0337	.0583	.0616	.0304
219	1504	AS	P1-8	2546.175	27.86	13.43	.1139	.0481	.0658	.0625	.0514
219	1505	AS	P2-12	2527.391	27.83	13.48	.0970	.0318	.0652	.0630	.0340
219	1507	AS	P1-9	2521.769	27.76	13.58	.1030	.0338	.0692	.0639	.0391
219	1510	AS	P1-10	2496.721	27.66	13.73	.1029	.0483	.0546	.0653	.0376
219	1512	AS	P2-8	2631.067	27.59	13.84	.1089	.0349	.0740	.0662	.0427
219	1430	AS	*P1-10	2665.219	27.41	13.94	.0782	.0362	.0420	.0470	.0312
219	1441	AS	*P2-4	2727.309	27.20	13.66	.0779	.0540	.0238	.0520	.0258
219	1445	AS	*P1-6	2767.968	27.12	13.56	.1170	.0811	.0359	.0538	.0632

* DENOTES LINES WHICH WERE EXCLUDED FROM THE CURVE FIT.

Table continues.

Table 2 — (Continued)

NRL OF LASER EXTINCTION MEASUREMENTS CAPISTRANO, 1975
DATA FILE: CREATED BY C10KMHI INTENDED FOR C08KMH, D11KMH, AND D14KMH

DAY	TIME	MODE	LINE	WAVENUMBER	T	P	EXT	CMA	DAE	AAE	AMA
220	1102	AS	P2-9	2631.067	22.30	14.69	.0732	.0370	.0362	.0347	.0385
220	1103	AS	P2-7	2665.863	22.32	14.68	.1336	.1035	.0301	.0356	.0980
220	1106	AS	P2-6	2680.179	22.38	14.66	.1100	.0617	.0483	.0382	.0718
220	1107	AS	P1-9	2691.606	22.40	14.66	.0878	.0474	.0404	.0390	.0488
220	1109	AS	P2-5	2703.999	22.44	14.65	.0751	.0308	.0443	.0405	.0346
220	1110	AS	P1-8	2717.538	22.46	14.64	.1831	.1477	.0354	.0412	.1419
220	1115	AS	P1-7	2742.997	22.56	14.61	.0711	.0356	.0355	.0442	.0269
220	1116	AS	P2-3	2750.094	22.59	14.61	.0892	.0433	.0459	.0447	.0445
220	1119	AS	P1-5	2792.434	22.67	14.60	.1140	.0718	.0422	.0459	.0681
220	1121	AS	P2-8	2631.067	22.73	14.60	.0804	.0368	.0436	.0466	.0338
220	1123	AS	P3-5	2617.386	22.79	14.60	.0687	.0233	.0454	.0472	.0215
220	1124	AS	P2-9	2605.806	22.82	14.60	.1004	.0523	.0481	.0474	.0530
220	1128	AS	P3-6	2584.197	22.93	14.59	.0752	.0314	.0438	.0480	.0272
220	1129	AS	P2-10	2580.096	22.96	14.59	.1280	.0679	.0601	.0480	.0800
220	1131	AS	P3-7	2570.522	23.00	14.59	.1209	.0652	.0557	.0480	.0729
220	1132	AS	P2-11	2553.952	23.01	14.60	.0851	.0367	.0484	.0480	.0371
220	1133	AS	P3-8	2546.375	23.02	14.60	.0986	.0511	.0475	.0479	.0507
220	1135	AS	P2-12	2527.391	23.03	14.60	.0902	.0347	.0555	.0476	.0426
220	1136	AS	P3-9	2521.769	23.04	14.61	.0800	.0366	.0434	.0475	.0325
220	1138	AS	P3-10	2496.721	23.06	14.61	.0893	.0513	.0380	.0470	.0423
220	1139	AS	P2-8	2631.067	23.07	14.61	.0829	.0368	.0461	.0467	.0362
220	1104	AS	*P1-10	2665.219	22.34	14.68	.0944	.0393	.0451	.0365	.0479
220	1114	AS	*P2-4	2727.309	22.54	14.62	.0790	.0547	.0203	.0436	.0354
220	1118	AS	*P1-6	2767.968	22.65	14.61	.1324	.0893	.0431	.0455	.0869
220	1424	AS	P2-8	2631.067	25.10	14.30	.1127	.0360	.0767	.0758	.0369
220	1424	AS	P2-7	2665.863	25.10	14.30	.1756	.1004	.0752	.0758	.0998
220	1427	AS	P2-6	2680.179	25.15	14.27	.1510	.0593	.0917	.0744	.0766
220	1428	AS	P1-9	2691.606	25.17	14.26	.1050	.0456	.0594	.0739	.0311
220	1430	AS	P2-5	2703.999	25.20	14.24	.0940	.0291	.0649	.0729	.0211
220	1431	AS	P1-8	2717.538	25.18	14.24	.2202	.1449	.0753	.0724	.1478
220	1436	AS	P1-7	2742.997	25.09	14.24	.1024	.0336	.0688	.0700	.0324
220	1437	AS	P2-3	2750.094	25.07	14.24	.1244	.0412	.0832	.0695	.0549
220	1440	AS	P1-5	2792.434	25.02	14.25	.1247	.0690	.0557	.0681	.0566
220	1441	AS	P2-8	2631.067	25.00	14.25	.1013	.0359	.0654	.0676	.0337
220	1442	AS	P3-5	2617.386	24.98	14.25	.0804	.0224	.0580	.0671	.0133
220	1443	AS	P2-9	2605.806	24.97	14.25	.1143	.0508	.0635	.0666	.0477
220	1449	AS	P3-6	2584.197	24.96	14.24	.1165	.0305	.0860	.0637	.0528
220	1453	AS	P2-10	2580.096	24.99	14.23	.1311	.0669	.0642	.0618	.0693
220	1454	AS	P3-7	2570.522	25.00	14.23	.1238	.0640	.0598	.0613	.0625
220	1459	AS	P2-12	2527.391	25.03	14.21	.0925	.0336	.0589	.0589	.0336
220	1500	AS	P3-9	2521.769	25.04	14.21	.0913	.0355	.0558	.0584	.0329
220	1502	AS	P3-10	2496.721	25.04	14.21	.1082	.0499	.0583	.0574	.0508
220	1503	AS	P2-8	2631.067	25.04	14.21	.0879	.0358	.0521	.0570	.0309
220	1426	AS	*P1-10	2665.219	25.13	14.28	.1354	.0375	.0979	.0749	.0605
220	1434	AS	*P2-4	2727.309	25.13	14.24	.1113	.0568	.0545	.0710	.0403
220	1438	AS	*P1-6	2767.968	25.06	14.25	.1401	.0961	.0540	.0691	.0710
224	1700	AS	P2-8	2631.067	19.60	11.77	.0721	.0300	.0421	.0480	.0241
224	1701	AS	P2-7	2665.863	19.57	11.77	.1378	.0821	.0557	.0480	.0898
224	1704	AS	P2-6	2680.179	19.47	11.76	.1045	.0493	.0552	.0480	.0565
224	1705	AS	P1-9	2691.606	19.43	11.75	.0763	.0396	.0367	.0480	.0283
224	1707	AS	P2-5	2703.999	19.37	11.75	.0709	.0249	.0460	.0480	.0229
224	1708	AS	P1-8	2717.538	19.33	11.74	.1718	.1156	.0562	.0480	.1238
224	1710	AS	P1-7	2742.997	19.27	11.74	.0790	.0295	.0495	.0480	.0310
224	1713	AS	P2-3	2750.094	19.17	11.73	.0846	.0355	.0491	.0480	.0366
224	1715	AS	P1-5	2792.434	19.10	11.72	.1018	.0583	.0435	.0480	.0538
224	1716	AS	P2-8	2631.067	19.09	11.72	.0681	.0299	.0382	.0480	.0201
224	1720	AS	P3-5	2617.386	19.05	11.73	.0698	.0195	.0503	.0480	.0218
224	1721	AS	P2-9	2605.806	19.04	11.74	.0967	.0431	.0536	.0480	.0487
224	1722	AS	P3-6	2584.197	19.03	11.74	.0759	.0263	.0496	.0480	.0279
224	1724	AS	P2-10	2580.096	19.01	11.74	.1219	.0644	.0575	.0480	.0739
224	1725	AS	P3-7	2570.522	19.00	11.75	.1168	.0615	.0553	.0480	.0688
224	1726	AS	P2-11	2553.952	18.99	11.75	.0862	.0336	.0526	.0480	.0382
224	1727	AS	P3-8	2546.375	18.98	11.75	.0970	.0478	.0492	.0480	.0490
224	1730	AS	P2-12	2527.391	18.95	11.76	.0734	.0312	.0422	.0480	.0254
224	1731	AS	P3-9	2521.769	18.95	11.76	.0757	.0331	.0426	.0480	.0277
224	1733	AS	P3-10	2496.721	18.94	11.76	.0940	.0472	.0468	.0480	.0460
224	1734	AS	P2-8	2631.067	18.94	11.76	.0669	.0300	.0369	.0480	.0189
224	1703	AS	*P1-10	2665.219	19.50	11.76	.0773	.0318	.0455	.0480	.0293
224	1709	AS	*P2-4	2727.309	19.30	11.74	.0845	.0469	.0376	.0480	.0365
224	1714	AS	*P1-6	2767.968	19.13	11.72	.1115	.0729	.0386	.0480	.0635

* DENOTES LINES WHICH WERE EXCLUDED FROM THE CURVE FIT.

Table continues.

Table 2 — (Continued)

NRL OF LASER EXTINCTION MEASUREMENTS CAPISTRANO, 1975
DATA FILE: CREATED BY C10KMH; INTENDED FOR C08KMH, D11KMH, AND D14KMH

DAY	TIME	MODE	LINE	WAVENUMBER	T	P	EXT	CMA	DAF	AAF	AMA
225	1157	AS	P2-8	2631.067	21.37	12.53	.0649	.0318	.0331	.0290	.0359
225	1158	AS	P2-7	2655.863	21.39	12.57	.1158	.0879	.0279	.0295	.0863
225	1201	AS	P2-6	2680.179	21.44	12.62	.0879	.0528	.0351	.0310	.0569
225	1202	AS	P1-9	2691.606	21.47	12.61	.0798	.0417	.0381	.0315	.0483
225	1203	AS	P2-5	2703.999	21.49	12.59	.0598	.0264	.0334	.0320	.0278
225	1204	AS	P1-8	2717.538	21.52	12.58	.1542	.1253	.0289	.0326	.1216
225	1206	AS	P1-7	2742.997	21.57	12.54	.0556	.0308	.0248	.0336	.0220
225	1207	AS	P2-3	2750.094	21.59	12.53	.0636	.0372	.0264	.0341	.0295
225	1209	AS	P1-5	2762.434	21.64	12.50	.0851	.0614	.0237	.0351	.0500
225	1210	AS	P2-8	2631.067	21.67	12.48	.0645	.0317	.0328	.0356	.0289
225	1214	AS	P3-5	2617.386	21.77	12.42	.0616	.0201	.0415	.0376	.0240
225	1215	AS	P2-9	2605.806	21.79	12.40	.0844	.0450	.0394	.0381	.0463
225	1216	AS	P3-6	2594.197	21.80	12.39	.0746	.0273	.0473	.0386	.0360
225	1217	AS	P2-10	2580.096	21.81	12.38	.1126	.0648	.0478	.0391	.0735
225	1218	AS	P3-7	2570.522	21.82	12.37	.1060	.0618	.0442	.0396	.0664
225	1218	AS	P2-11	2563.952	21.82	12.37	.0707	.0339	.0368	.0396	.0311
225	1219	AS	P3-8	2546.375	21.83	12.36	.0976	.0481	.0495	.0401	.0575
225	1220	AS	P2-12	2527.391	21.84	12.35	.0717	.0316	.0401	.0406	.0311
225	1221	AS	P3-9	2521.769	21.85	12.34	.0717	.0334	.0383	.0411	.0306
225	1223	AS	P3-10	2496.721	21.88	12.32	.0886	.0475	.0411	.0421	.0465
225	1225	AS	P2-8	2631.067	21.90	12.30	.0649	.0313	.0336	.0431	.0218
225	1200	AS	*P1-10	2665.219	21.42	12.64	.0749	.0339	.0410	.0305	.0444
225	1205	AS	*P2-4	2727.309	21.54	12.56	.0697	.0501	.0196	.0331	.0366
225	1208	AS	*P1-6	2767.968	21.62	12.51	.0976	.0769	.0207	.0346	.0630
225	1427	A6	P2-8	2631.067	22.43	12.07	.0677	.0307	.0370	.0310	.0367
225	1428	A6	P2-7	2655.863	22.42	12.05	.1161	.0840	.0321	.0330	.0831
225	1430	A6	P2-6	2680.179	22.41	12.00	.0977	.0499	.0478	.0365	.0612
225	1431	A6	P1-9	2691.606	22.40	12.00	.0700	.0398	.0302	.0381	.0319
225	1432	A6	P2-5	2703.999	22.38	12.00	.0696	.0248	.0448	.0396	.0300
225	1433	A6	P1-8	2717.538	22.37	12.00	.1485	.1196	.0289	.0409	.1076
225	1434	A6	P1-7	2742.997	22.36	11.99	.0656	.0291	.0365	.0422	.0234
225	1434	A6	P2-3	2750.094	22.36	11.99	.0734	.0353	.0381	.0422	.0312
225	1434	A6	P1-5	2762.434	22.36	11.99	.0969	.0586	.0383	.0422	.0547
225	1435	A6	P2-8	2631.067	22.35	11.99	.0684	.0305	.0379	.0433	.0251
225	1438	A6	P3-5	2617.386	22.31	11.99	.0654	.0194	.0460	.0458	.0196
225	1439	A6	P2-9	2605.806	22.30	11.99	.0899	.0435	.0464	.0464	.0435
225	1440	A6	P3-6	2594.197	22.28	11.99	.0845	.0265	.0580	.0469	.0376
225	1441	A6	P2-10	2580.096	22.27	11.99	.1158	.0642	.0516	.0472	.0686
225	1441	A6	P3-7	2570.522	22.27	11.99	.1082	.0611	.0471	.0472	.0610
225	1442	A6	P2-11	2563.952	22.26	11.98	.0858	.0333	.0525	.0474	.0384
225	1443	A6	P3-8	2546.375	22.25	11.98	.0961	.0474	.0487	.0475	.0486
225	1444	A6	P2-12	2527.391	22.23	11.98	.0899	.0309	.0590	.0475	.0424
225	1446	A6	P3-9	2521.769	22.20	11.98	.0743	.0327	.0416	.0471	.0272
225	1447	A6	P3-10	2496.721	22.18	11.98	.0925	.0468	.0457	.0467	.0458
225	1447	A6	P2-8	2631.067	22.18	11.98	.0677	.0305	.0372	.0467	.0210
225	1429	A6	*P1-10	2665.219	22.42	12.02	.0795	.0321	.0474	.0348	.0447
225	1433	A6	*P2-4	2727.309	22.37	12.00	.0763	.0477	.0286	.0409	.0354
225	1434	A6	*P1-6	2767.968	22.36	11.99	.0967	.0735	.0232	.0422	.0545
226	1359	AS	P2-8	2631.067	21.46	12.22	.0692	.0311	.0381	.0368	.0324
226	1400	AS	P2-7	2655.863	21.44	12.23	.1235	.0854	.0381	.0382	.0853
226	1401	AS	P2-6	2680.179	21.44	12.23	.0922	.0511	.0411	.0395	.0527
226	1402	AS	P1-9	2691.606	21.44	12.23	.0796	.0406	.0390	.0407	.0389
226	1403	AS	P2-5	2703.999	21.44	12.24	.0687	.0256	.0431	.0418	.0269
226	1404	AS	P1-8	2717.538	21.44	12.24	.1694	.1217	.0477	.0427	.1267
226	1405	AS	P1-7	2742.997	21.44	12.24	.0698	.0300	.0398	.0436	.0262
226	1406	AS	P2-3	2750.094	21.44	12.24	.0830	.0364	.0466	.0443	.0387
226	1408	AS	P1-5	2762.434	21.45	12.25	.0969	.0602	.0367	.0455	.0514
226	1409	AS	P2-8	2631.067	21.45	12.25	.0680	.0312	.0368	.0459	.0221
226	1413	AS	P3-5	2617.386	21.45	12.26	.0735	.0199	.0536	.0464	.0271
226	1413	AS	P2-9	2605.806	21.45	12.26	.0937	.0445	.0492	.0464	.0473
226	1414	AS	P3-6	2594.197	21.45	12.26	.0770	.0271	.0499	.0463	.0307
226	1415	AS	P2-10	2580.096	21.45	12.26	.1116	.0647	.0469	.0460	.0656
226	1415	AS	P3-7	2570.522	21.45	12.26	.1037	.0617	.0420	.0460	.0577
226	1416	AS	P2-11	2563.952	21.44	12.26	.0820	.0338	.0482	.0457	.0363
226	1417	AS	P3-8	2546.375	21.43	12.26	.0978	.0480	.0498	.0452	.0526
226	1418	AS	P2-12	2527.391	21.42	12.26	.0735	.0315	.0420	.0446	.0289
226	1420	AS	P3-9	2521.769	21.39	12.25	.0766	.0333	.0433	.0431	.0335
226	1421	AS	P3-10	2496.721	21.38	12.25	.0936	.0475	.0461	.0422	.0514
226	1422	AS	P2-8	2631.067	21.37	12.25	.0654	.0312	.0342	.0412	.0242
226	1401	AS	*P1-10	2665.219	21.44	12.23	.0870	.0328	.0542	.0395	.0475
226	1404	AS	*P2-4	2727.309	21.44	12.24	.0825	.0488	.0337	.0427	.0398
226	1407	AS	*P1-6	2767.968	21.44	12.24	.0991	.0753	.0238	.0449	.0542

* DENOTES LINES WHICH WERE EXCLUDED FROM THE CURVE FIT.

Table continues.

Table 2 — (Continued)

NRL OF LASER EXTINCTION MEASUREMENTS CAPISTRANO, 1975
DATA FILE: CREATED BY D10KMH1 INTENDED FOR D08KMH, D11KMH, AND D14KMH

DAY	TIME	MODE	LINE	WAVENUMBER	T	P	EXT	CMA	DAE	AAE	AMA
226	1556	R6	P2-8	2631.067	20.57	12.22	.0666	.0311	.0355	.0385	.0281
226	1557	R6	P2-7	2655.863	20.55	12.23	.1238	.0854	.0384	.0385	.0853
226	1558	R6	P2-6	2680.179	20.52	12.24	.0940	.0513	.0427	.0385	.0555
226	1559	R6	P1-9	2691.606	20.50	12.24	.0778	.0408	.0370	.0385	.0393
226	1600	R6	P2-5	2703.999	20.47	12.25	.0657	.0258	.0399	.0385	.0272
226	1609	R6	P1-8	2717.538	20.57	12.26	.1605	.1216	.0389	.0385	.1220
226	1610	R6	P1-7	2742.997	20.58	12.26	.0620	.0304	.0316	.0385	.0235
226	1611	R6	P2-3	2750.094	20.59	12.26	.0778	.0367	.0411	.0385	.0393
226	1613	R6	P1-5	2792.434	20.62	12.27	.0889	.0606	.0283	.0385	.0504
226	1614	R6	P2-8	2631.067	20.63	12.27	.0649	.0312	.0337	.0385	.0264
226	1616	R6	P3-5	2617.386	20.60	12.27	.0599	.0201	.0398	.0385	.0214
226	1617	R6	P2-9	2605.806	20.55	12.26	.0987	.0447	.0540	.0385	.0602
226	1618	R6	P3-6	2594.197	20.51	12.26	.0723	.0272	.0451	.0385	.0338
226	1619	R6	P2-10	2580.096	20.46	12.25	.1085	.0649	.0436	.0385	.0700
226	1619	R6	P3-7	2570.522	20.46	12.25	.1083	.0620	.0463	.0385	.0698
226	1621	R6	P3-8	2546.375	20.38	12.24	.0909	.0482	.0427	.0385	.0524
226	1622	R6	P2-12	2527.391	20.33	12.24	.0678	.0317	.0361	.0385	.0293
226	1623	R6	P3-9	2521.769	20.29	12.23	.0684	.0335	.0349	.0385	.0299
226	1624	R6	P3-10	2496.721	20.24	12.23	.0862	.0478	.0384	.0385	.0477
226	1625	R6	P2-8	2631.067	20.20	12.22	.0531	.0311	.0220	.0385	.0146
226	1557	R6	*P1-10	2665.219	20.55	12.23	.0832	.0329	.0503	.0385	.0447
226	1610	R6	*P2-4	2727.309	20.58	12.26	.0783	.0490	.0293	.0385	.0398
226	1612	R6	*P1-6	2767.968	20.61	12.27	.0911	.0757	.0154	.0385	.0526
227	1207	R5	P2-8	2631.067	20.98	11.50	.0568	.0294	.0274	.0281	.0287
227	1208	R5	P2-7	2655.863	21.03	11.52	.1124	.0802	.0322	.0285	.0839
227	1209	R5	P2-6	2680.179	21.08	11.53	.0812	.0481	.0331	.0289	.0523
227	1210	R5	P1-9	2691.606	21.12	11.55	.0616	.0387	.0229	.0293	.0323
227	1211	R5	P2-5	2703.999	21.17	11.57	.0531	.0241	.0290	.0297	.0234
227	1211	R5	P1-8	2717.538	21.17	11.57	.1448	.1145	.0303	.0297	.1151
227	1213	R5	P1-7	2742.997	21.27	11.60	.0530	.0285	.0245	.0305	.0225
227	1213	R5	P2-3	2750.094	21.27	11.60	.0657	.0345	.0312	.0305	.0352
227	1215	R5	P1-5	2792.434	21.36	11.63	.0838	.0571	.0267	.0313	.0525
227	1215	R5	P2-8	2631.067	21.36	11.63	.0557	.0297	.0260	.0313	.0244
227	1218	R5	P3-5	2617.386	21.36	11.62	.0525	.0190	.0335	.0325	.0200
227	1219	R5	P2-9	2605.806	21.37	11.62	.0769	.0424	.0345	.0329	.0440
227	1219	R5	P3-6	2594.197	21.37	11.62	.0669	.0259	.0410	.0329	.0340
227	1220	R5	P2-10	2580.096	21.37	11.61	.1034	.0638	.0396	.0333	.0701
227	1220	R5	P3-7	2570.522	21.37	11.61	.1008	.0607	.0401	.0333	.0675
227	1221	R5	P2-11	2553.552	21.37	11.61	.0681	.0329	.0352	.0337	.0344
227	1222	R5	P3-8	2546.375	21.37	11.61	.0876	.0471	.0405	.0340	.0536
227	1223	R5	P2-12	2527.391	21.37	11.60	.0601	.0305	.0296	.0344	.0257
227	1223	R5	P3-9	2521.769	21.37	11.60	.0642	.0323	.0319	.0344	.0298
227	1224	R5	P3-10	2496.721	21.37	11.60	.0819	.0463	.0356	.0348	.0471
227	1225	R5	P2-8	2631.067	21.37	11.60	.0540	.0296	.0244	.0352	.0188
227	1209	R5	*P1-10	2665.219	21.08	11.53	.0641	.0310	.0331	.0289	.0352
227	1212	R5	*P2-4	2727.309	21.22	11.58	.0632	.0461	.0171	.0301	.0331
227	1214	R5	*P1-6	2767.968	21.31	11.61	.0879	.0715	.0164	.0309	.0570
227	1644	R6	P2-7	2655.863	20.95	11.66	.0999	.0813	.0186	.0185	.0814
227	1645	R6	P2-6	2680.179	20.92	11.65	.0736	.0496	.0250	.0194	.0542
227	1646	R6	P1-9	2691.606	20.91	11.66	.0559	.0391	.0168	.0203	.0356
227	1647	R6	P2-5	2703.999	20.91	11.67	.0465	.0244	.0221	.0211	.0254
227	1647	R6	P1-8	2717.538	20.91	11.67	.1344	.1155	.0189	.0211	.1133
227	1648	R6	P1-7	2742.997	20.90	11.68	.0452	.0288	.0164	.0220	.0232
227	1649	R6	P2-3	2750.094	20.90	11.69	.0618	.0349	.0269	.0229	.0389
227	1651	R6	P1-5	2792.434	20.89	11.71	.0752	.0576	.0176	.0246	.0506
227	1652	R6	P2-8	2631.067	20.88	11.72	.0520	.0299	.0221	.0255	.0265
227	1653	R6	P3-5	2617.386	20.88	11.72	.0502	.0192	.0310	.0264	.0238
227	1654	R6	P2-9	2605.806	20.87	11.73	.0715	.0428	.0287	.0272	.0443
227	1655	R6	P3-6	2594.197	20.87	11.74	.0560	.0262	.0298	.0281	.0279
227	1656	R6	P2-10	2580.096	20.86	11.75	.0962	.0641	.0321	.0290	.0672
227	1656	R6	P3-7	2570.522	20.86	11.75	.0900	.0611	.0289	.0290	.0610
227	1657	R6	P2-11	2553.552	20.86	11.76	.0595	.0332	.0263	.0299	.0296
227	1658	R6	P3-8	2546.375	20.85	11.77	.0961	.0474	.0487	.0307	.0654
227	1659	R6	P2-12	2527.391	20.85	11.78	.0565	.0309	.0256	.0316	.0249
227	1700	R6	P3-9	2521.769	20.84	11.79	.0684	.0327	.0357	.0325	.0359
227	1701	R6	P3-10	2496.721	20.81	11.79	.0813	.0468	.0345	.0334	.0479
227	1701	R6	P2-8	2631.067	20.81	11.79	.0510	.0301	.0209	.0334	.0176
227	1645	R6	*P1-10	2665.219	20.92	11.65	.0594	.0313	.0281	.0194	.0400
227	1648	R6	*P2-4	2727.309	20.90	11.68	.0565	.0465	.0100	.0220	.0345
227	1650	R6	*P1-6	2767.968	20.89	11.70	.0858	.0722	.0136	.0237	.0621

* DENOTES LINES WHICH WERE EXCLUDED FROM THE CURVE FIT.

Table continues.

Table 2 — (Continued)

NRL DF LASER EXTINCTION MEASUREMENTS CAPISTRANO, 1975
DATA FILE: CREATED BY D10KMH1 INTENDED FOR D08KMH, D11KMH, AND D14KMH

DAY	TIME	MODE	LINE	WAVENUMBER	T	P	EXT	CMA	DAE	AAE	AMA
255	1127	R5	P2-8	2631.067	17.52	12.17	.0481	.0310	.0171	.0155	.0326
255	1128	R5	P2-7	2655.863	17.55	12.15	.1078	.0850	.0228	.0167	.0911
255	1131	R5	P2-6	2680.179	17.63	12.07	.0737	.0511	.0226	.0200	.0537
255	1132	R5	P1-9	2691.606	17.66	12.05	.0588	.0408	.0180	.0210	.0378
255	1135	R5	P2-5	2703.999	17.72	12.00	.0437	.0258	.0179	.0238	.0199
255	1137	R5	P1-8	2717.538	17.77	11.96	.1402	.1172	.0230	.0255	.1147
255	1142	R5	P1-7	2742.997	17.88	11.87	.0524	.0303	.0221	.0289	.0235
255	1143	R5	P2-3	2750.094	17.90	11.85	.0684	.0363	.0321	.0295	.0389
255	1147	R5	P1-5	2792.434	18.01	11.83	.0888	.0592	.0296	.0314	.0574
255	1149	R5	P2-8	2631.067	18.08	11.84	.0541	.0302	.0239	.0321	.0220
255	1152	R5	P3-5	2617.386	18.17	11.87	.0558	.0198	.0360	.0329	.0229
255	1154	R5	P2-9	2605.806	18.23	11.89	.0791	.0437	.0354	.0332	.0459
255	1155	R5	P3-6	2594.197	18.26	11.90	.0681	.0266	.0415	.0332	.0349
255	1157	R5	P2-10	2580.096	18.33	11.91	.1052	.0647	.0405	.0333	.0719
255	1158	R5	P3-7	2570.522	18.36	11.92	.0961	.0619	.0342	.0333	.0628
255	1200	R5	P2-11	2553.952	18.42	11.94	.0643	.0340	.0303	.0331	.0312
255	1202	R5	P3-8	2546.375	18.47	12.00	.0851	.0483	.0368	.0328	.0523
255	1204	R5	P2-12	2527.391	18.51	12.07	.0647	.0318	.0329	.0323	.0324
255	1206	R5	P3-9	2521.769	18.56	12.13	.0638	.0338	.0300	.0316	.0322
255	1207	R5	P3-10	2496.721	18.58	12.16	.0782	.0481	.0301	.0312	.0470
255	1209	R5	P2-8	2631.067	18.62	12.23	.0559	.0312	.0247	.0303	.0256
255	1130	R5	*P1-10	2665.219	17.61	12.09	.0600	.0331	.0269	.0189	.0411
255	1139	R5	*P2-4	2727.309	17.81	11.92	.0563	.0479	.0084	.0270	.0293
255	1145	R5	*P1-6	2767.968	17.95	11.81	.0900	.0738	.0162	.0305	.0595
255	1358	R6	P2-8	2631.067	19.43	12.55	.0991	.0319	.0672	.0647	.0344
255	1400	R6	P2-7	2655.863	19.50	12.58	.1537	.0881	.0656	.0639	.0898
255	1403	R6	P2-6	2680.179	19.44	12.56	.1185	.0529	.0656	.0628	.0557
255	1404	R6	P1-9	2691.606	19.42	12.55	.1039	.0419	.0620	.0624	.0415
255	1405	R6	P2-5	2703.999	19.40	12.55	.0855	.0267	.0588	.0621	.0234
255	1407	R6	P1-8	2717.538	19.36	12.53	.1851	.1239	.0612	.0613	.1238
255	1410	R6	P1-9	2691.606	19.30	12.51	.0919	.0418	.0501	.0602	.0317
255	1411	R6	P2-3	2750.094	19.28	12.51	.0979	.0379	.0600	.0598	.0381
255	1415	R6	P1-5	2792.434	19.20	12.48	.1207	.0622	.0585	.0583	.0624
255	1417	R6	P2-8	2631.067	19.16	12.48	.0785	.0317	.0468	.0576	.0209
255	1419	R6	P3-5	2617.386	19.11	12.47	.0787	.0207	.0580	.0568	.0219
255	1420	R6	P2-9	2605.806	19.09	12.47	.1008	.0456	.0552	.0565	.0443
255	1424	R6	P3-6	2594.197	19.00	12.47	.0890	.0277	.0613	.0550	.0340
255	1422	R6	P2-10	2580.096	19.05	12.47	.1295	.0655	.0640	.0557	.0738
255	1424	R6	P3-7	2570.522	19.00	12.47	.1252	.0627	.0625	.0550	.0702
255	1426	R6	P2-11	2553.952	18.96	12.47	.0895	.0347	.0548	.0542	.0353
255	1427	R6	P3-8	2546.375	18.94	12.46	.1107	.0489	.0618	.0539	.0568
255	1429	R6	P2-12	2527.391	18.89	12.46	.0859	.0324	.0535	.0531	.0328
255	1431	R6	P3-9	2521.769	18.86	12.46	.0895	.0342	.0553	.0524	.0371
255	1432	R6	P3-10	2496.721	18.85	12.46	.0953	.0486	.0467	.0520	.0433
255	1434	R6	P2-8	2631.067	18.84	12.46	.0719	.0317	.0402	.0513	.0206
255	1401	R6	*P1-10	2665.219	19.48	12.57	.1061	.0341	.0720	.0636	.0425
255	1409	R6	*P2-4	2727.309	19.32	12.52	.0976	.0502	.0474	.0606	.0370
255	1413	R6	*P1-6	2767.968	19.24	12.49	.1216	.0776	.0440	.0591	.0625
258	1212	R5	P2-8	2631.067	24.79	13.19	.1116	.0334	.0782	.0762	.0354
258	1215	R5	P2-7	2655.863	24.63	13.20	.1666	.0923	.0743	.0762	.0904
258	1218	R5	P2-6	2680.179	24.52	13.21	.1301	.0547	.0754	.0762	.0539
258	1219	R5	P1-9	2691.606	24.49	13.21	.1164	.0428	.0736	.0762	.0402
258	1221	R5	P2-5	2703.999	24.42	13.22	.0945	.0271	.0674	.0762	.0183
258	1222	R5	P1-8	2717.538	24.38	13.22	.2124	.1336	.0788	.0762	.1362
258	1224	R5	P1-7	2742.997	24.31	13.23	.1071	.0314	.0757	.0762	.0309
258	1226	R5	P2-3	2750.094	24.24	13.24	.1198	.0385	.0813	.0762	.0436
258	1228	R5	P1-5	2792.434	24.17	13.24	.1394	.0642	.0752	.0762	.0632
258	1229	R5	P2-8	2631.067	24.14	13.25	.1004	.0335	.0669	.0762	.0242
258	1230	R5	P3-5	2617.386	24.10	13.25	.1015	.0210	.0805	.0762	.0253
258	1232	R5	P2-9	2605.806	24.21	13.23	.1296	.0474	.0822	.0762	.0534
258	1233	R5	P3-6	2594.197	24.26	13.23	.1191	.0287	.0904	.0762	.0429
258	1234	R5	P2-10	2580.096	24.31	13.22	.1493	.0656	.0837	.0762	.0731
258	1236	R5	P3-7	2570.522	24.42	13.20	.1569	.0625	.0943	.0762	.0806
258	1237	R5	P2-11	2553.952	24.47	13.19	.1126	.0344	.0782	.0762	.0364
258	1239	R5	P3-8	2546.375	24.58	13.18	.1374	.0486	.0888	.0762	.0612
258	1240	R5	P2-12	2527.391	24.63	13.17	.0943	.0322	.0621	.0762	.0181
258	1241	R5	P3-9	2521.769	24.69	13.16	.1041	.0340	.0701	.0762	.0279
258	1242	R5	P3-10	2496.721	24.74	13.15	.1175	.0482	.0693	.0762	.0413
258	1244	R5	P2-8	2631.067	24.85	13.14	.0870	.0332	.0538	.0762	.0108
258	1216	R5	*P1-10	2665.219	24.59	13.20	.1206	.0348	.0858	.0762	.0444
258	1223	R5	*P2-4	2727.309	24.35	13.23	.1143	.0526	.0617	.0762	.0381
258	1227	R5	*P1-6	2767.968	24.21	13.24	.1396	.0803	.0593	.0762	.0634

* DENOTES LINES WHICH WERE EXCLUDED FROM THE CURVE FIT.

Table continues.

Table 2 — (Continued)

NRL DF LASER EXTINCTION MEASUREMENTS CAPISTRANO, 1975
DATA FILE: CREATED BY D10KMH: INTENDED FOR D08KMH, D11KMH, AND D14KMH

DAY	TIME	MODE	LINE	WAVENUMBER	T	P	EXT	CMA	DAE	AAE	AMA
259	1507	A5	P2-A	2631.067	30.50	11.20	.0422	.0285	.0137	.0095	.0327
259	1509	A5	P2-7	2655.863	30.49	11.10	.0882	.0766	.0116	.0129	.0753
259	1511	A5	P2-6	2680.179	30.48	10.99	.0631	.0441	.0190	.0161	.0470
259	1512	A5	P1-9	2691.606	30.48	10.94	.0528	.0356	.0172	.0175	.0353
259	1513	A5	P2-5	2703.999	30.47	10.89	.0416	.0209	.0207	.0189	.0227
259	1516	A5	P1-8	2717.538	30.49	10.77	.1260	.1096	.0164	.0226	.1034
259	1518	A5	P1-7	2742.997	30.56	10.76	.0445	.0235	.0210	.0248	.0197
259	1520	A5	P2-3	2750.094	30.63	10.74	.0554	.0293	.0261	.0266	.0288
259	1523	A5	P1-5	2762.434	30.74	10.72	.0722	.0497	.0225	.0288	.0434
259	1524	A5	P2-A	2631.067	30.77	10.71	.0522	.0274	.0248	.0293	.0229
259	1525	A5	P3-5	2617.386	30.81	10.71	.0489	.0163	.0326	.0298	.0191
259	1527	A5	P2-9	2605.806	30.88	10.69	.0649	.0381	.0268	.0306	.0343
259	1528	A5	P3-6	2594.197	30.91	10.68	.0584	.0276	.0348	.0309	.0275
259	1530	A5	P2-10	2580.096	30.98	10.67	.0994	.0609	.0385	.0313	.0681
259	1531	A5	P3-7	2570.522	30.99	10.66	.0944	.0573	.0371	.0313	.0631
259	1533	A5	P2-11	2553.952	31.00	10.65	.0600	.0298	.0302	.0312	.0288
259	1535	A5	P3-8	2546.375	31.01	10.63	.0791	.0438	.0353	.0308	.0483
259	1538	A5	P2-12	2527.391	31.02	10.61	.0560	.0272	.0288	.0297	.0263
259	1540	A5	P3-9	2521.769	31.03	10.59	.0613	.0289	.0324	.0286	.0327
259	1542	A5	P3-10	2496.721	31.04	10.57	.0670	.0423	.0247	.0271	.0399
259	1543	A5	P2-8	2631.067	31.05	10.57	.0475	.0270	.0205	.0263	.0212
259	1510	A5	*P1-10	2665.219	30.49	11.04	.0577	.0282	.0295	.0145	.0432
259	1517	A5	*P2-4	2727.309	30.53	10.77	.0540	.0417	.0123	.0237	.0303
259	1521	A5	*P1-6	2767.968	30.67	10.74	.0690	.0635	.0055	.0274	.0416
260	1338	A6	P2-A	2631.067	29.14	12.89	.0500	.0326	.0174	.0134	.0366
260	1339	A6	P2-7	2655.863	29.13	12.91	.1009	.0898	.0111	.0152	.0857
260	1342	A6	P2-6	2680.179	29.10	12.96	.0853	.0527	.0326	.0201	.0652
260	1343	A6	P1-9	2691.606	29.09	12.98	.0639	.0412	.0227	.0216	.0423
260	1344	A6	P2-5	2703.999	29.08	13.00	.0478	.0255	.0223	.0230	.0248
260	1346	A6	P1-8	2717.538	29.06	13.02	.1500	.1337	.0163	.0256	.1244
260	1349	A6	P1-7	2742.997	29.02	13.04	.0525	.0291	.0234	.0291	.0234
260	1351	A6	P2-3	2750.094	29.00	13.05	.0690	.0363	.0327	.0311	.0379
260	1355	A6	P1-5	2762.434	28.95	13.07	.0854	.0615	.0239	.0342	.0512
260	1359	A6	P2-A	2631.067	28.90	13.09	.0568	.0331	.0237	.0362	.0206
260	1400	A6	P3-5	2617.386	28.89	13.09	.0587	.0200	.0387	.0365	.0222
260	1402	A6	P2-9	2605.806	28.88	13.11	.0811	.0463	.0348	.0369	.0442
260	1403	A6	P3-6	2594.197	28.87	13.12	.0761	.0281	.0480	.0371	.0390
260	1404	A6	P2-10	2580.096	28.86	13.13	.1096	.0645	.0451	.0371	.0725
260	1406	A6	P3-7	2570.522	28.85	13.15	.1092	.0613	.0479	.0370	.0722
260	1407	A6	P2-11	2553.952	28.84	13.16	.0667	.0333	.0334	.0369	.0298
260	1409	A6	P3-8	2546.375	28.83	13.17	.0871	.0475	.0396	.0363	.0508
260	1410	A6	P2-12	2527.391	28.82	13.18	.0775	.0312	.0463	.0360	.0415
260	1412	A6	P3-9	2521.769	28.81	13.20	.0744	.0330	.0414	.0351	.0393
260	1413	A6	P3-10	2496.721	28.80	13.21	.0754	.0471	.0283	.0345	.0409
260	1414	A6	P2-8	2631.067	28.80	13.22	.0504	.0334	.0170	.0338	.0166
260	1341	A6	*P1-10	2665.219	29.11	12.95	.0656	.0332	.0324	.0185	.0471
260	1348	A6	*P2-4	2727.309	29.03	13.03	.0603	.0512	.0051	.0280	.0323
260	1354	A6	*P1-6	2767.968	28.96	13.06	.0978	.0775	.0203	.0335	.0643
260	1440	A7	P2-A	2631.067	28.99	13.19	.0560	.0333	.0227	.0220	.0340
260	1440	A7	P2-7	2655.863	28.99	13.19	.1115	.0919	.0196	.0220	.0895
260	1441	A7	P2-7	2655.863	29.01	13.18	.1115	.0918	.0197	.0226	.0889
260	1444	A7	P2-6	2680.179	29.05	13.17	.0877	.0536	.0341	.0244	.0633
260	1447	A7	P1-9	2691.606	29.08	13.13	.0658	.0416	.0242	.0262	.0396
260	1450	A7	P1-8	2717.538	29.09	13.06	.1543	.1341	.0202	.0280	.1263
260	1453	A7	P2-8	2631.067	29.11	12.99	.0596	.0328	.0268	.0298	.0298
260	1456	A7	P2-9	2605.806	29.12	12.93	.0863	.0457	.0406	.0316	.0547
260	1459	A7	P3-7	2570.522	29.14	12.86	.0967	.0608	.0359	.0334	.0633
260	1502	A7	P3-8	2546.375	29.21	12.79	.0848	.0469	.0379	.0352	.0496
260	1505	A7	P2-8	2631.067	29.32	12.72	.0631	.0322	.0309	.0370	.0261

* DENOTES LINES WHICH WERE EXCLUDED FROM THE CURVE FIT.

Table continues.

Table 2 (Concluded)

NRL OF LASER EXTINCTION MEASUREMENTS CAPISTRANO, 1975
DATA FILE: CREATED BY D10KMHI INTENDED FOR D08KMH, D11KMH, AND D14KMH

DAY	TIME	MODE	LINE	WAVENUMBER	T	P	EXT	CMA	DAE	AAE	AMA
261	1043	AS	P2-8	2631.067	26.31	13.62	.0702	.0344	.0358	.0272	.0430
261	1049	AS	P2-7	2655.863	26.20	13.63	.1180	.0954	.0226	.0272	.0908
261	1053	AS	P2-6	2680.179	26.03	13.61	.0901	.0561	.0340	.0272	.0629
261	1054	AS	P1-9	2691.606	25.99	13.60	.0777	.0436	.0341	.0272	.0505
261	1055	AS	P2-5	2703.999	25.95	13.59	.0589	.0275	.0314	.0272	.0317
261	1057	AS	P1-8	2717.538	25.87	13.58	.1568	.1381	.0187	.0272	.1296
261	1111	AS	P1-7	2742.997	25.73	13.23	.0451	.0309	.0142	.0272	.0179
261	1111	AS	P2-3	2750.094	25.73	13.23	.0634	.0379	.0255	.0272	.0362
261	1113	AS	P1-5	2762.474	25.72	13.17	.0782	.0633	.0149	.0272	.0510
261	1114	AS	P2-8	2631.067	25.72	13.14	.0456	.0332	.0124	.0272	.0184
261	1116	AS	P3-5	2617.386	25.73	13.09	.0441	.0205	.0236	.0272	.0169
261	1118	AS	P2-9	2605.806	25.76	13.04	.0794	.0466	.0328	.0272	.0522
261	1120	AS	P3-6	2594.197	25.78	13.00	.0656	.0282	.0374	.0272	.0384
261	1121	AS	P2-10	2580.096	25.79	12.97	.1027	.0649	.0378	.0272	.0755
261	1122	AS	P3-7	2570.522	25.80	12.95	.0891	.0618	.0273	.0272	.0619
261	1123	AS	P2-11	2553.952	25.82	12.93	.0598	.0337	.0261	.0272	.0326
261	1125	AS	P3-8	2546.375	25.84	12.88	.0783	.0479	.0304	.0272	.0511
261	1126	AS	P2-12	2527.391	25.85	12.86	.0583	.0314	.0269	.0272	.0311
261	1128	AS	P3-9	2521.769	25.88	12.82	.0702	.0332	.0370	.0272	.0430
261	1129	AS	P3-10	2496.721	25.89	12.79	.0796	.0472	.0324	.0272	.0524
261	1131	AS	P2-8	2631.067	25.93	12.75	.0491	.0323	.0168	.0272	.0219
261	1051	AS	*P1-10	2665.219	26.12	13.62	.0745	.0356	.0389	.0272	.0473
261	1059	AS	*P2-4	2727.309	25.78	13.57	.0789	.0538	.0251	.0272	.0517
261	1112	AS	*P1-6	2767.968	25.72	13.20	.0825	.0795	.0030	.0272	.0553
262	1101	AS	P2-8	2631.067	24.94	11.68	.0740	.0297	.0443	.0419	.0321
262	1102	AS	P2-7	2655.863	24.96	11.66	.1298	.0810	.0488	.0427	.0871
262	1109	AS	P2-6	2680.179	25.08	11.55	.0956	.0474	.0482	.0469	.0487
262	1111	AS	P1-9	2691.606	25.14	11.49	.0861	.0379	.0482	.0487	.0374
262	1112	AS	P2-5	2703.999	25.16	11.47	.0738	.0231	.0507	.0493	.0245
262	1114	AS	P1-8	2717.538	25.20	11.43	.1629	.1147	.0482	.0505	.1124
262	1118	AS	P1-7	2742.997	25.42	11.46	.0664	.0267	.0397	.0525	.0139
262	1120	AS	P2-3	2750.094	25.55	11.49	.0926	.0329	.0597	.0534	.0392
262	1126	AS	P1-5	2762.474	25.95	11.59	.1036	.0554	.0482	.0558	.0478
262	1128	AS	P2-8	2631.067	26.09	11.63	.0731	.0296	.0435	.0565	.0166
262	1136	AS	P3-5	2617.386	26.00	12.06	.0776	.0189	.0587	.0584	.0192
262	1139	AS	P2-9	2605.806	25.88	12.25	.1115	.0439	.0676	.0588	.0527
262	1149	AS	P3-6	2594.197	25.66	12.65	.0927	.0275	.0652	.0592	.0335
262	1151	AS	P2-10	2580.096	25.66	12.65	.1299	.0645	.0654	.0590	.0709
262	1152	AS	P3-7	2570.522	25.66	12.65	.1254	.0613	.0641	.0590	.0664
262	1154	AS	P2-11	2553.952	25.66	12.65	.0882	.0334	.0548	.0587	.0295
262	1156	AS	P3-8	2546.375	25.66	12.65	.1169	.0476	.0693	.0584	.0585
262	1159	AS	P2-12	2527.391	25.66	12.65	.0934	.0312	.0622	.0578	.0356
262	1201	AS	P3-9	2521.769	25.66	12.65	.0830	.0330	.0500	.0574	.0256
262	1203	AS	P3-10	2496.721	25.66	12.65	.1015	.0470	.0545	.0568	.0447
262	1207	AS	P2-8	2631.067	25.66	12.65	.0781	.0321	.0460	.0555	.0226
262	1106	AS	*P1-10	2665.219	25.04	11.58	.0869	.0304	.0565	.0455	.0414
262	1115	AS	*P2-4	2727.309	25.22	11.41	.0863	.0449	.0414	.0510	.0353
262	1121	AS	*P1-6	2767.968	25.62	11.51	.1110	.0695	.0415	.0539	.0571

* DENOTES LINES WHICH WERE EXCLUDED FROM THE CURVE FIT.

Table 3 — Coefficients for the Molecular Absorption Algorithm
(CMA = A0+A1*T+A2*PH20+A3*T*PH20+A4*PH20*PH20+A5*T*PH20*PH20)

DF LINE	A0	A1	A2	A3	A4	A5
$P_3$10	2.780E-02	-1.594E-05	2.102E-03	-7.438E-06	3.014E-05	-2.852E-07
$P_3$9	1.552E-02	-9.069E-07	1.862E-03	-7.376E-06	2.460E-05	-2.148E-07
$P_2$12	1.390E-02	-2.444E-06	1.848E-03	7.699E-06	2.298E-05	-1.901E-07
$P_3$8	3.012E-02	2.889E-05	2.094E-03	-1.384E-05	8.605E-06	8.232E-08
$P_2$11	1.678E-02	2.862E-05	1.992E-03	1.323E-05	9.179E-06	6.249E-08
$P_3$7	4.172E-02	5.021E-05	2.475E-03	-1.966E-05	6.723E-06	3.918E-07
$P_2$10	4.704E-02	1.879E-05	1.886E-03	9.963E-06	1.094E-05	1.358E-08
$P_3$6	7.406E-03	-3.380E-05	1.445E-03	4.047E-06	3.073E-05	-3.543E-07
$P_2$9	4.978E-03	-7.649E-06	3.500E-03	-5.028E-06	1.397E-05	-5.240E-08
$P_3$5	2.203E-03	4.115E-06	1.707E-03	-5.656E-06	2.009E-05	-1.505E-07
$P_2$8	6.353E-03	-6.577E-05	1.627E-03	1.096E-05	3.620E-05	-5.064E-07
$P_2$7	2.822E-03	-4.498E-05	6.321E-03	5.121E-06	5.253E-05	-3.650E-07
$P_1$10	1.965E-03	-1.805E-06	2.722E-03	-5.121E-06	3.052E-05	-2.363E-07
$P_2$6	1.619E-04	2.168E-06	4.358E-03	-6.776E-06	3.576E-05	-1.948E-07
$P_1$9	8.718E-03	-1.558E-05	2.670E-03	-1.725E-06	4.235E-05	-4.276E-07
$P_2$5	1.176E-04	-1.961E-06	2.393E-03	-6.411E-06	3.072E-05	-2.610E-07
$P_1$8	1.459E-02	-2.934E-04	5.935E-03	6.229E-05	1.147E-04	-1.493E-06
$P_2$4	3.074E-03	-5.804E-05	3.482E-03	6.176E-06	5.183E-05	-5.574E-07
$P_1$7	2.337E-03	-7.795E-06	3.131E-03	-1.457E-05	2.394E-05	-1.012E-07
$P_2$3	1.156E-04	1.903E.05	3.566E-03	-1.324E-05	3.449E-05	-2.311E-07
$P_1$6	3.954E-03	2.244E-05	6.354E-03	-1.487E-05	4.787E-05	-2.226E-07
$P_1$5	1.076E-03	7.367E-06	5.321E-03	-1.224E-05	5.032E-05	-3.352E-07

3.5 Aerosol Extinction and Meteorological Measurements

The derived aerosol extinction (DAE) values corresponding to each long-path optical measurement obtained by processing the data with programs D09KMH and D10KMH and which are tabulated in Table 2 are plotted in Figs. 16 through 29 together with plots of supporting meteorological data. The solid squares shown in Figs. 16a, 17a, etc. are DAE values for the $P_2 8$ laser line, and the open squares correspond to values for the remaining DF laser lines measured in the sequence described in Section 2.4. The legend at the upper right of Fig. 16a applies to the symbols and curves shown in Figs. 16a, 17a, etc. Included in the plots Figs. 16 through 29 are 15-min averages of aerosol particle distributions as measured by the NRL meteorology van, graphed once per hour on the hour during the optical extinction measurement times. These figures contain records of additional aerosol data plus other meteorological parameters recorded throughout the entire day during which the optical data were taken: particle counts for each of the four PMS spectrometer ranges, wind speed and direction, effective aerosol cross-sectional area calculated for each of the four PMS ranges, partial pressure of water vapor, relative humidity, air temperature, barometric pressure, CO_2 concentration, and solar radiation. The water-vapor concentration and relative humidity shown are calculated from the measured values of dew point. The discontinuities in the smooth records of the meteorological data are due to meteorological sensor and data acquisition system adjustments (usually performed when optical data were not being taken).

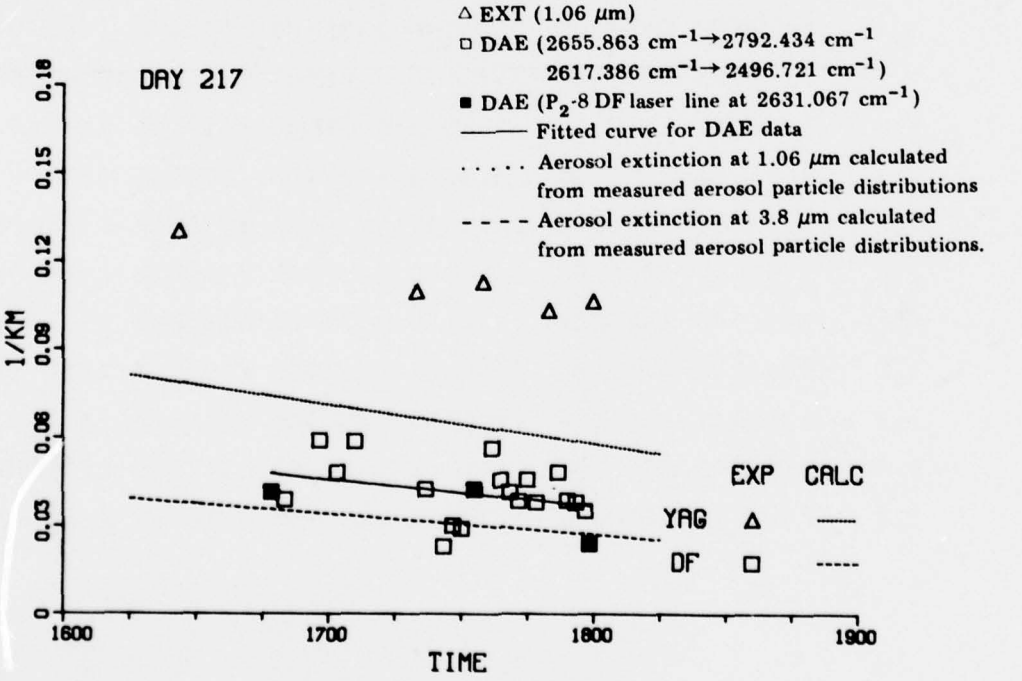

Fig. 16a — Aerosol extinction vs time

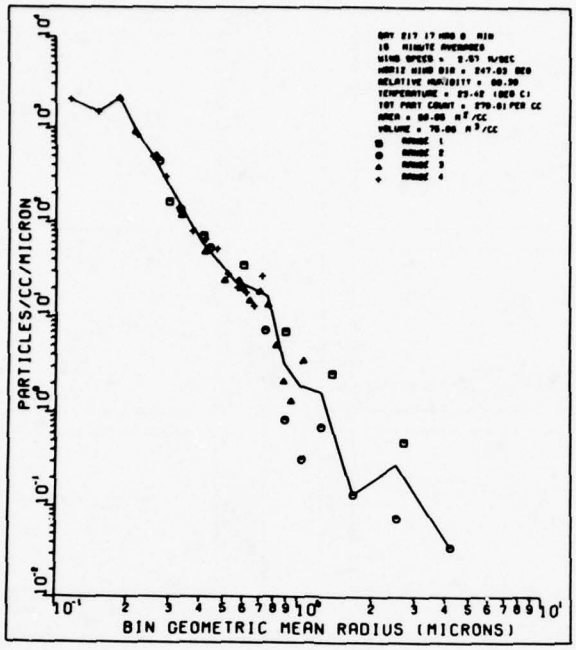

Fig. 16b — Particle distribution during optical extinction measurements

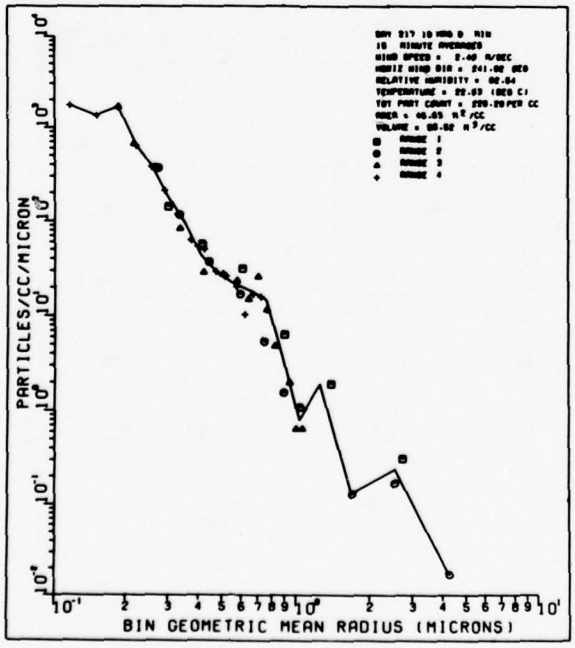

Fig. 16c — Particle distribution

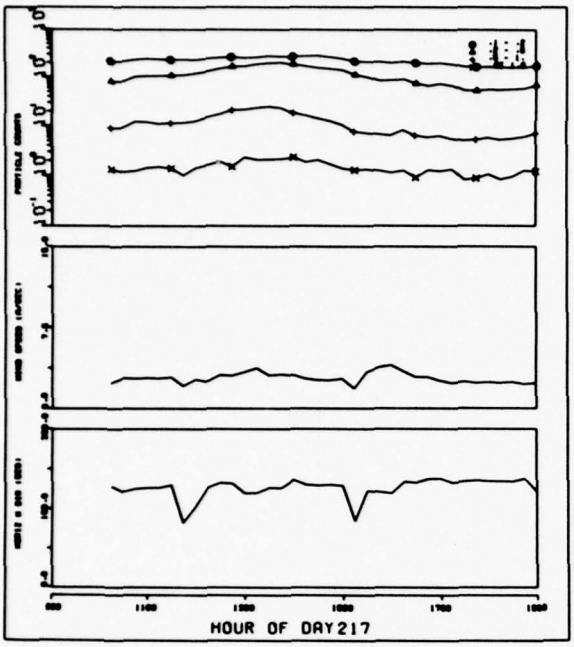

Fig. 16d — Particle counts, wind speed, and horizontal wind direction vs time

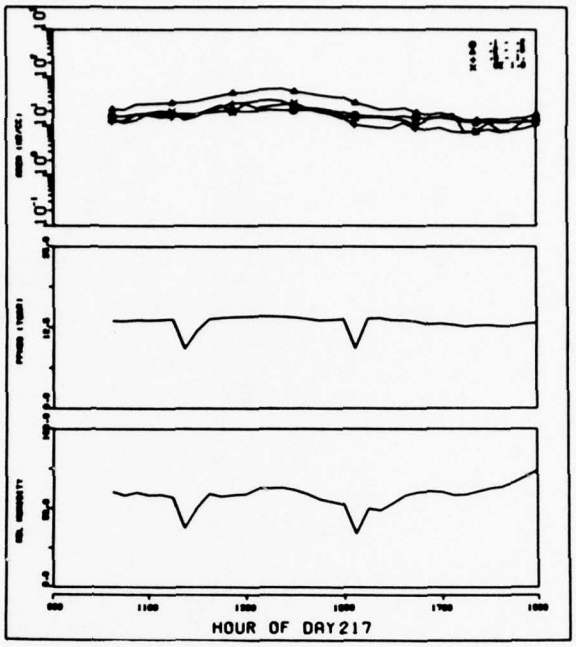

Fig. 16e — Area, water-vapor pressure, and relative humidity vs time

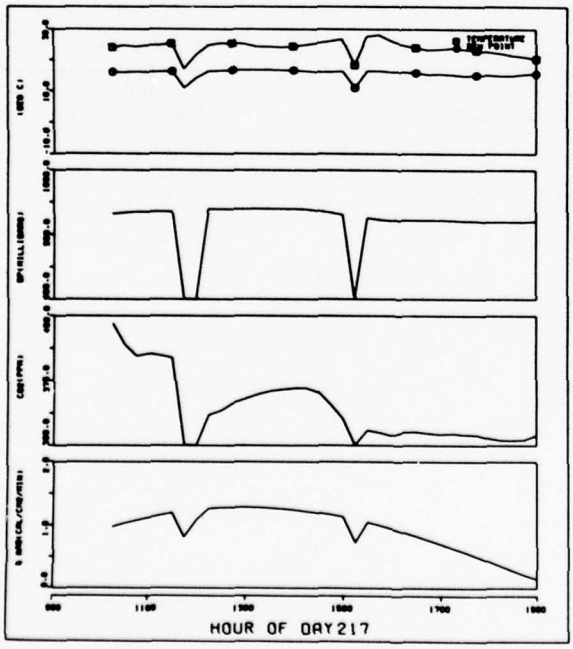

Fig. 16f — Air temperature, barometric pressure, CO_2 concentration, and solar radiation vs time

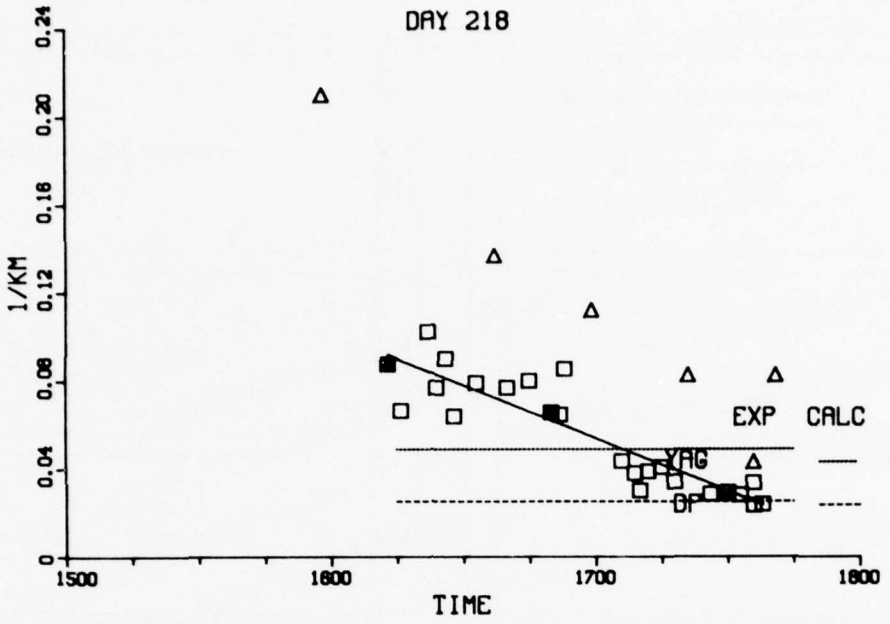

Fig. 17a — Aerosol extinction vs time

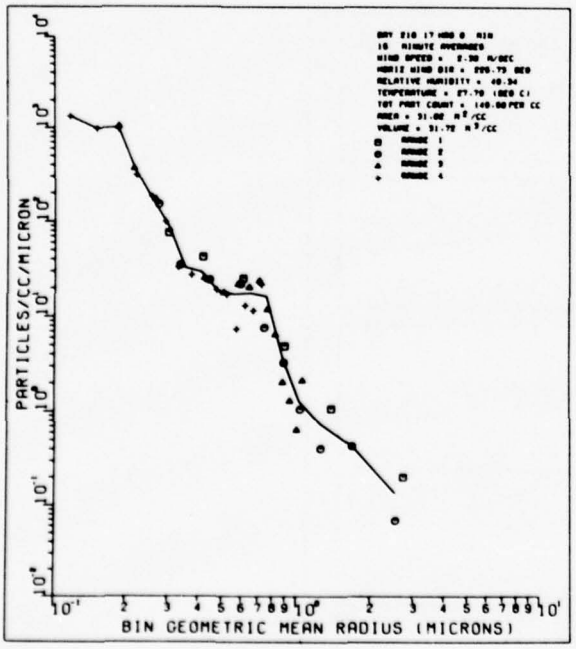

Fig. 17b — Particle distribution

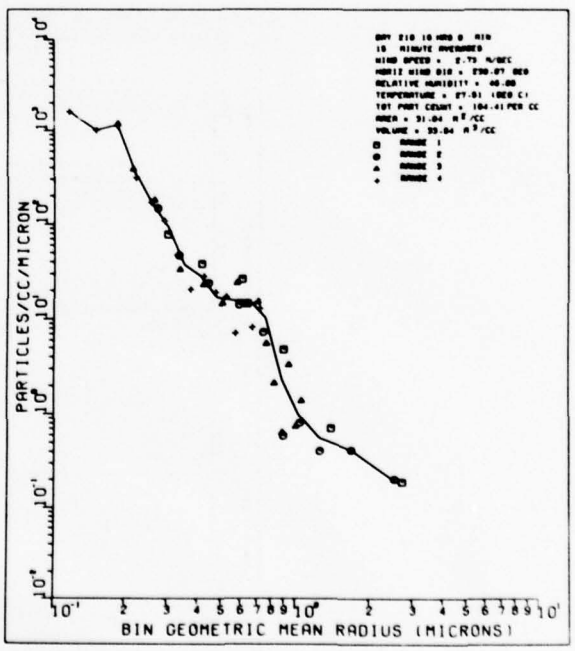

Fig. 17c — Particle distribution

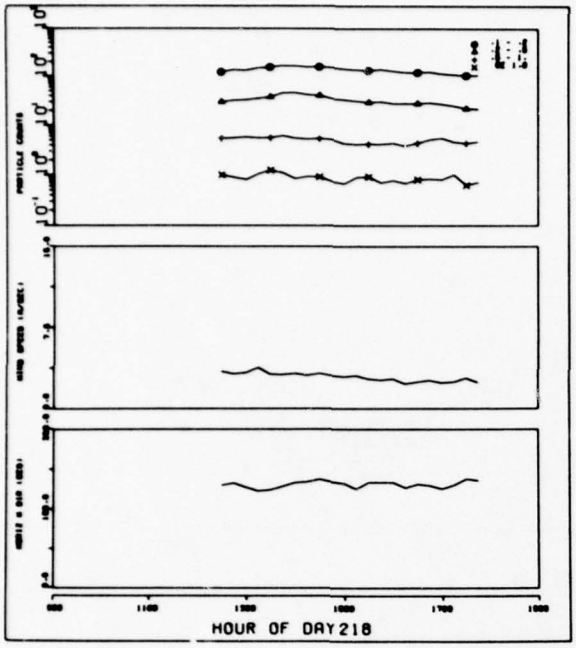

Fig. 17d — Particle counts, wind speed, and horizontal wind direction vs time

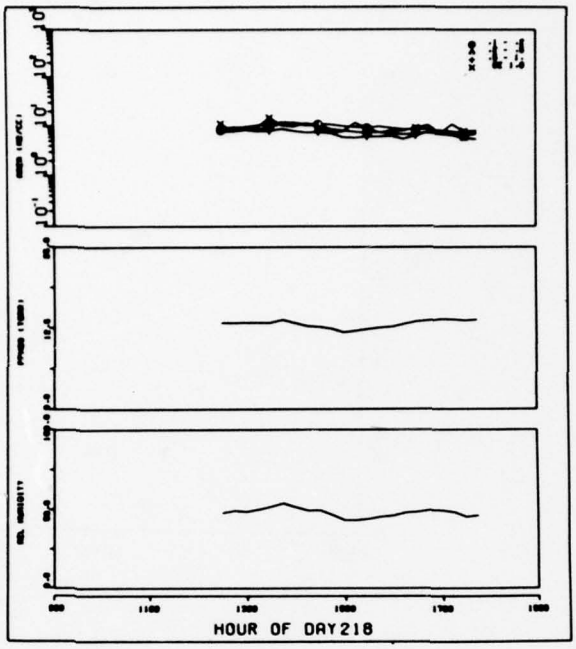

Fig. 17e — Area, water-vapor pressure, and relative humidity vs time

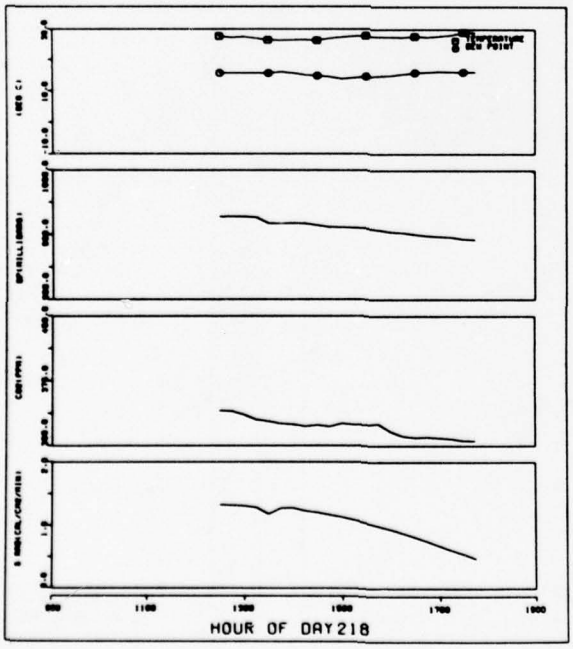

Fig. 17f — Air temperature, barometric pressure, CO_2 concentration, and solar radiation vs time

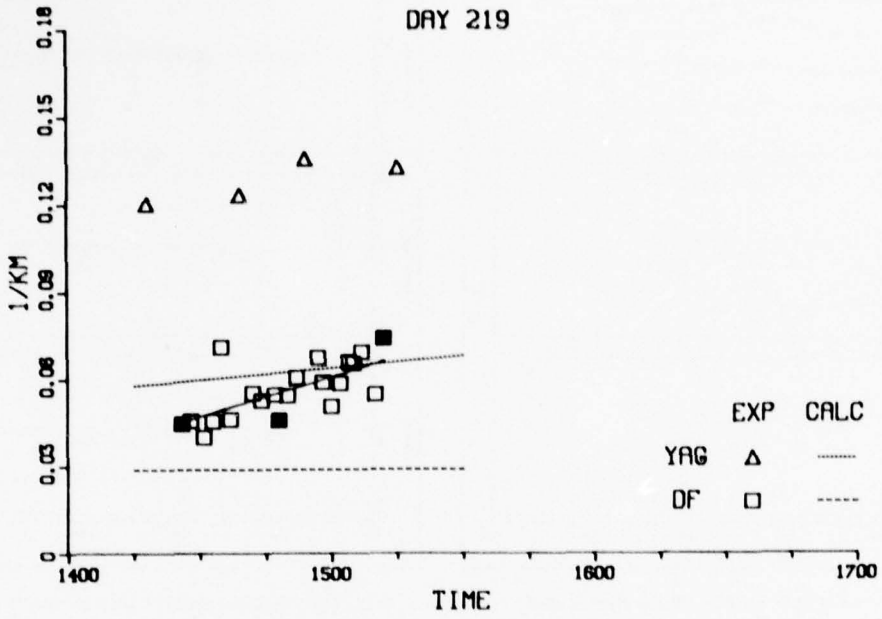

Fig. 18a — Aerosol extinction vs time

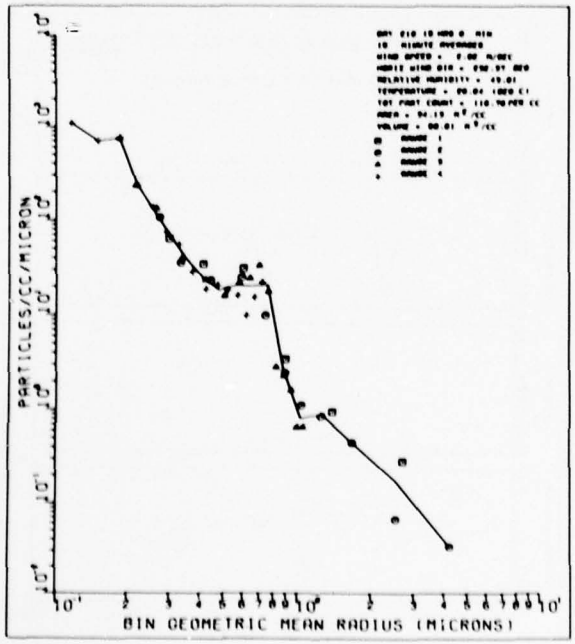

Fig. 18b — Particle distribution

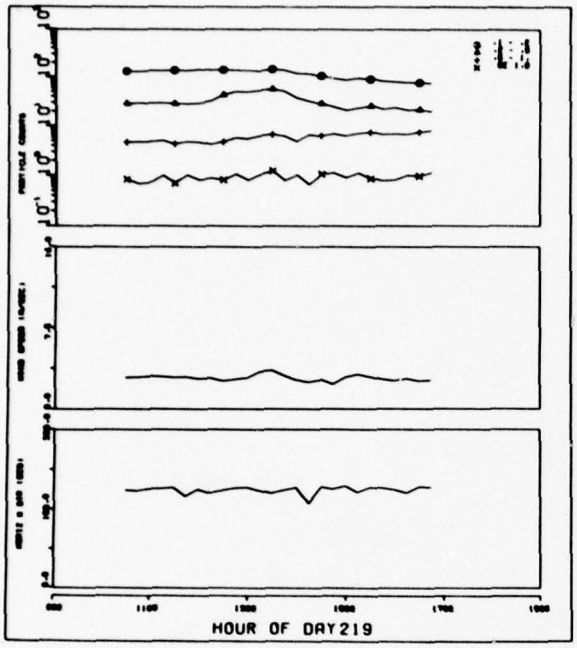

Fig. 18c — Particle counts, wind speed, and horizontal wind direction vs time

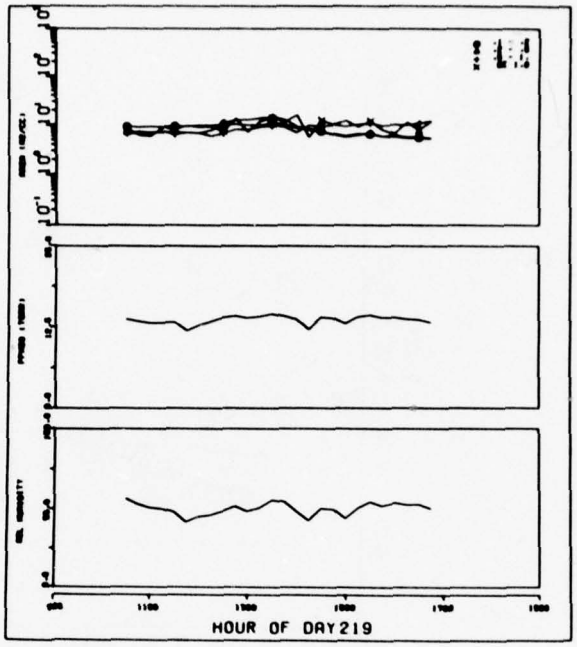

Fig. 18d — Area, water-vapor pressure, and relative humidity vs time

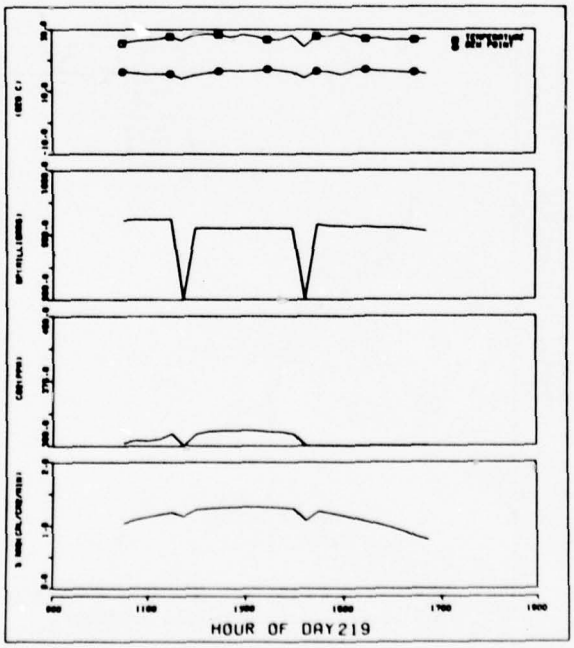

Fig. 18e — Air temperature, barometric pressure, CO_2 concentration, and solar radiation vs time

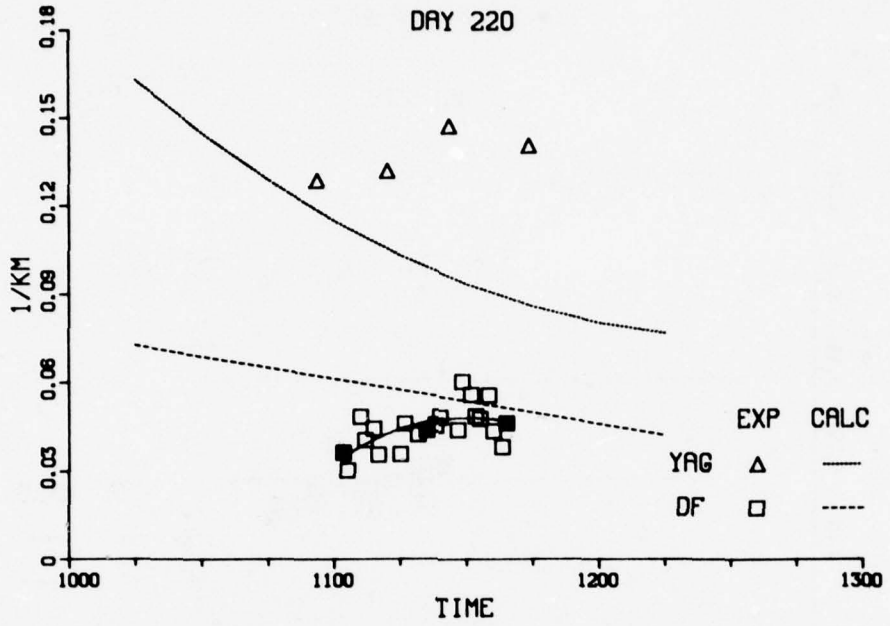

Fig. 19a — Aerosol extinction vs time

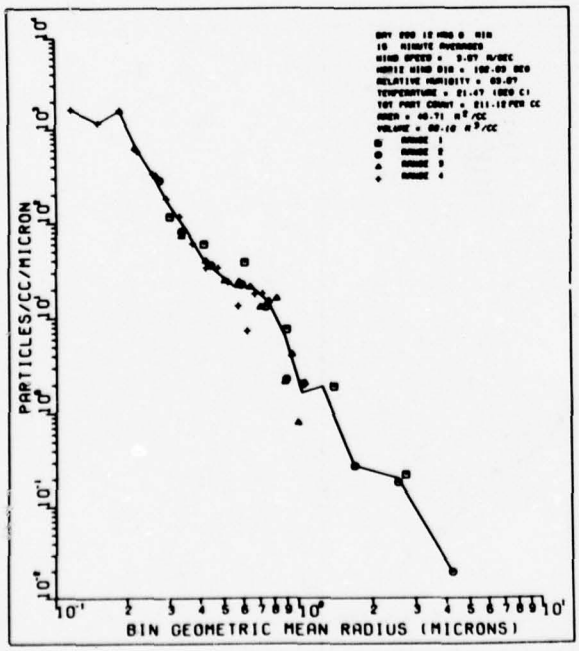

Fig. 19b — Paritcle distribution

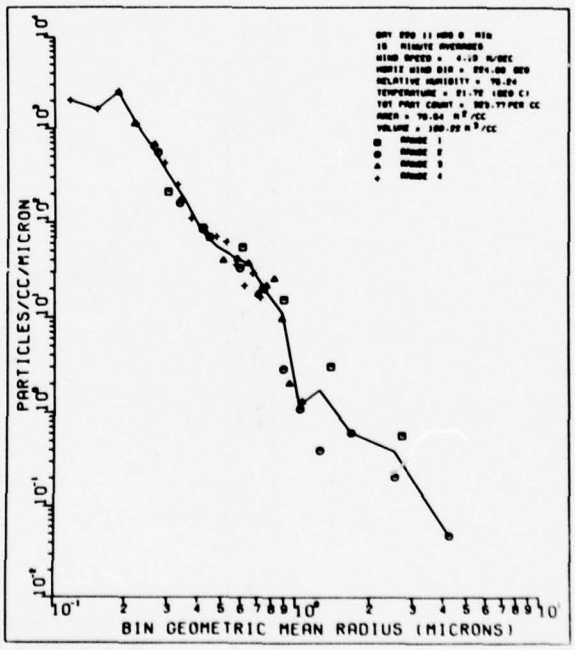

Fig. 19c — Particle distribution

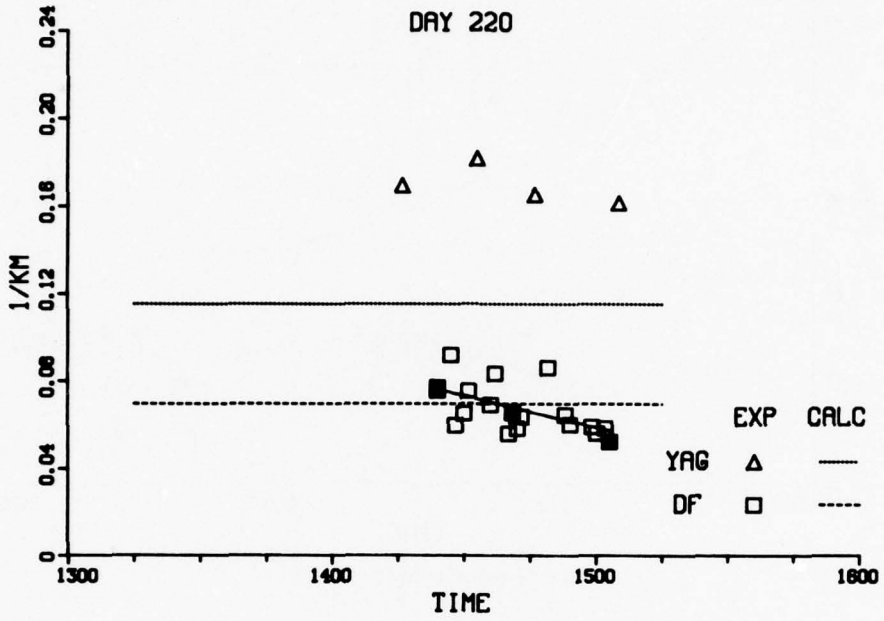

Fig. 19d — Aerosol extinction vs time

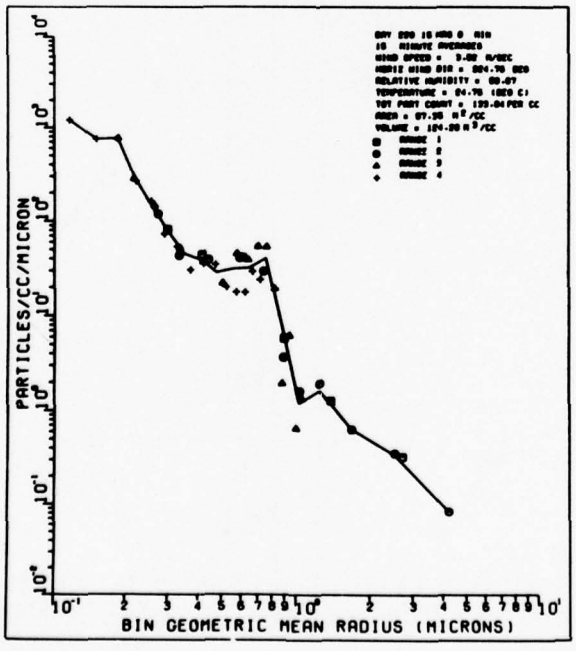

Fig. 19e — Particle distribution

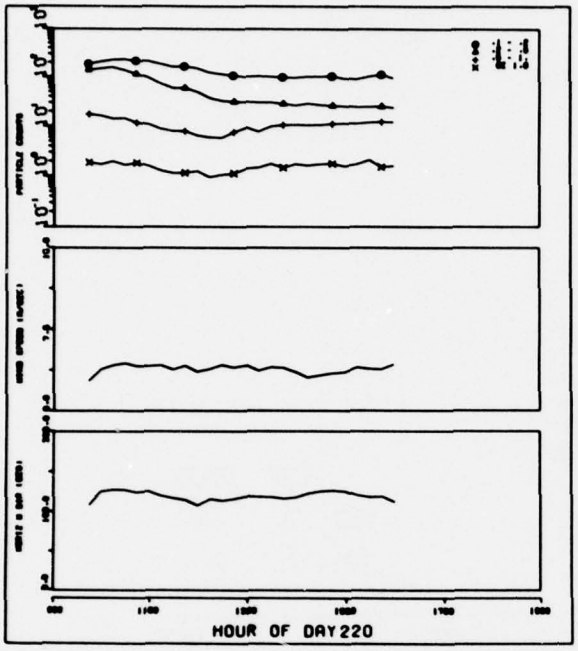

Fig. 19f — Particle counts, wind speed, and horizontal wind direction vs time

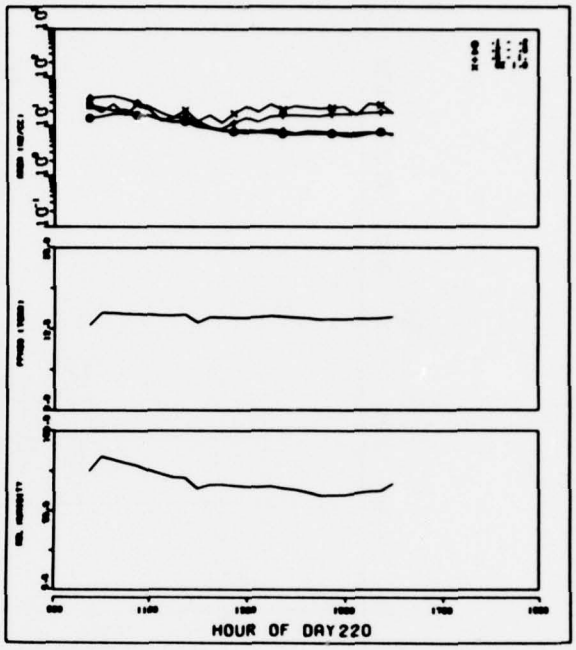

Fig. 19g — Area, water-vapor pressure, and relative humidity vs time

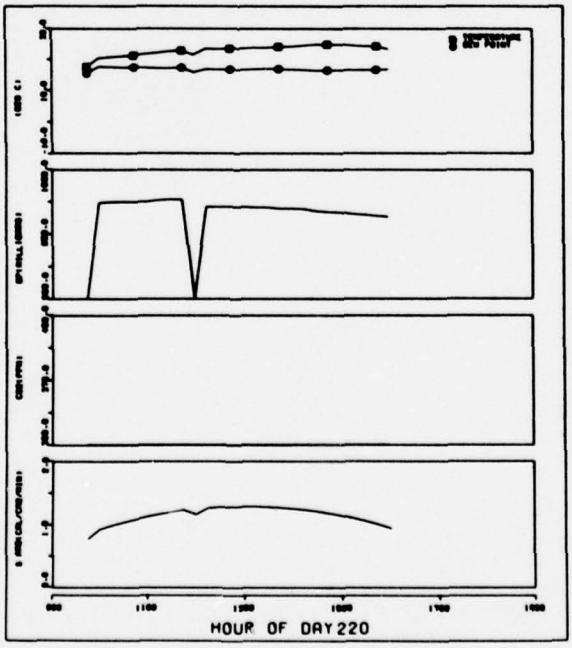

Fig. 19h - Air temperature, barometric pressure, CO_2 concentration, and solar radiation vs time

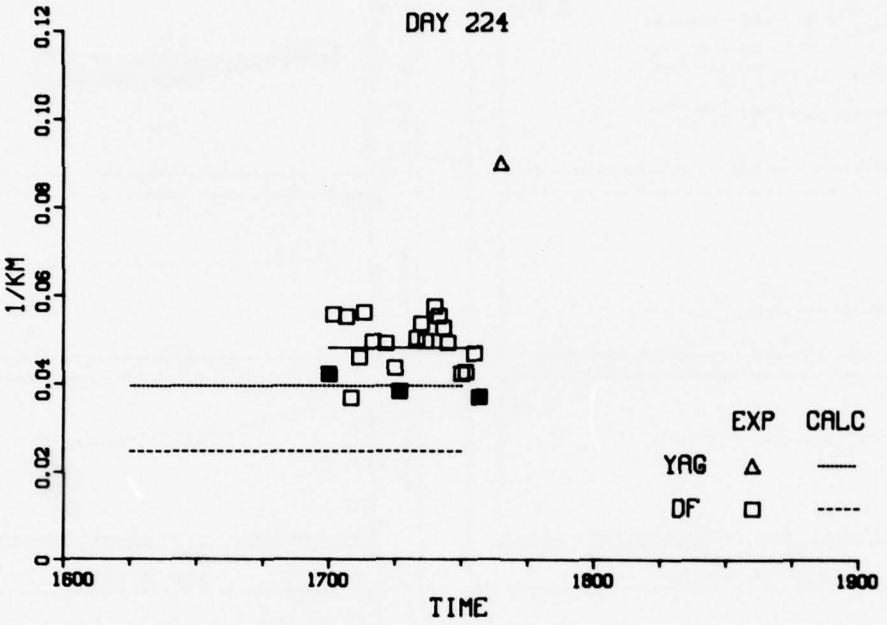

Fig. 20a — Aerosol extinction vs time

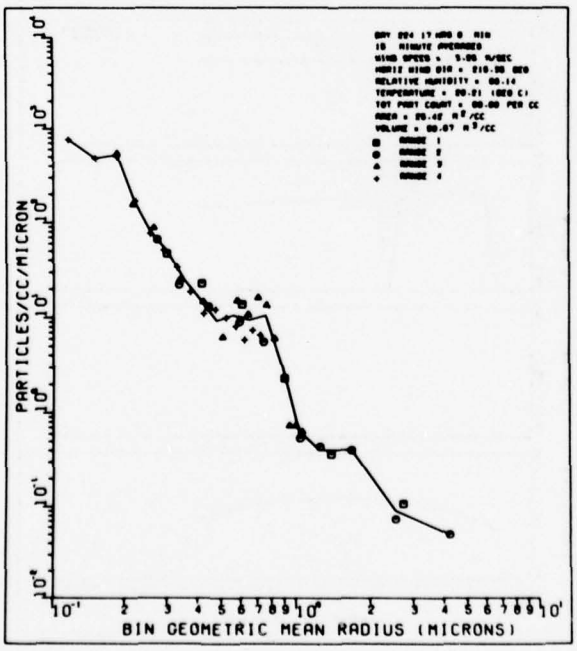

Fig. 20b — Particle distribution

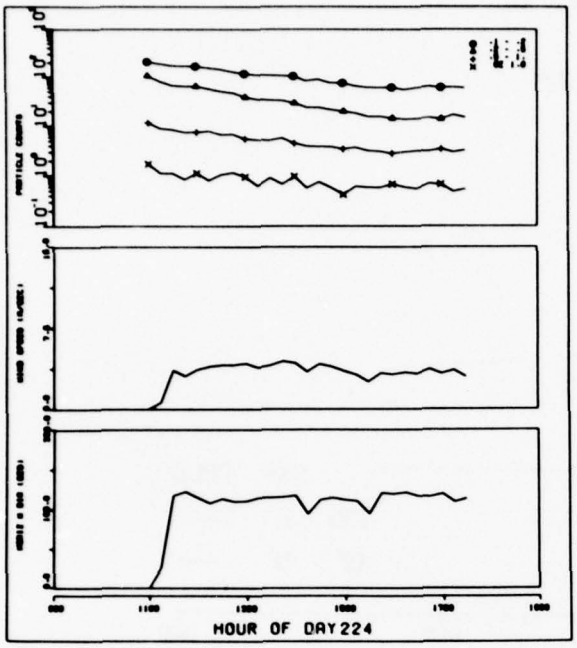

Fig. 20c — Particle counts, wind speed, and horizontal wind direction vs time

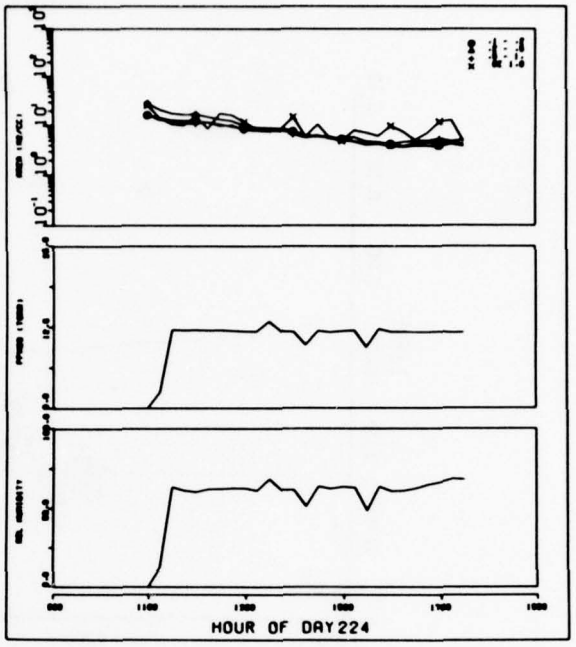

Fig. 20d — Area, water-vapor pressure, and relative humidity vs time

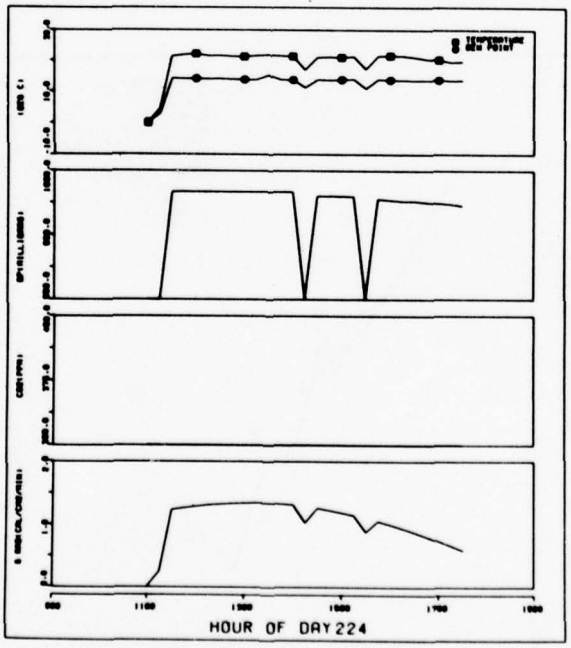

Fig. 20e — Air temperature, barometric pressure, CO_2 concentration, and solar radiation vs time

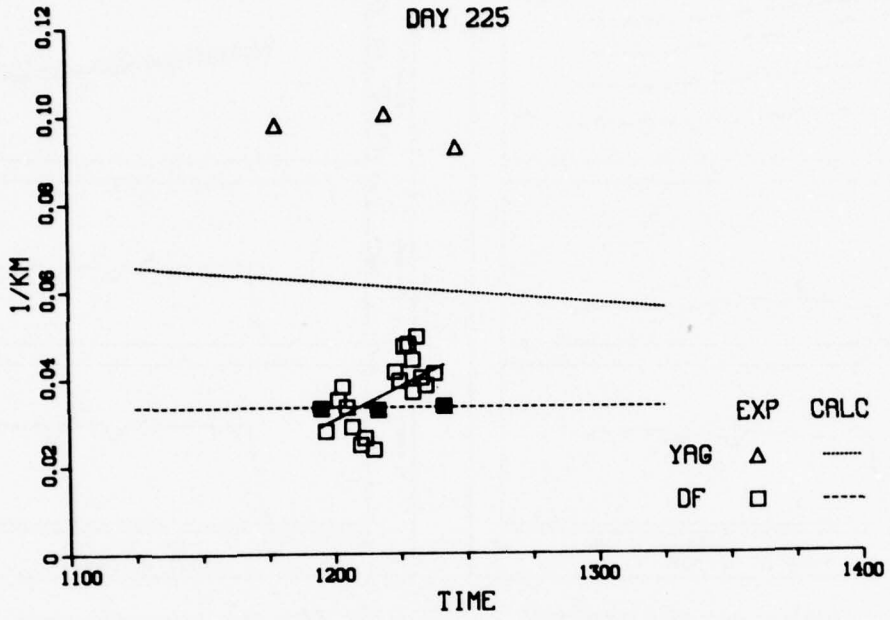

Fig. 21a — Aerosol extinction vs time

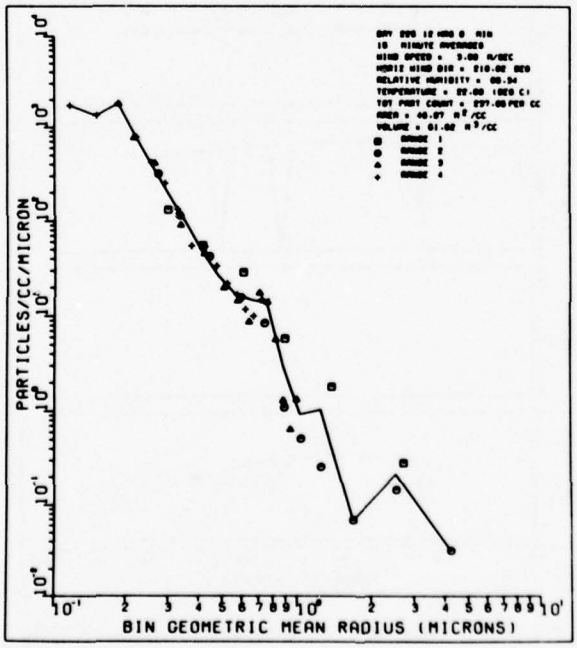

Fig. 21b — Particle distribution

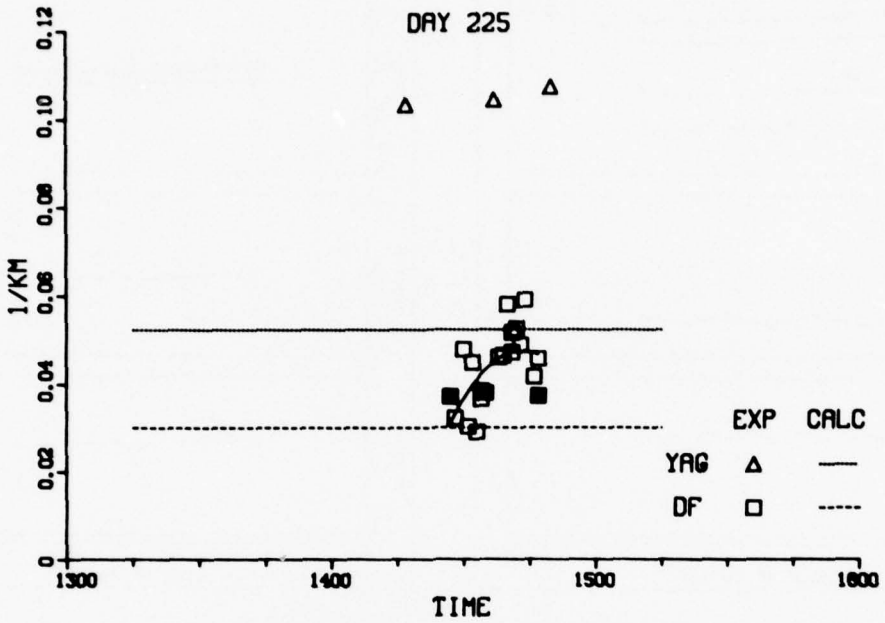

Fig. 21c — Aerosol extinction vs time

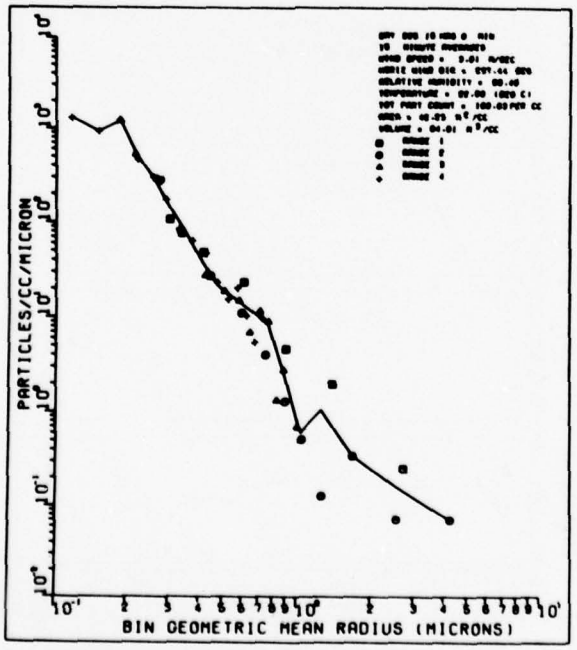

Fig. 21d — Particle distribution

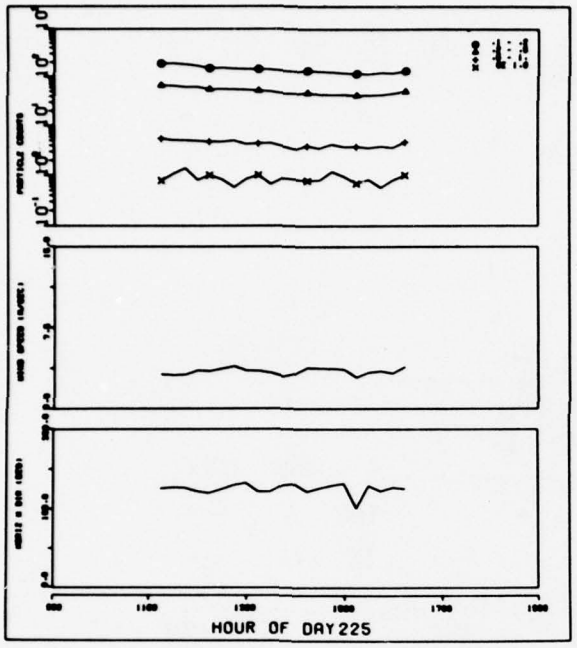

Fig. 21e — Particle counts, wind speed, and horizontal wind direction vs time

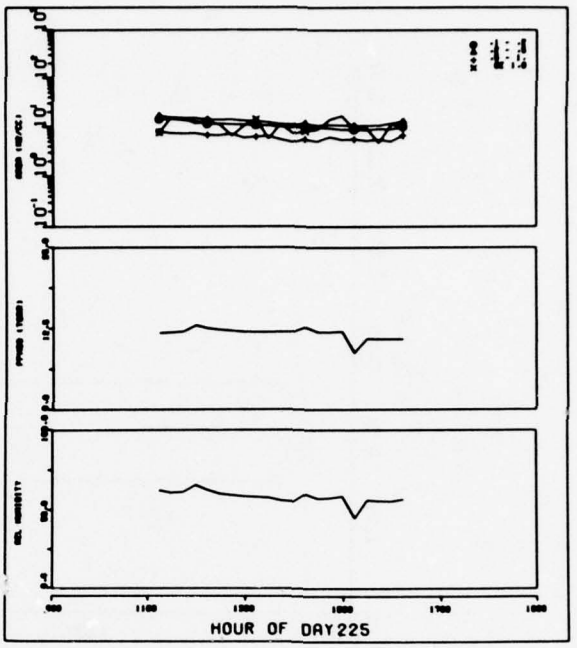

Fig. 21f — Area, water-vapor pressure, and relative humidity vs time

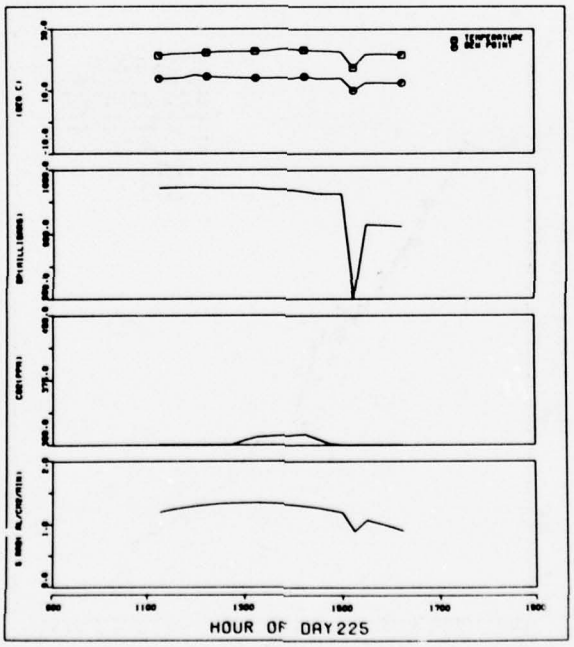

Fig. 21g — Air temperature, barometric pressure, CO_2 concentration, and solar radiation vs time

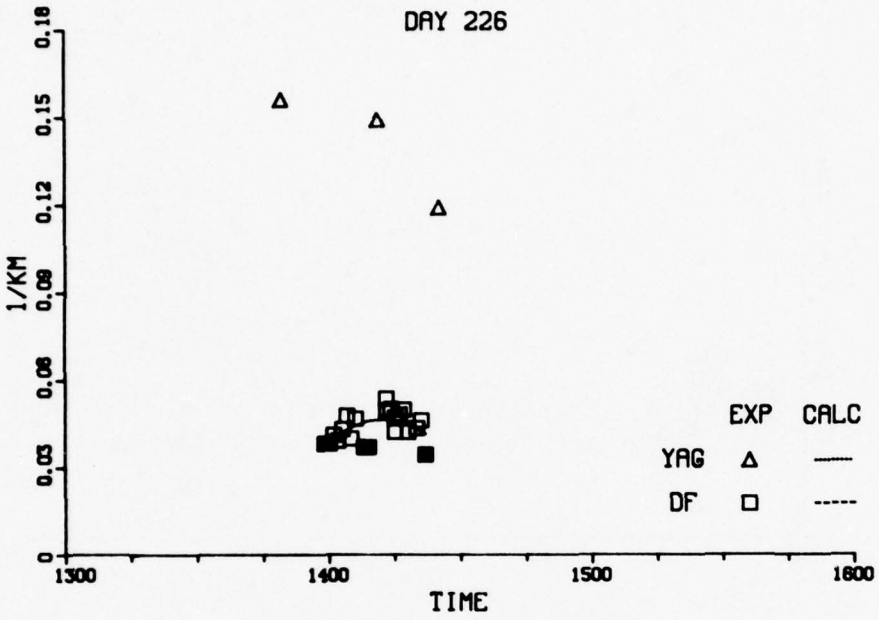

Fig. 22a — Aerosol extinction vs time

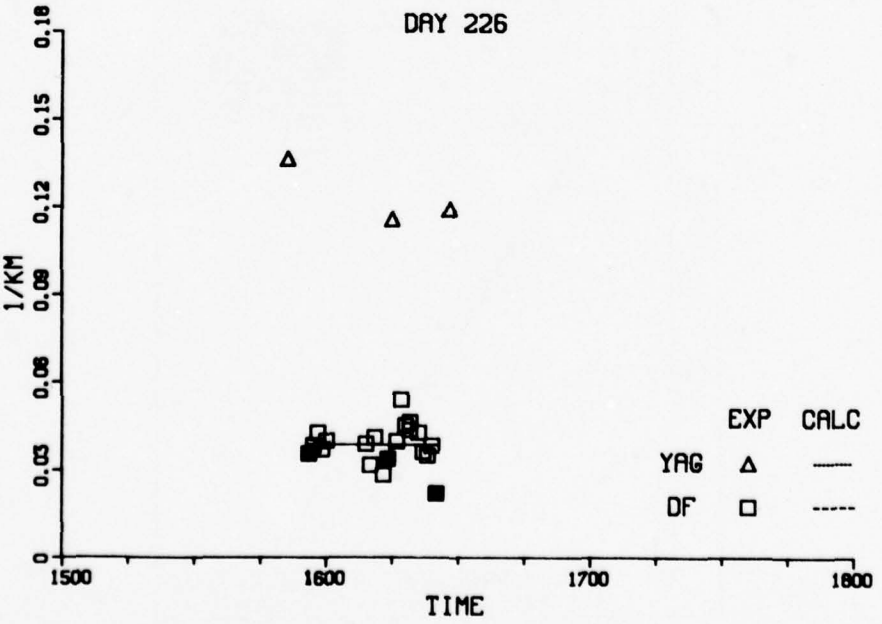

Fig. 22b — Aerosol extinction vs time

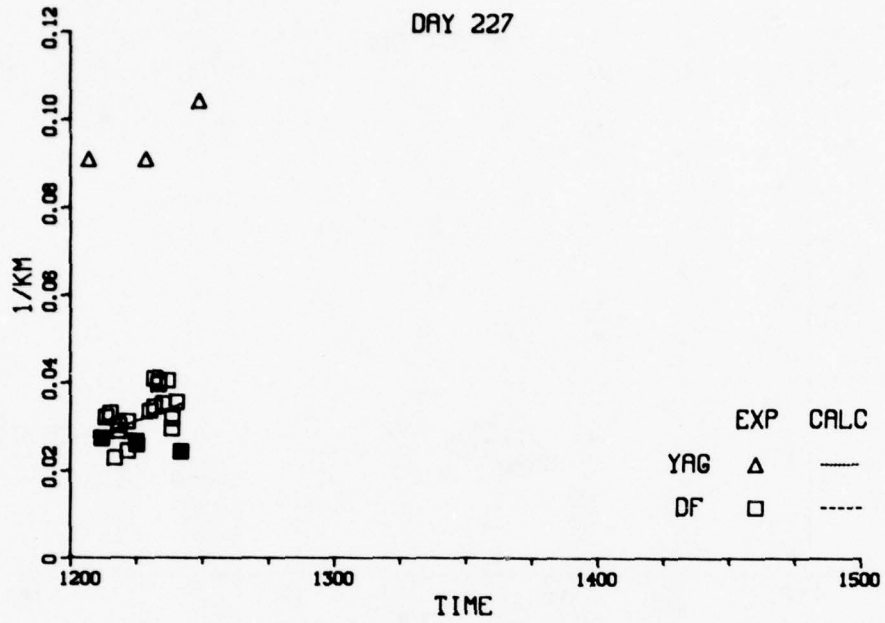

Fig. 23a — Aerosol extinction vs time

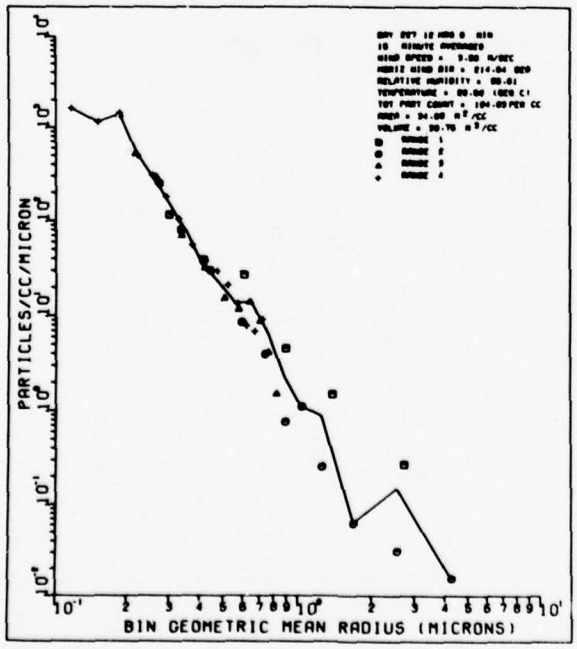

Fig. 23b — Particle distribution

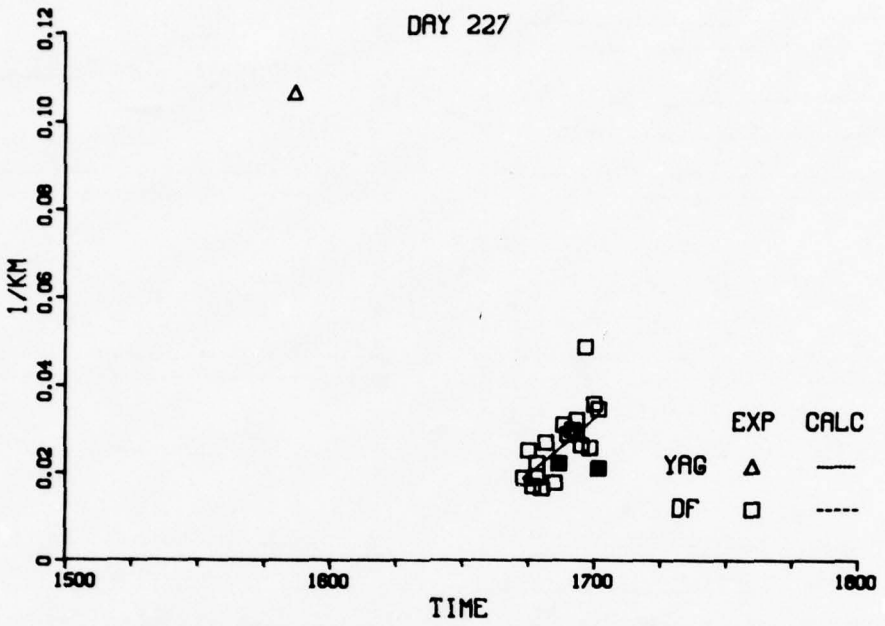

Fig. 23c — Aerosol extinction vs time

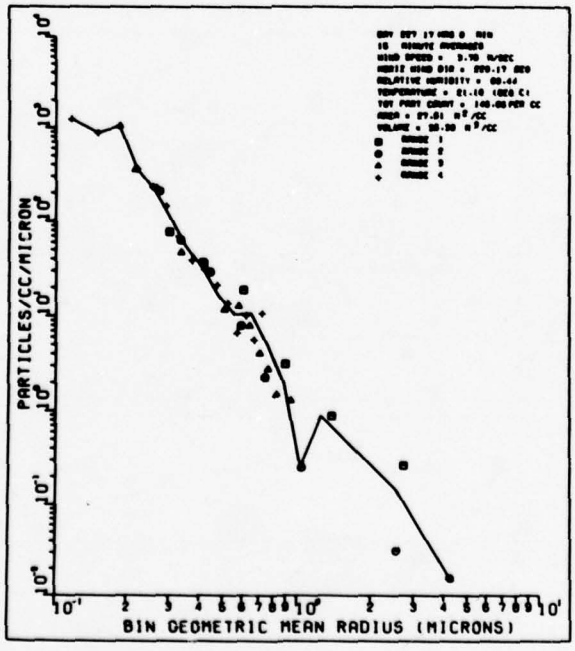

Fig. 23d — Particle distribution

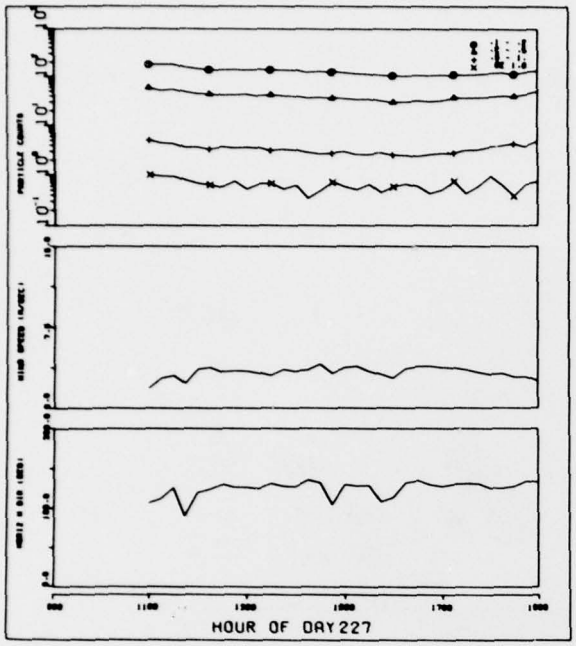

Fig. 23e — Particle counts, wind speed, and horizontal wind direction vs time

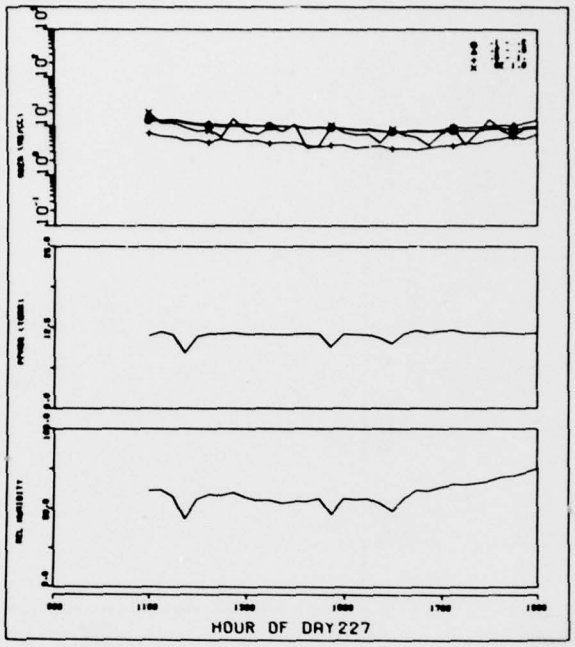

Fig. 23f — Area, water-vapor pressure, and relative humidity vs time

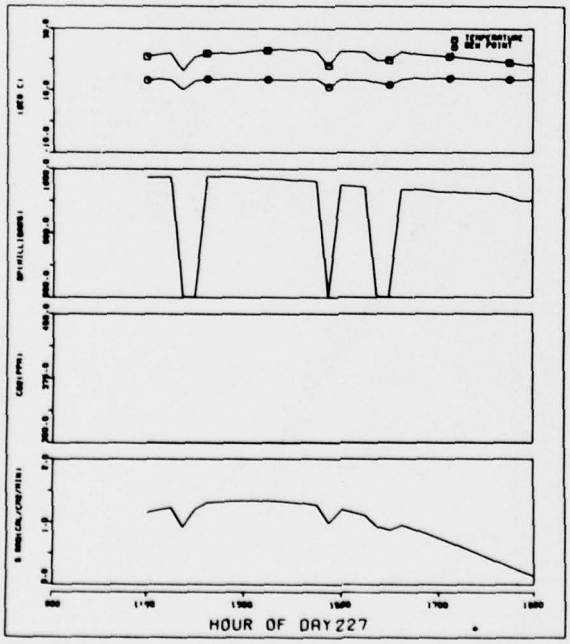

Fig. 23g — Air temperature, barometric pressure, CO_2 concentration, and solar radiation vs time

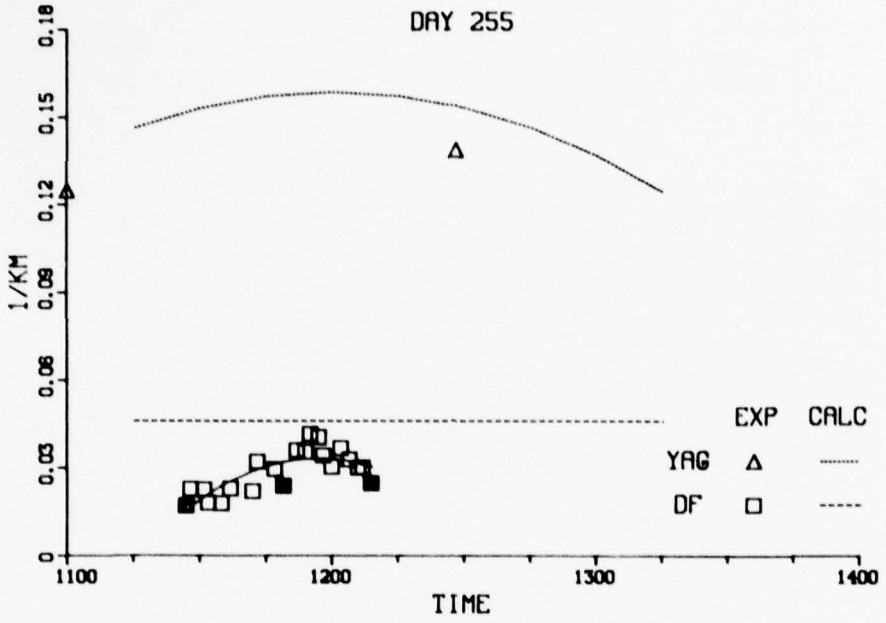

Fig. 24a — Aerosol extinction vs time

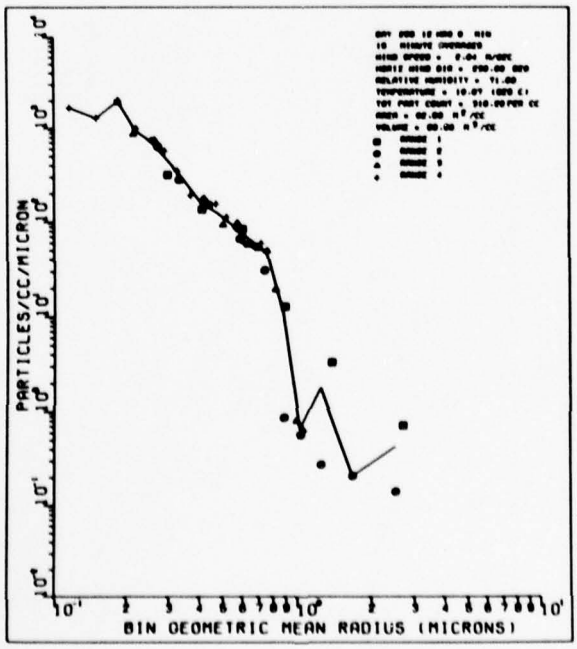

Fig. 24b — Particle distribution

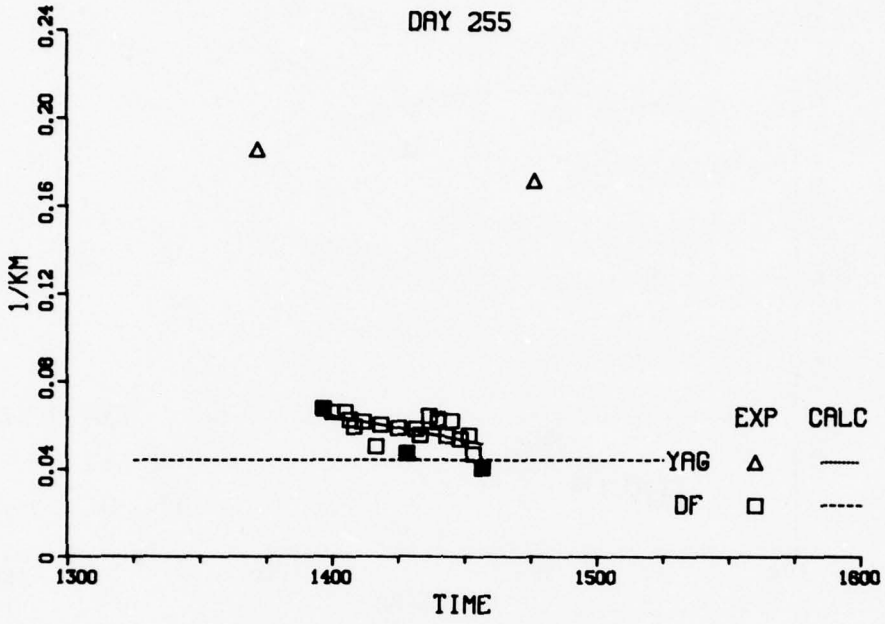

Fig. 24c — Aerosol extinction vs time

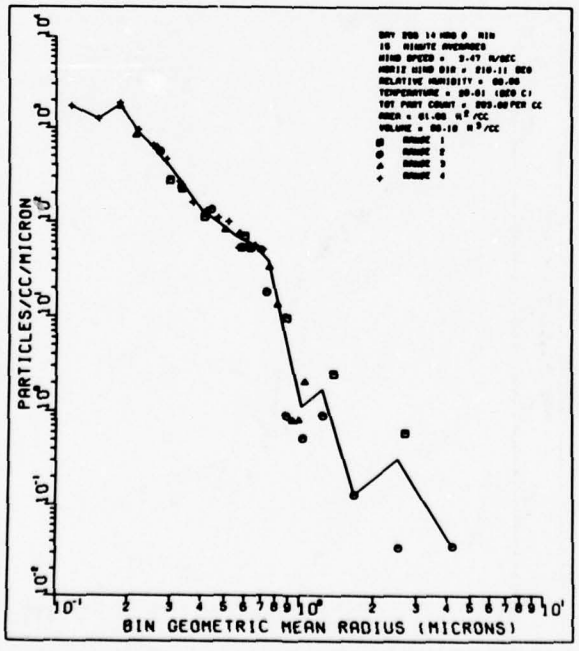

Fig. 24d — Particle distribution

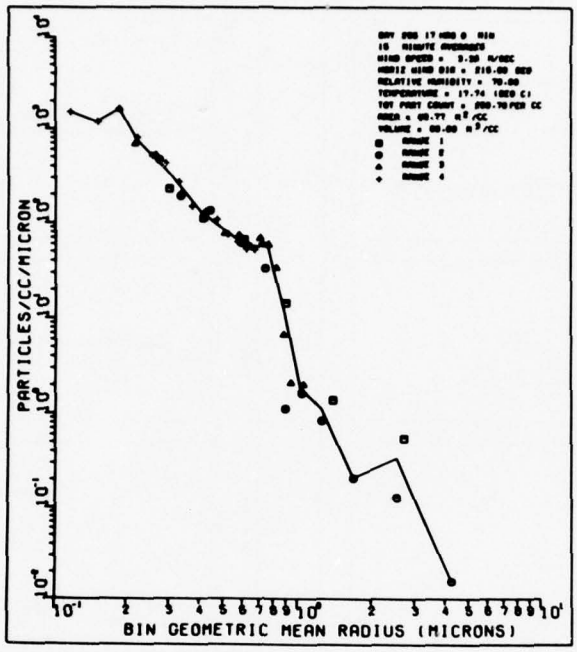

Fig. 24e — Particle distribution

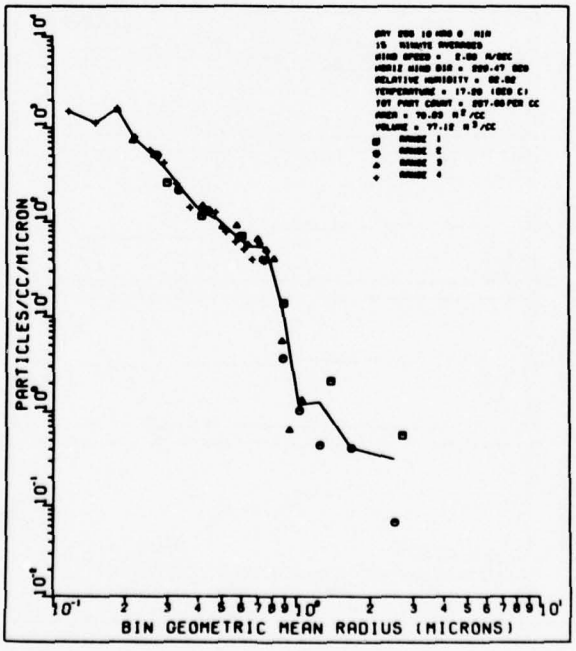

Fig. 24f — Particle distribution

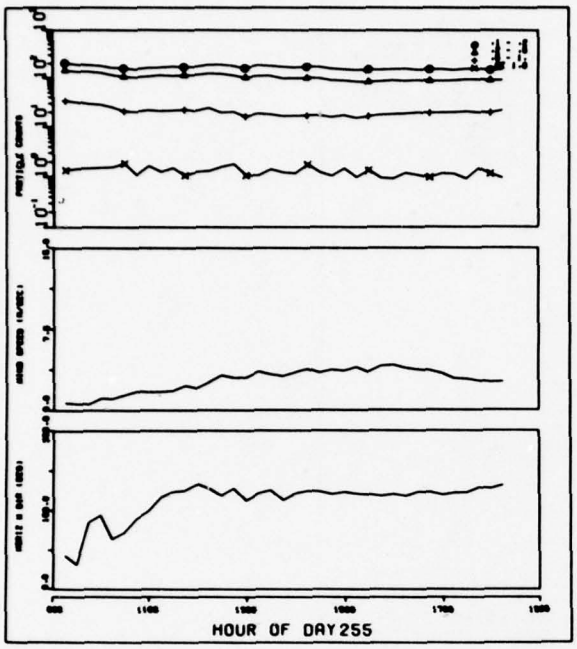

Fig. 24g — Particle counts, wind speed, and horizontal wind direction vs time

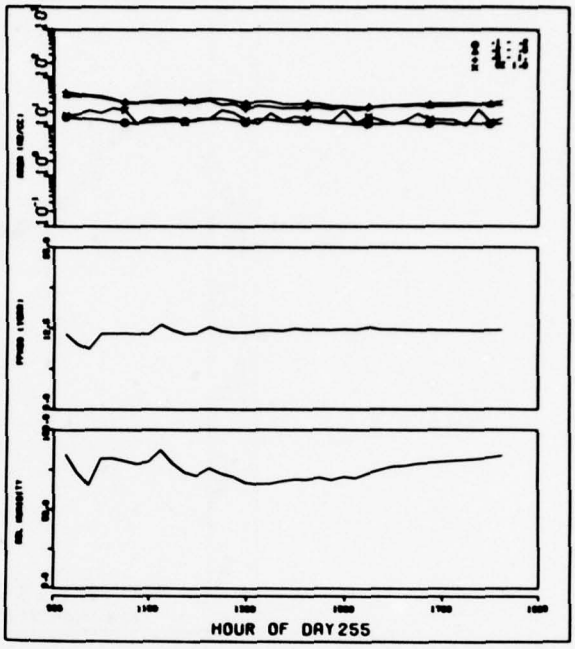

Fig. 24h — Area, water-vapor pressure, and relative humidity vs time

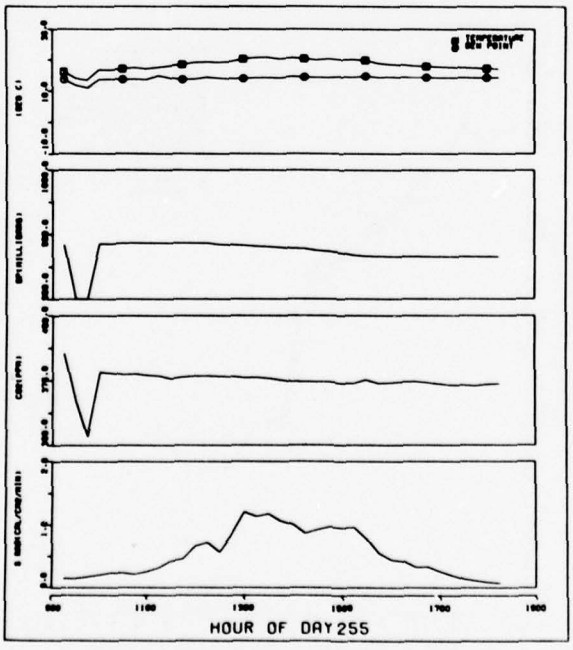

Fig. 24i — Air temperature, barometric pressure, CO_2 concentration, and solar radiation vs time

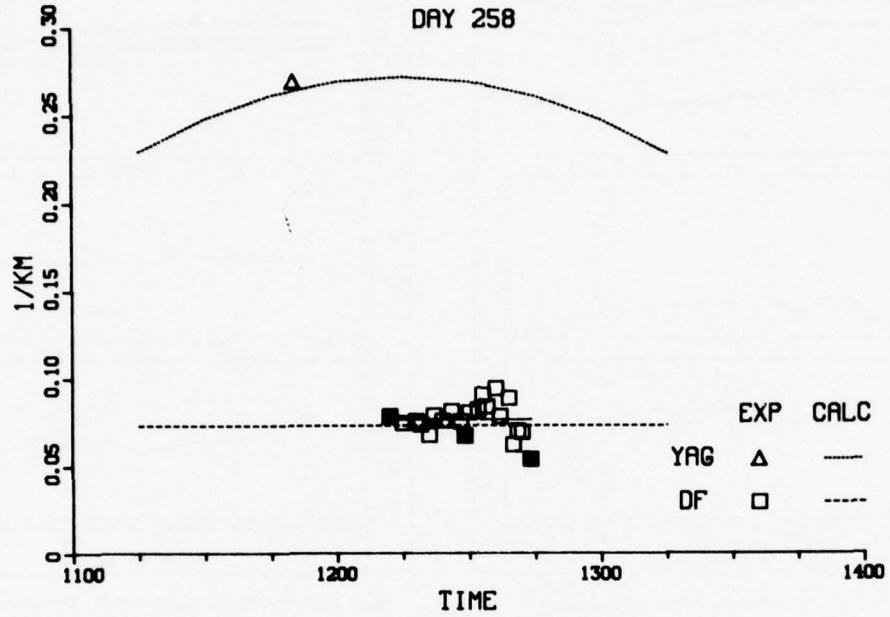

Fig. 25a — Aerosol extinction vs time

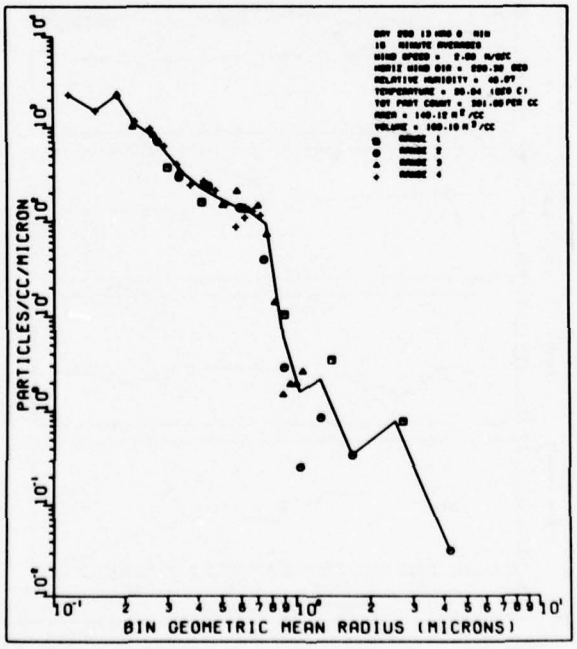

Fig. 25b — Particle distribution

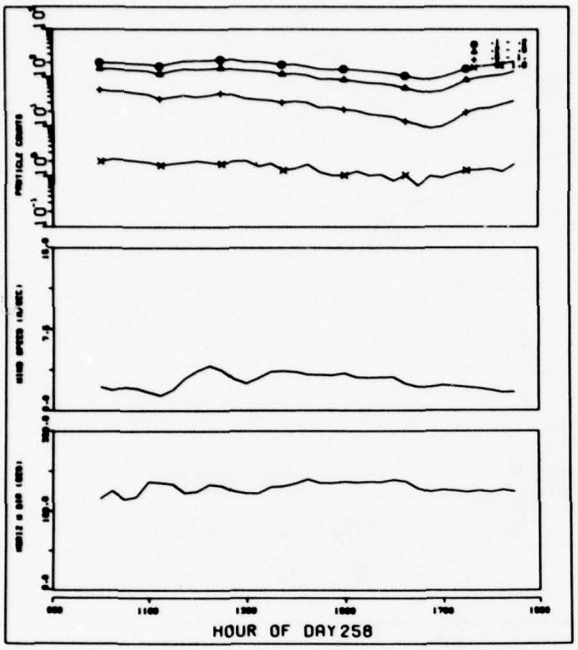

Fig. 25c — Particle counts, wind speed, and horizontal wind direction vs time

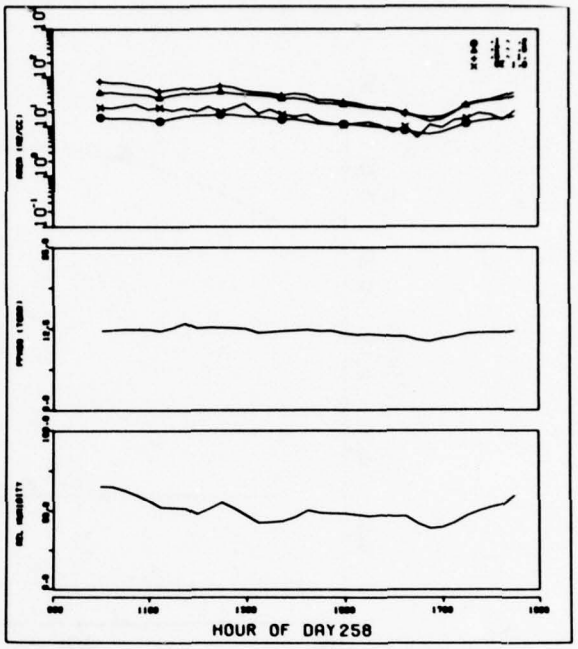

Fig. 25d — Area, water-vapor pressure, and relative humidity vs time

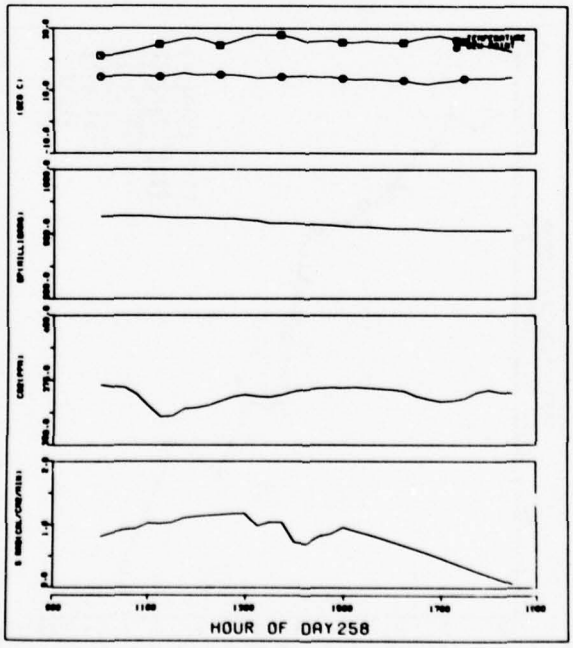

Fig. 25e — Air temperature, barometric pressure, CO_2 concentration, and solar radiation vs time

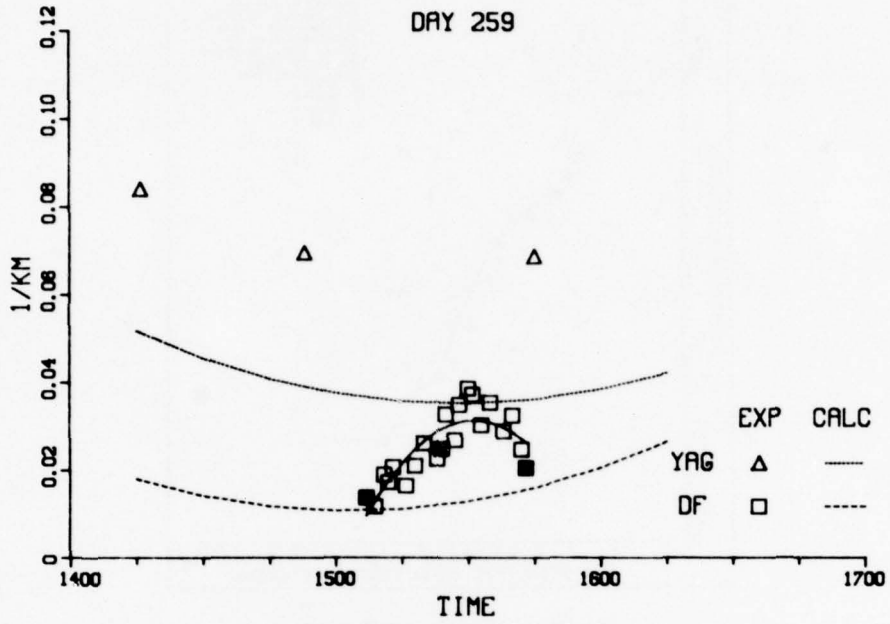

Fig. 26a — Aerosol extinction vs time

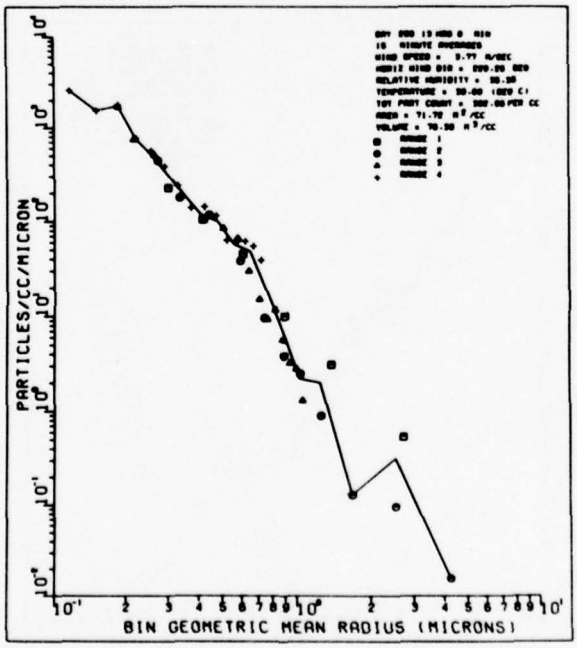

Fig. 26b — Particle distribution

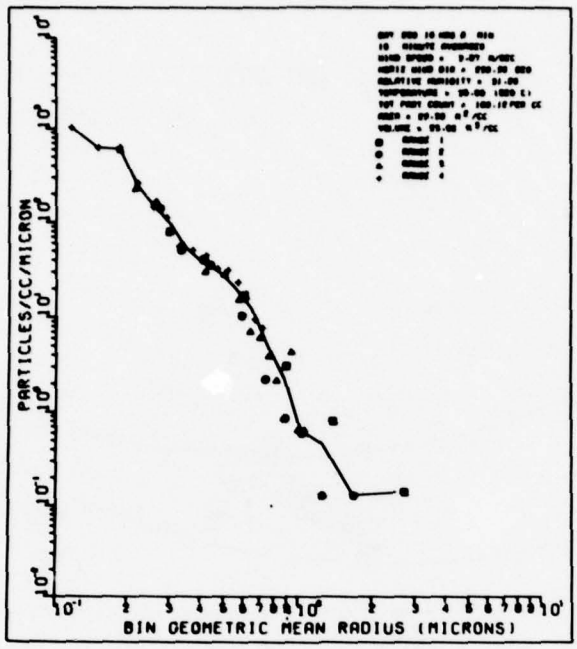

Fig. 26c — Particle distribution

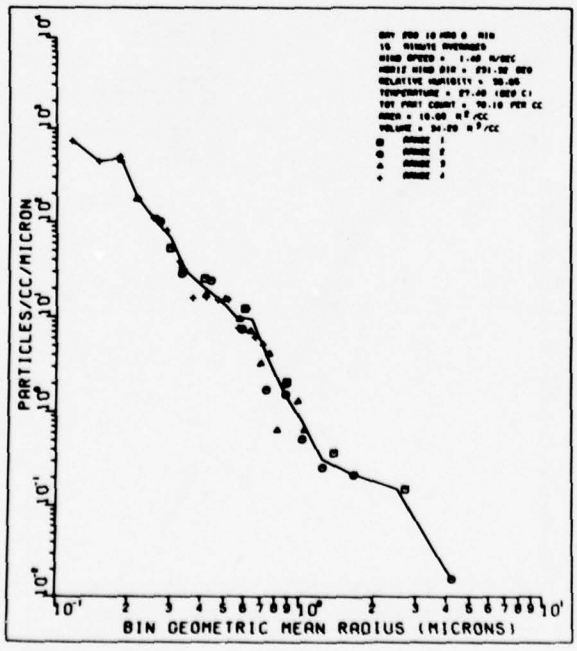

Fig. 26d — Particle distribution

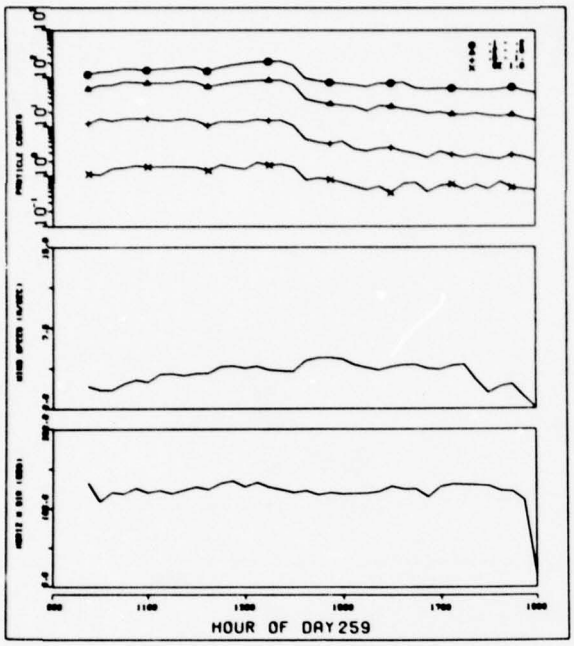

Fig. 26e — Particle counts, wind speed, and horizontal wind direction vs time

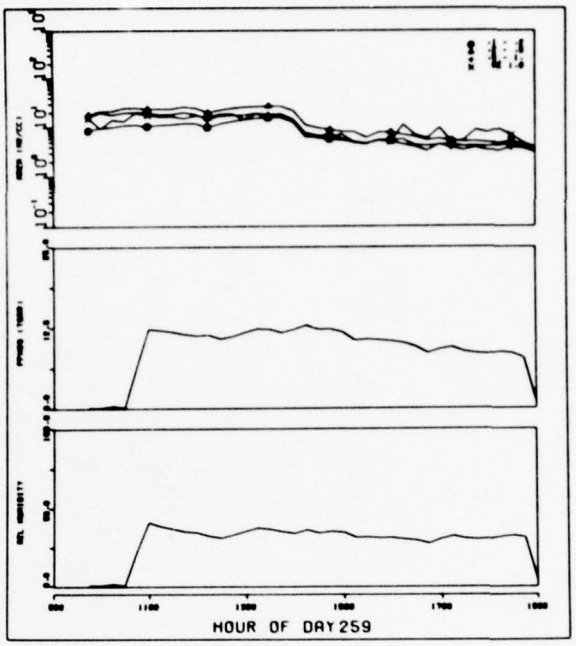

Fig. 26f — Area, water-vapor pressure, and relative humidity vs time

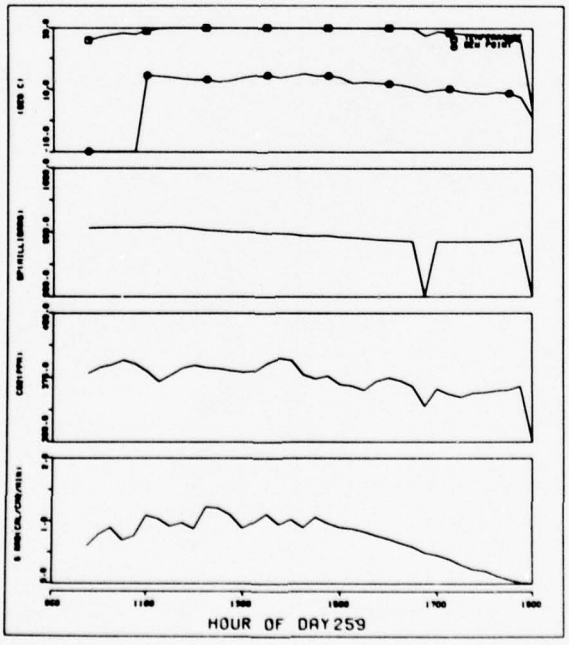

Fig. 26g — Air temperature, barometric pressure, CO_2 concentration, and solar radiation vs time

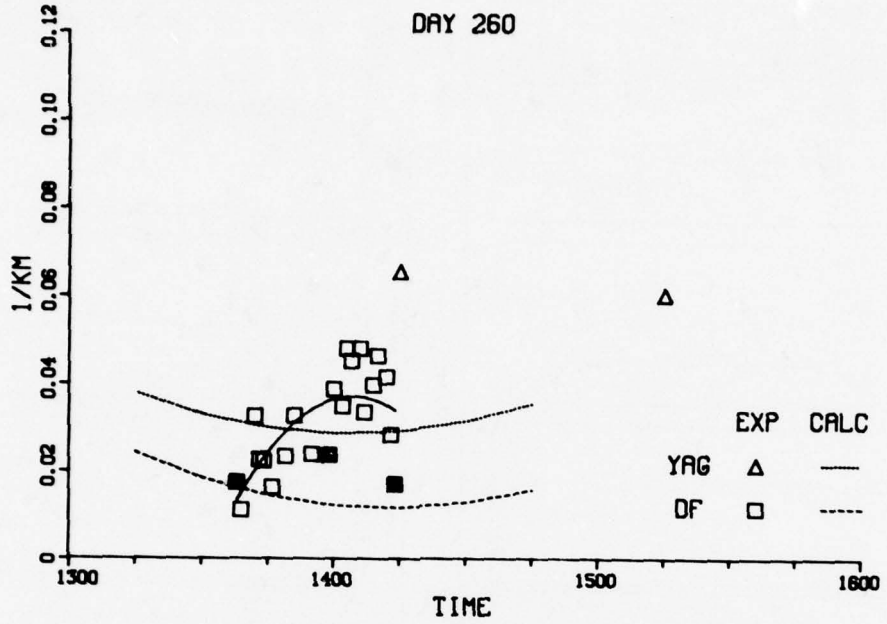

Fig. 27a — Aerosol extinction vs time

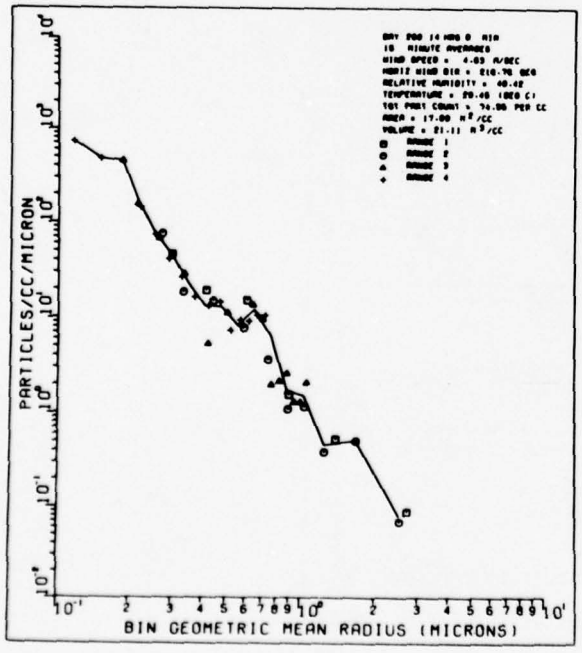

Fig. 27b - Aerosol extinction vs time

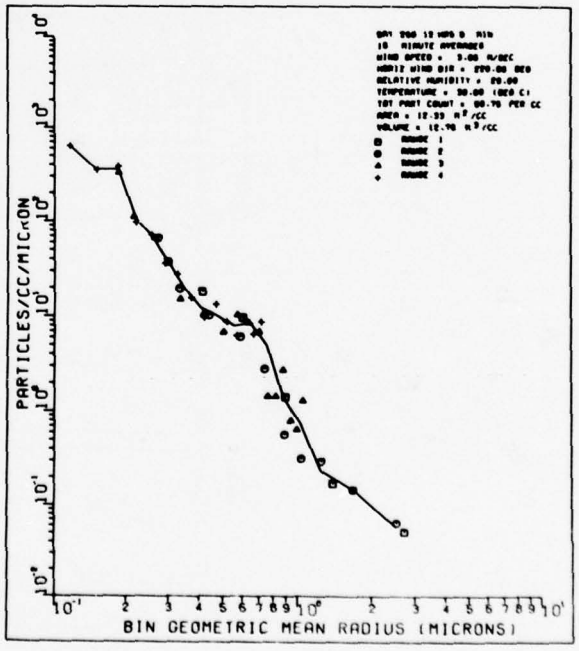

Fig. 27c — Particle distribution

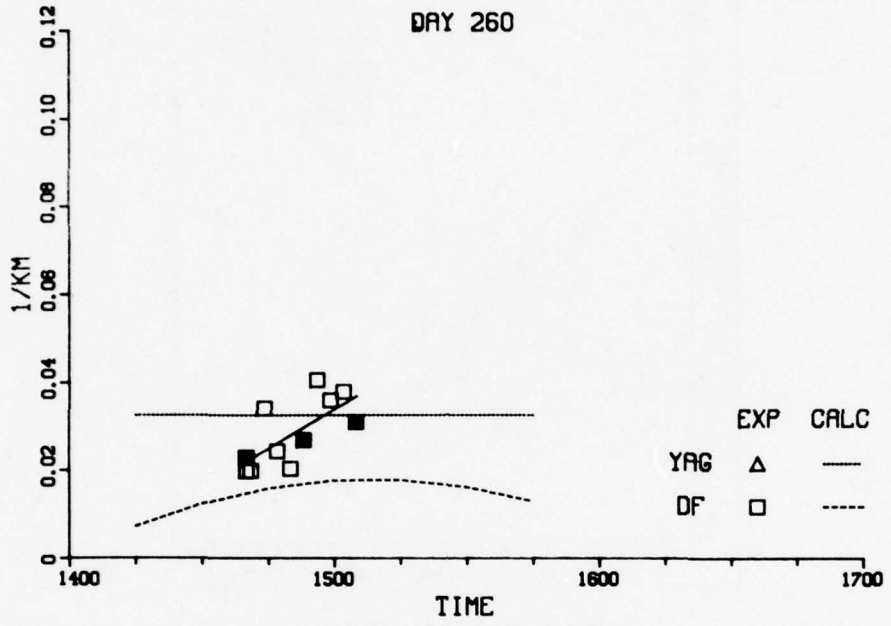

Fig. 27d — Aerosol extinction vs time

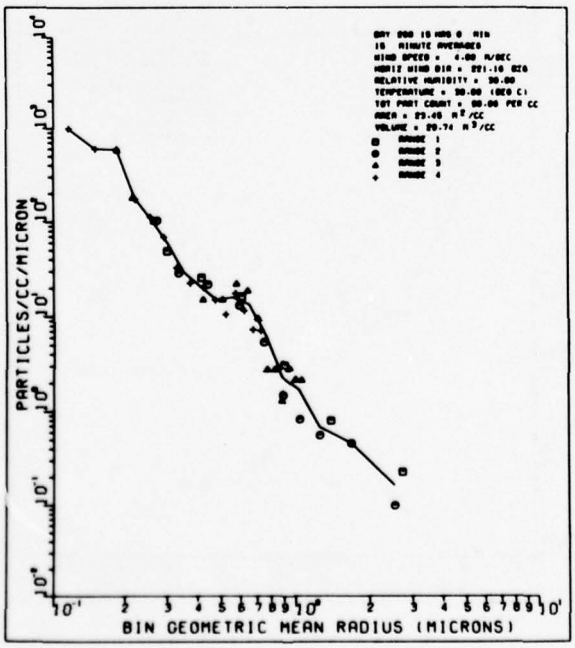

Fig. 27e — Particle distribution

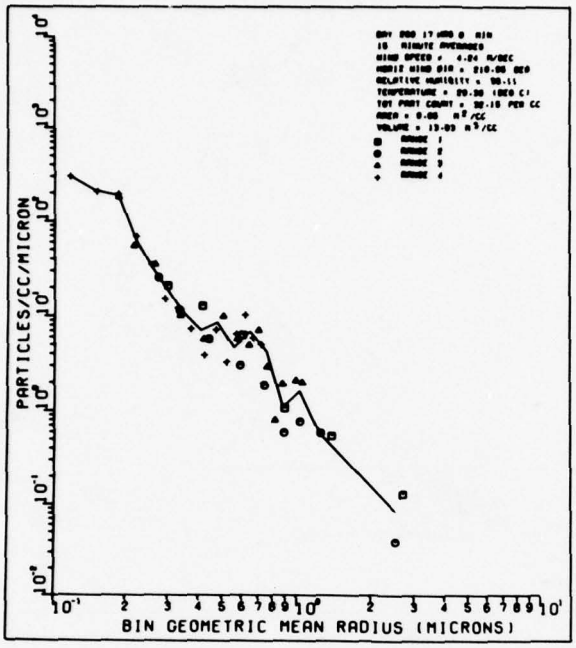

Fig. 27f — Particle distribution

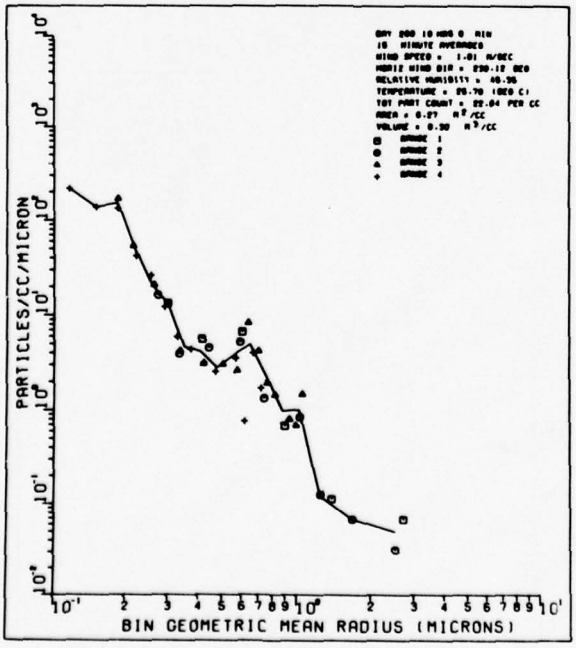

Fig. 27g — Particle distribution

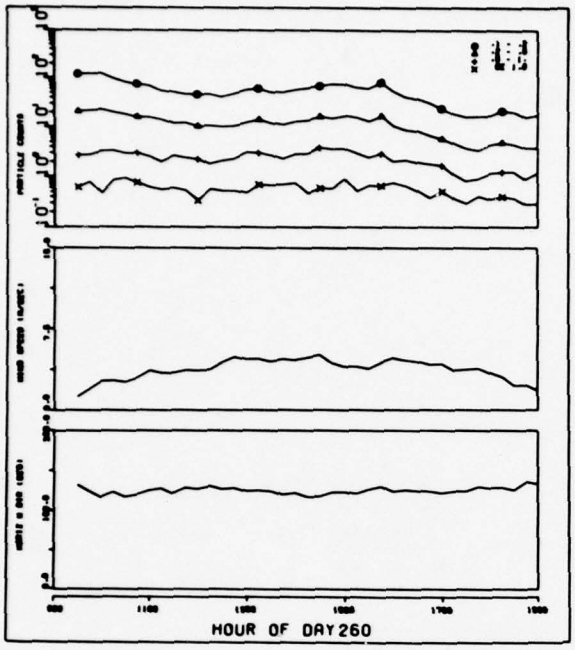

Fig. 27h — Particle counts, wind speed, and horizontal wind direction vs time

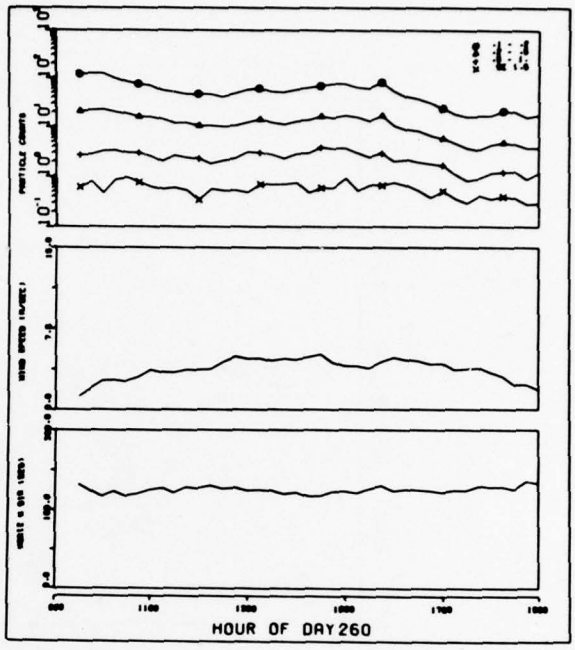

Fig. 27i — Area, water-vapor pressure, and relative humidity vs time

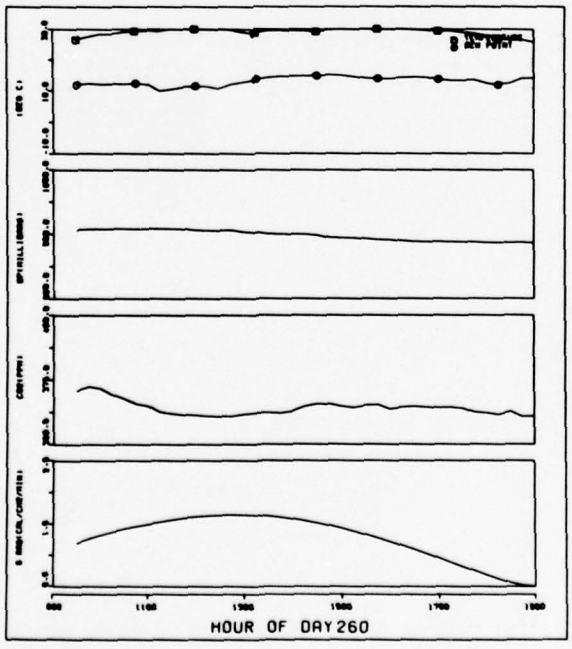

Fig. 27j — Air temperature, barometric pressure, CO_2 concentration, and solar radiation vs time

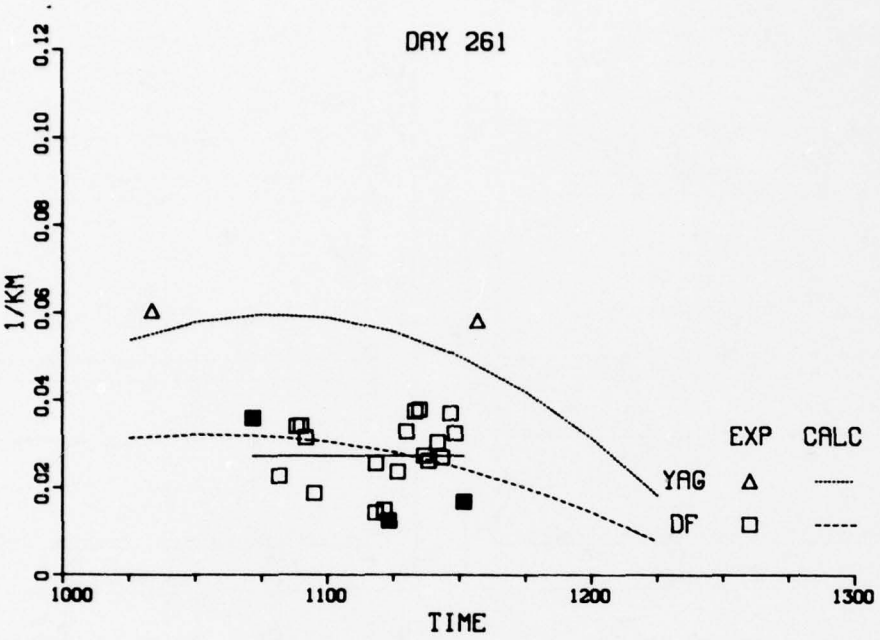

Fig. 28a — Aerosol extinction vs time

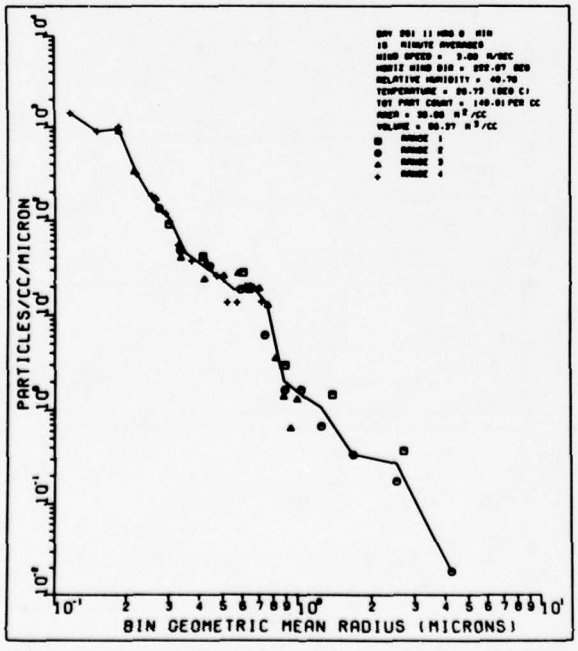

Fig. 28b — Particle distribution

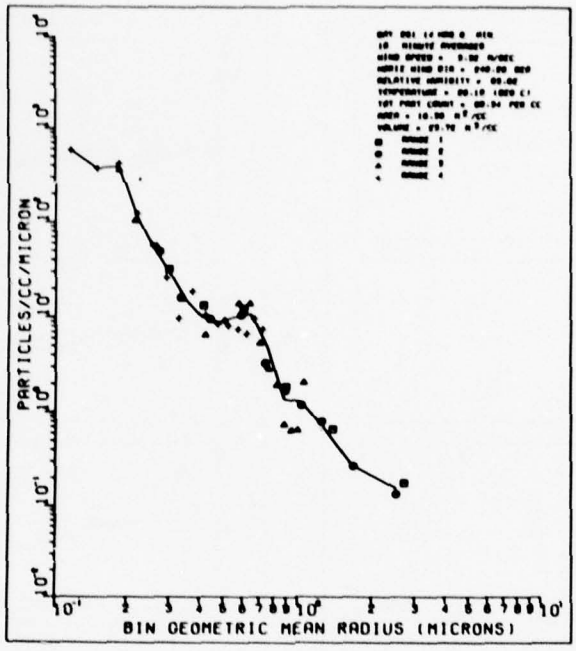

Fig. 28c — Particle distribution

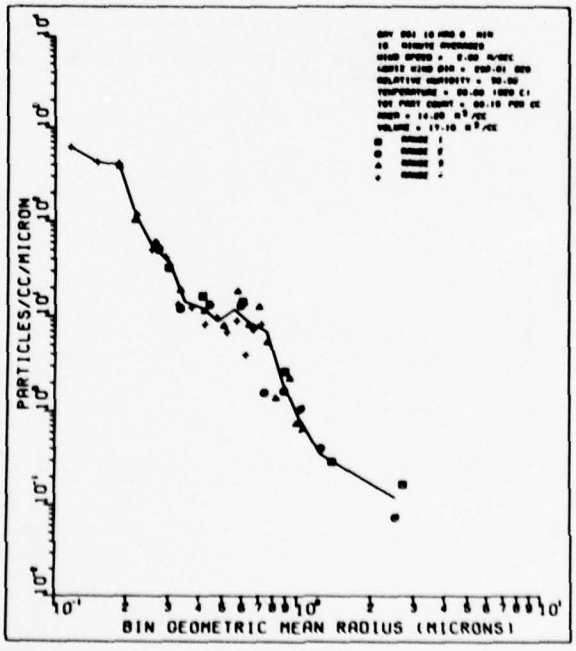

Fig. 28d — Particle distribution

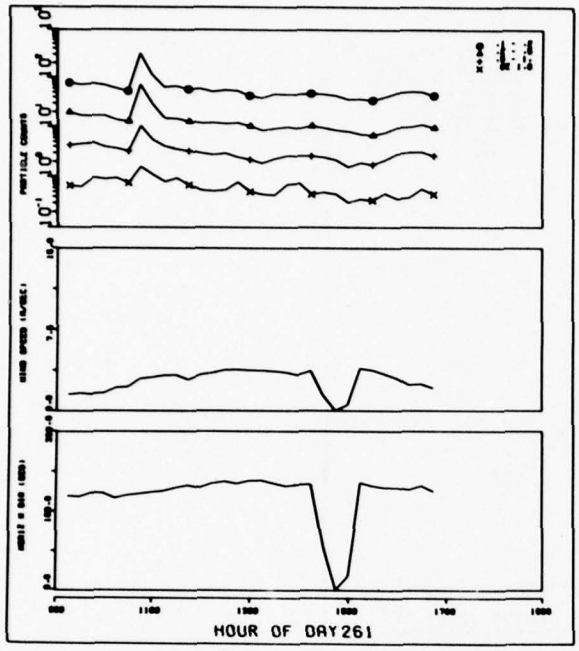

Fig. 28e — Particle counts, wind speed, and horizontal wind direction vs time

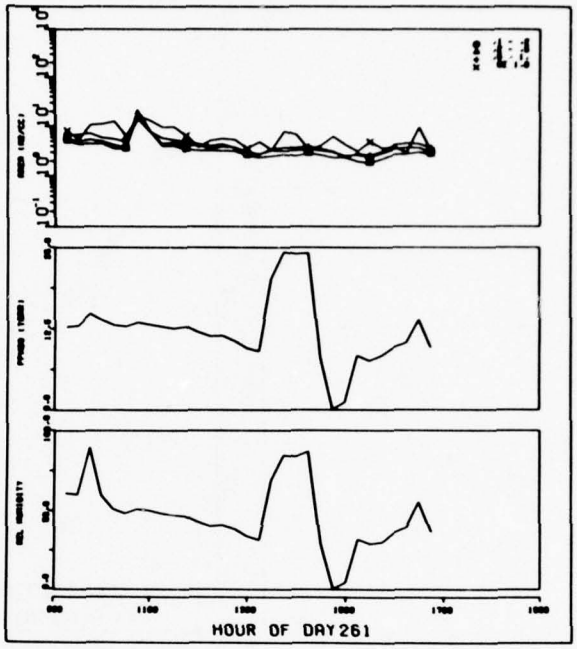

Fig. 28f — Area, water-vapor pressure, and relative humidity vs time

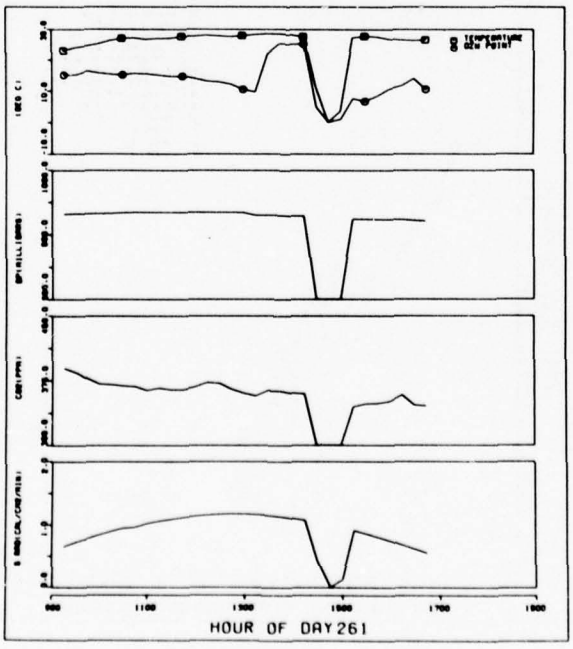

Fig. 28g — Air temperature, barometric pressure, CO_2 concentration, and solar radiation vs time

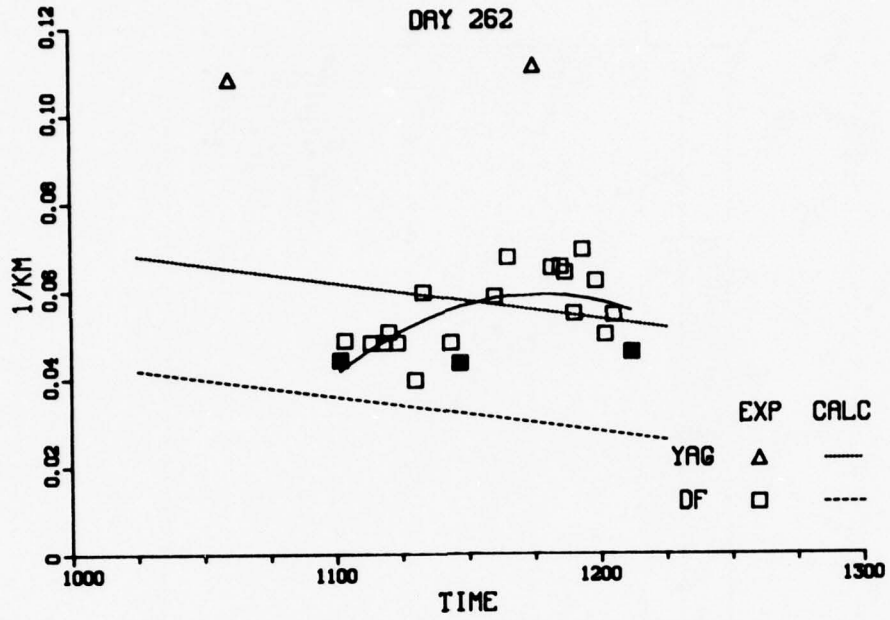

Fig 29a — Aerosol extinction vs time

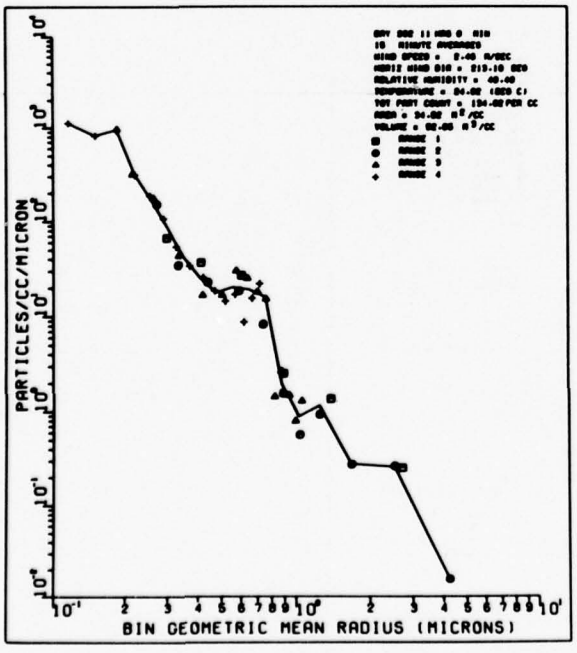

Fig. 29b — Particle distribution

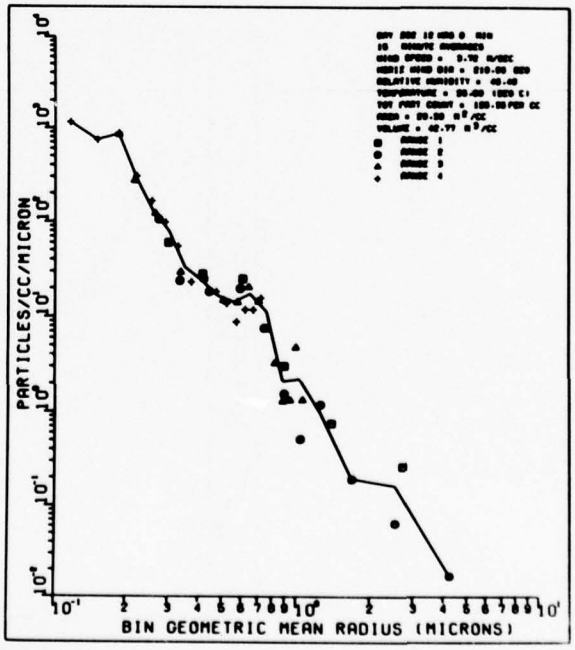

Fig. 29c — Particle distribution

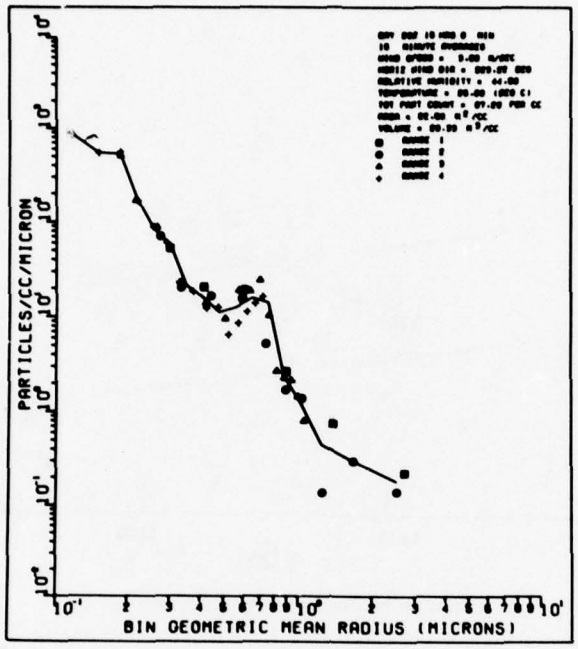

Fig. 29d — Particle distribution

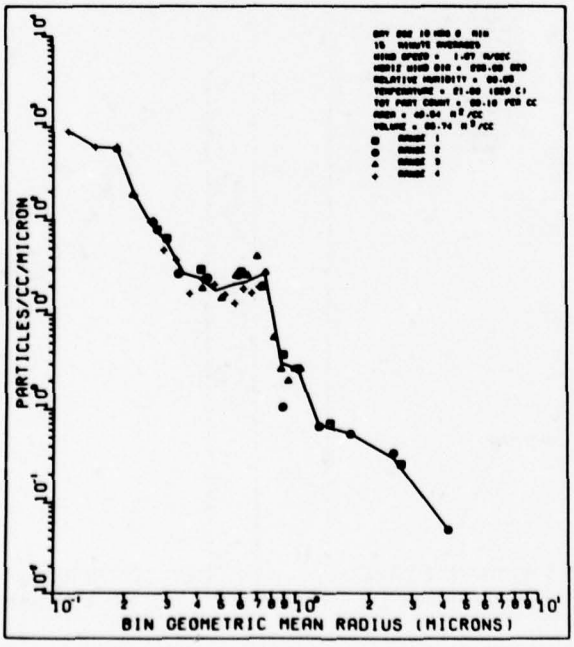

Fig. 29e — Particle distribution

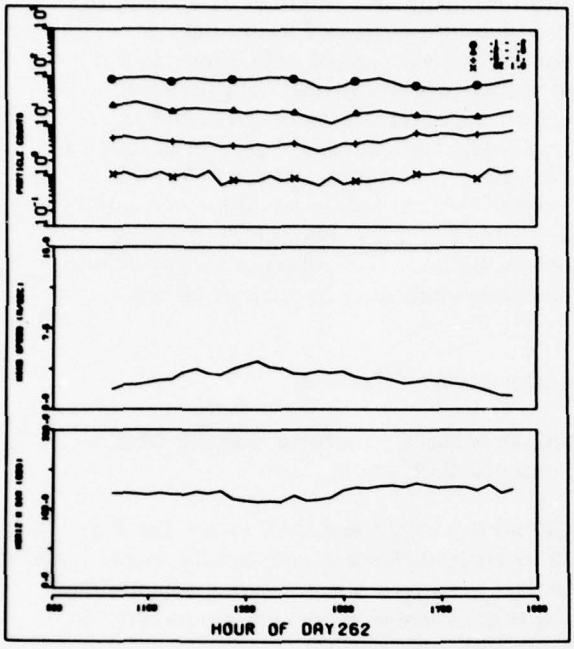

Fig. 29f — Particle counts, wind speed, and horizontal wind direction vs time

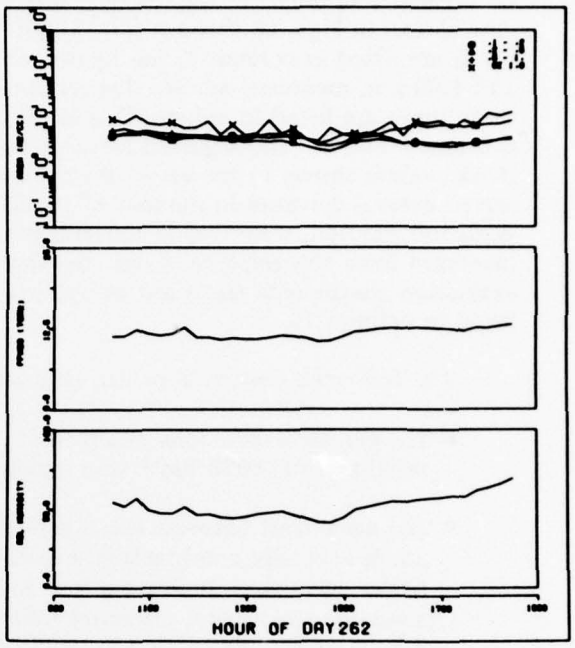

Fig. 29g — Area, water-vapor pressure, and relative humidity vs time

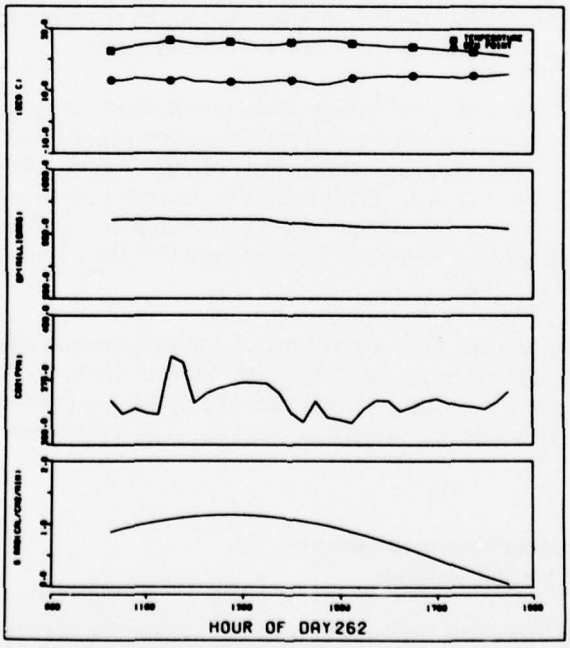

Fig. 29h — Air temperature, barometric pressure, CO_2 concentration, and solar radiation vs time

Table 4 summarizes the observations which can be made as a result of examining the data shown in Figs. 16 through 29. The days on which long-path extinction data were taken are listed in column 1; the figures which show observed aerosol extinctions at 3.8 and 1.06 μm, measured aerosol distributions, and related meteorological data for each of these times are listed in column 2; and the extinction measurement times are listed in columns 3 and 4. The adjusted aerosol extinction (AAE) and calculated aerosol extinction (CAE) values shown in the set of figures are summarized in columns 5 through 8. Observed aerosol densities in number of particles per cm^3 per μm radius are listed in column 9. Wind information, water-vapor concentration, air temperature, and barometric pressure (averaged from the graphical data) are summarized in the next five columns. Atmospheric extinction coefficients measured at 650 nm for the times indicated in column 16 are listed in column 15.

The following observations can be made on inspection of Table 4:

- The aerosol extinctions observed at 3.8 μm are relatively uniform, varying from a minimum of 0.025 km^{-1} to a maximum value of 0.08 km^{-1}.

- The agreement between the observed AAE and the calculated CAE values for 3.8 μm is generally good, within a factor of 2 extreme difference and usually much better agreement, indicating that the PMS data used in a Mie scattering calculation (assuming the aerosol refractive index to be that of water vapor) gives numbers for 3.8-μm aerosol extinction in good agreement with observations.

- The agreement between measured and calculated aerosol extinction (AAE and CAE) for 1.06 μm is not as good as for 3.8 μm; the calculated results are consistently 50% to 60% of the observed values. Possibly the assumption of water index of refraction for the smaller particles, which are more effective in scattering 1.06-μm radiation, is not as reliable as it is for the 3.8-μm case.

- The summary meteorological information in columns 10 through 14 show that uniform weather conditions persisted throughout the experiment, with winds generally between 2 and 4 m/s from the southwest, off the Pacific Ocean. (The site was approximately 10 km inland). Little variation in water-vapor pressure was observed, as can be seen in column 12 and also by an examination of Figs. 30a through 30v, which show the molecular absorption for each DF laser line studied as a function of water-vapor pressure.

- The local hazes present during portions of the experiment give rise to some of the moderately high scattering observations at 650/μm (column 15 of Table 4). It is interesting to note that the 1.06-nm data do not show the large increases observed in the visible, although the trends in the two observations are consistently in the same direction.

3.6 Molecular-Absorption Measurements and Comparisons to Calculations

Figs. 30a through 30v show the variation of the apparent molecular absorption with water-vapor pressure for each of the 22 DF laser lines studied. The molecular absorptions obtained

Table 4 — Summary Observation Of Adjusted Aerosol Extinction (AAE), Calculated Aerosol Extinction (CAE), Aerosol Density as Measured with the PMS Particle-Size Spectrometer, and Meteorological Data (Wind Speed, Wind Direction, Partial Pressure of H_2O, Air Temperature, and Barometric Pressure).

Day	Figures	Time		AAE (km^{-1})		CAE (km^{-1})		PMS Data at 1 μm (particle cm^{-3} μm^{-1})	WS (m/s)	WD (deg)	PPH_2O (torr)	AT (°C)	BP (mbar)	Visible Extinction	
		Start	Stop	3.8 μm	1.06 μm	3.8 μm	1.06 μm							(km^{-1})	Time
217	16a-16f	1700	1800	0.045	0.11	0.035	0.070	2.0	11.8	~240	12.5	20	992	0.17	1710
218	17a-17f	1615	1745	0.060↓	0.12	0.030	0.050	1-1.5	2.0	~250	13↑	15	990↓	0.084	1630
219	18a-18e	1430	1515	0.050↑	0.13↑	0.030	0.060	0.9	2.8	~225	13	26	991	0.073	1430
220	19a-19h	1100	1145	0.045	0.13	0.050	0.10	2.0	3.8	210	14.5	26	995	0.123	1845
		1430	1500	0.065	0.17	0.070	0.115	1.3	3.8	230	14.5	25	993	0.110	1445
224	20a-20e	1700	1745	0.050	0.09	0.025	0.040	0.9	3.5	195	11.5	20	994	0.121	1700
225	21a-21g	1200	1230	0.035	0.090	0.030	0.060	1.0	3.6	230	12.5	23	998	0.156	1225
		1415	1445	0.040↑	0.105	0.030	0.050	0.08	3.8	240	12.0	23	997	0.141	1430
226	22a	1400	1430	0.045	0.135↓	—	—	—	—	—	—	—	—	0.205	1425
	22b	1545	1630	0.040	0.130	—	—	—	—	—	--	—	—	0.166	1545
227	23a-23g	1200	1230	0.030	0.095↑	—	—	1.3	3.5	225	12.0	23	997	—	—
		1645	1715	0.025↑	0.110	—	—	0.4	4.0	240	12.5	21	996	0.108	1730
255	24a-24i	1130	1215	0.030	0.13	0.045	0.16	1.1	2.0↑	180	12.0	19	989	0.296	1130
		1345	1430	0.060	0.18	0.050	—	1.3	3.8	225	12.5	20	988	0.30	1430
		1700*	—	—	—	—	—	2.0	3.5↓	225	12.5	18	986	—	—
		1800*	—	—	—	—	—	1.3	2.7	240	12.5	18	986	—	—
258	25a-25e	1200	1245	0.080	0.27	0.075	0.27	2.0	3.5	225	12.5	27	992	0.55	1200
259	26a-26g	1500	1545	0.025↑	0.070	0.015	0.035	0.65	3.8	210	11.0	30†	989	0.09	1600
		1300*	—	—	—	—	—	2.7	3.8	225	12.0	30†	990	—	—
		1600*	—	—	—	—	—	0.90	3.8	225	11.0	30†	989	0.09	1600
260	27a-27j	1200*		—	—	—	—	0.80	3.6	225	9.3	30†	990	—	—
		1330	1415	0.03↑	0.060	0.01	0.03	1.6	4.7	220	12.0	30†	990	0.074	1415
		1430	1515	0.03↑	0.06	0.02	0.035	1.7	4.0	225	12.5	30†	989	0.071	1515
		1700		—	—	—	—	1.5	3.8	225	11.8	29	988	0.04	1730
		1900		—	—	—	—	1.0	1.9	230	12.0	25	988	—	—
261	28a-28g	1030	1130	0.027	0.059	0.030	0.58	1.4	3.0	225	13	26	993	0.089	1025
		1400*		—	—	—	—	1.1	3.8	240	—	29	992	0.048	1435
		1600*		—	—	—	—	1.0	3.2	230	9.3	28	992	—	—
262	29a-29h	1100	1215	0.055	0.11	0.030	0.055	0.9	3.0↑	220	11.0	26	992	0.094	1145
		1200		—	—	—	—	2.0	3.8	220	11.0	25	992	0.094	1145
		1500		—	—	—	—	1.2	3.0	230	11.5	27	991	0.084	1440
		1600		—	—	—	—	2.7	2.3	240	12.5	26	991	0.098	1635

↑(↓) Indicates increasing (decreasing) size of parameter during observation time.

* Particle distributions associated with BDL shot times included.

† Graphic presentation limited to 30°C; actual recorded data can exceed this value.

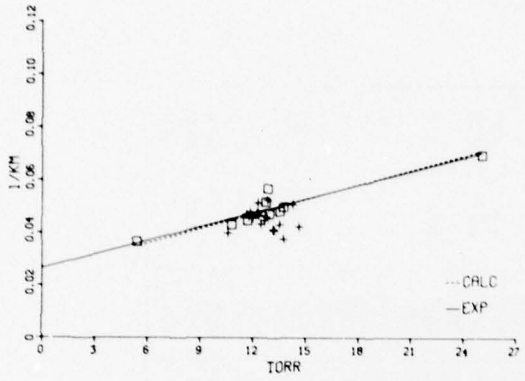

Fig. 30a — Molecular absorption vs water-vapor pressure, $P_3$10 DF laser line

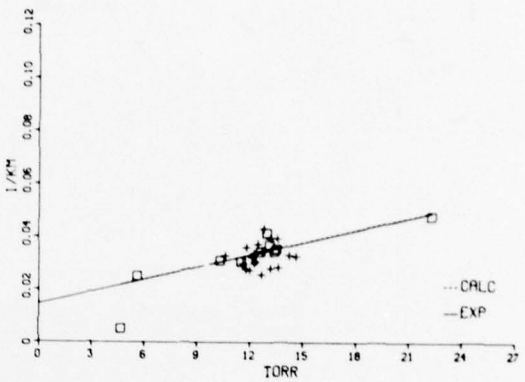

Fig. 30b — Molecular absorption vs water-vapor pressure, $P_3$9 DF laser line

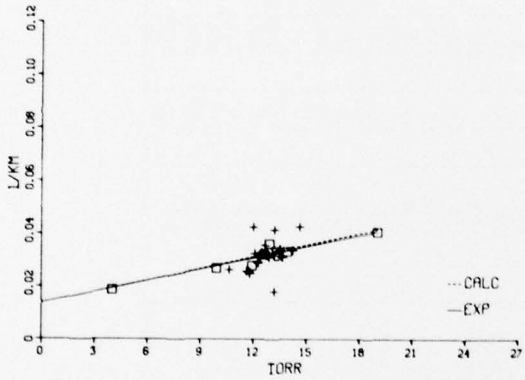

Fig. 30c — Molecular absorption vs water-vapor pressure, $P_2$12 DF laser line

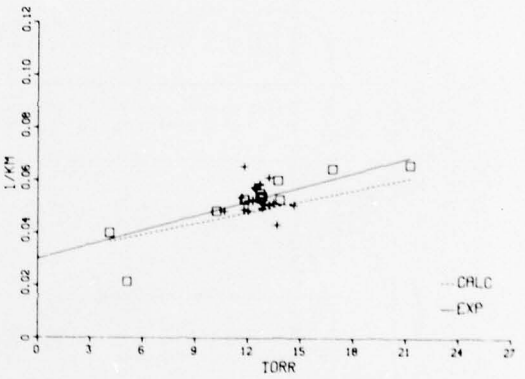

Fig. 30d — Molecular absorption vs water-vapor pressure, $P_3$8 DF laser line

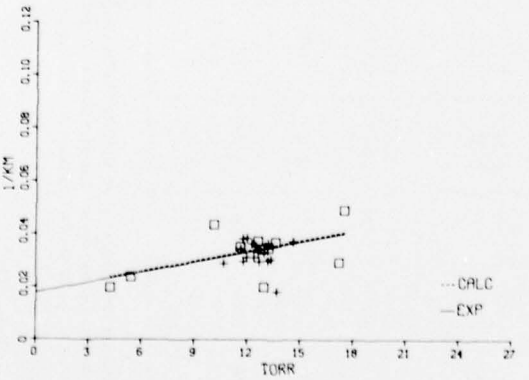

Fig. 30e — Molecular absorption vs water-vapor pressure, $P_2$11 DF laser line

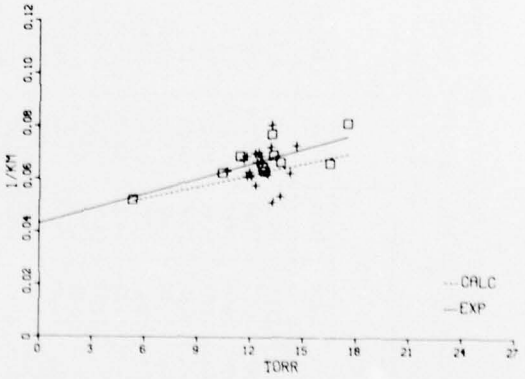

Fig. 30f — Molecular absorption vs water-vapor pressure, $P_3$7 DF laser line

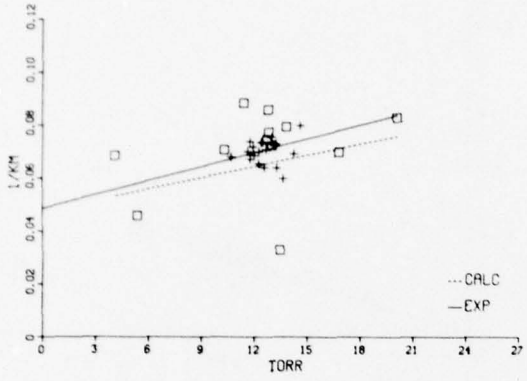

Fig. 30g — Molecular absorption vs water-vapor pressure, $P_2$10 DF laser line

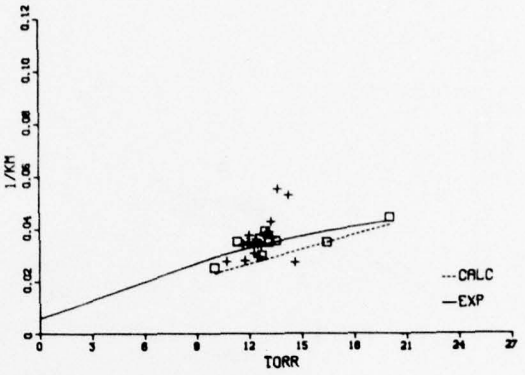

Fig. 30h — Molecular absorption vs water-vapor pressure, $P_3$6 DF laser line

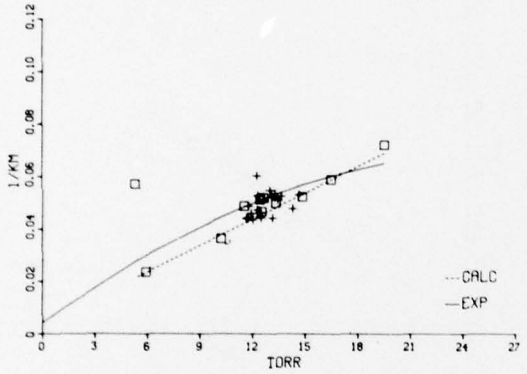

Fig. 30i — Molecular absorption vs water-vapor pressure, $P_2$9 DF laser line

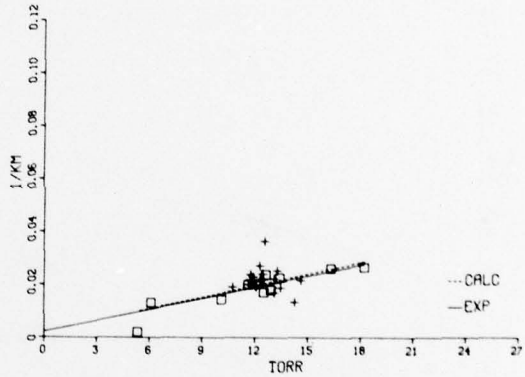

Fig. 30j — Molecular absorption vs water-vapor pressure, $P_3$5 DF laser line

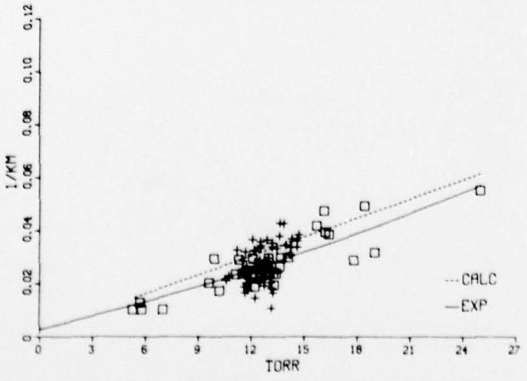

Fig. 30k — Molecular absorption vs water-vapor pressure, $P_2$8 DF laser line

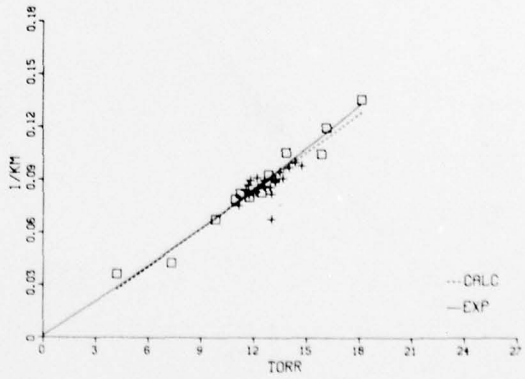

Fig. 30l — Molecular absorption vs water-vapor pressure, $P_2$7 DF laser line

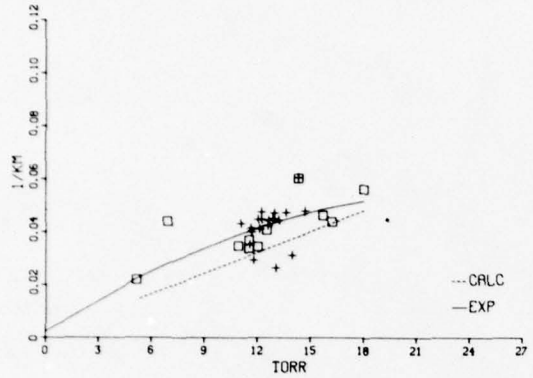

Fig. 30m — Molecular absorption vs water-vapor pressure, $P_1$10 DF laser line

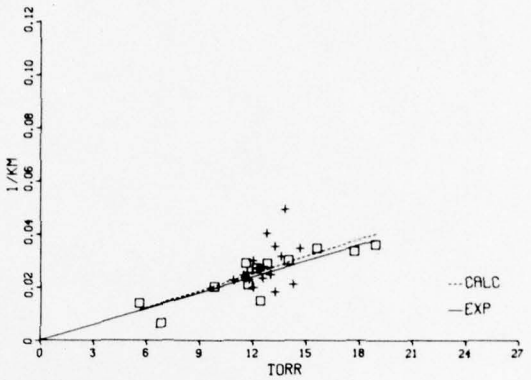

Fig. 30n — Molecular absorption vs water-vapor pressure, $P_2$6 DF laser line

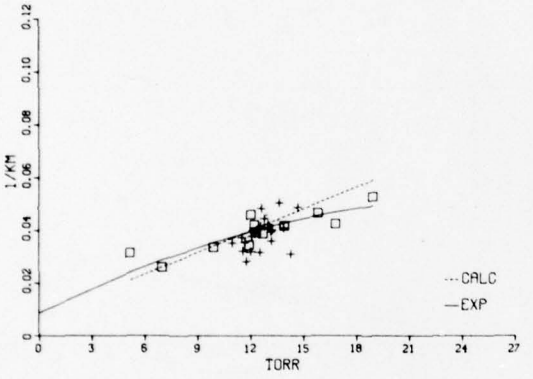

Fig. 30o — Molecular absorption vs water-vapor pressure, $P_1$9 DF laser line

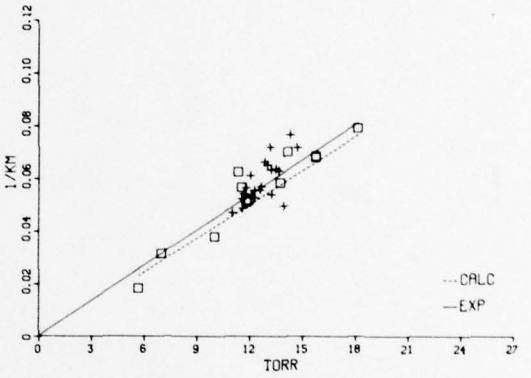

Fig. 30p — Molecular absorption vs water-vapor pressure, $P_2$5 DF laser line

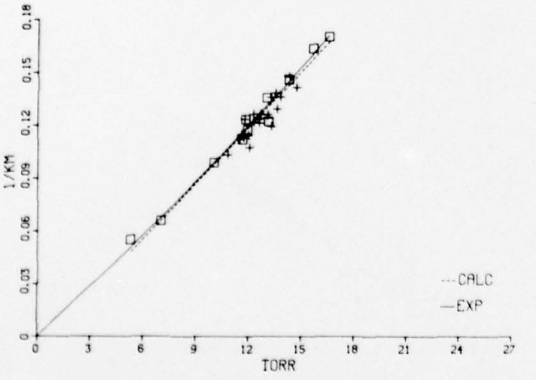

Fig. 30q — Molecular absorption vs water-vapor pressure, $P_1$8 DF laser line

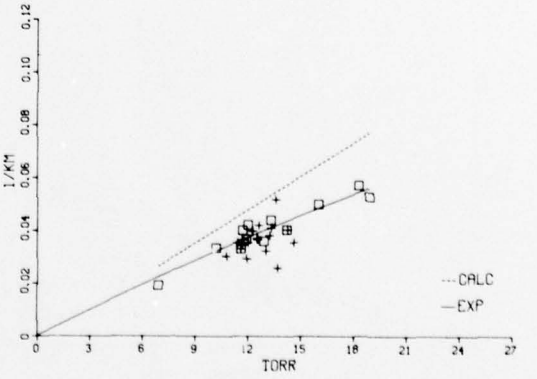

Fig. 30r — Molecular absorption vs water-vapor pressure, $P_2$4 DF laser line

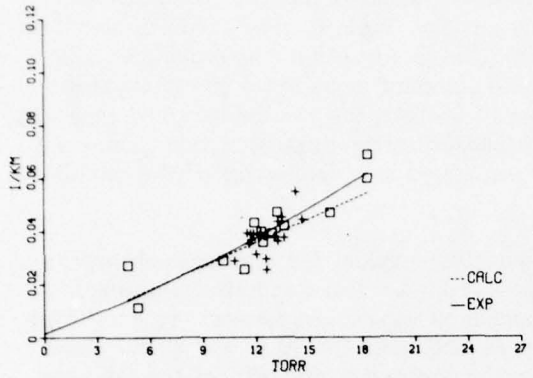

Fig. 30s — Molecular absorption vs water-vapor pressure, $P_1 7$ DF laser line

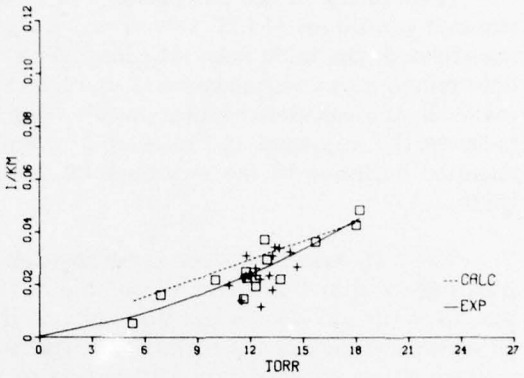

Fig. 30t — Molecular absorption vs water-vapor pressure, $P_2 3$ DF laser line

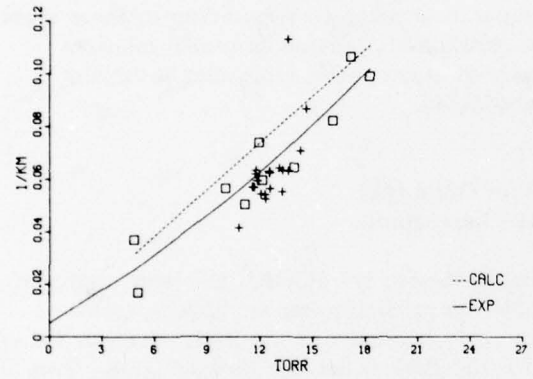

Fig. 30u — Molecular absorption vs water-vapor pressure, $P_1 6$ DF laser line

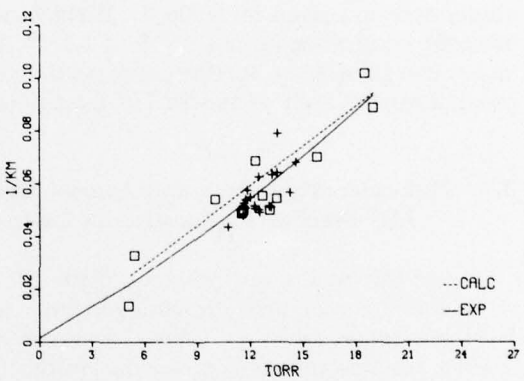

Fig. 30v — Molecular absorption vs water-vapor pressure, $P_1 5$ DF laser line

from the Capistrano measurements are shown as crosses; similiar data taken earlier in 1975 at Cape Canaveral, Florida, are shown as open boxes. The latter data are included because the wider range of water-vapor pressures encountered in Florida permits the molecular-absorption algorithms to be tested under more demanding conditions.

The solid line on each graph is a least-squares fit of the Florida data against water-vapor pressure. The dashed line indicates the molecular absorptions predicted by the algorithm. In most cases the agreement between the experimental and calculated values is good. Larger discrepancies are observed for the $P_1 6$, $P_1 10$, and $P_2 4$ lines, since these were not included in the curve fits used to estimate the aerosol extinction. The solid curve provides a better estimate of the molecular absorption for these lines.

A summary of the comparisons of measured and calculated values for midlatitude summer conditions (14.26 torr of water vapor) is given in Table 5. For each DF laser line investigated, the table lists: the line identification, the line position, the experimentally determined molecular absorption at 14.26 torr, the standard deviation of the empirical curve fit, the calculated molecular absorption for 14.26 torr, the percentage difference between the measured and calculated values (normalized to the calculated value), and the standard deviation of the experimental curve fit expressed as a percentage of the calculated value.

The differences between experimental and calculated values for molecular-absorption values are within ± 20% for all but the $P_1 10$ and $P_2 4$ lines. The standard deviations of the curve fits are always less than 20% of the calculated values. At present the good overall agreement between modeling and experiment, as evidenced for 20 of the 22 DF lines studied, shows that existing calculations of molecular absorption for 90% of the DF laser lines of current interest should prove quite reliable.

The coefficients for the least-squares fits of the experimentally determined molecular absorptions are given in Table 6. Within the temperature range corresponding to these measurement conditions (about 15°C to 35°C), these coefficients provide empirical relations which can be used to further increase the accuracy of atmospheric molecular-absorption predictions for each of the 22 DF laser lines investigated.

3.7 Molecular Absorption and Aerosol Extinction During the JAN Baseline Demonstration Laser (BDL) Laser Shots

Analysis of the optical transmission data obtained with the IMORL DF laser improved or validated the computational algorithms available for predicting molecular absorption at DF laser frequencies. By using the known relative line strengths of the BDL (given in Table 7 [5]), the line-weighted molecular absorption for the BDL beam can be calculated. This calculation and the best-estimate aerosol extinction (obtained from section 3.5) are listed in Table 8 for each of the BDL shots. These results permit BDL molecular-absorption effects to be distinguished from aerosol-scattering effects, thereby aiding the interpretation of the BDL data.

4. CONCLUSIONS

The measurements of optical system efficiency shown in Figs. 12 and 13 represent the largest source of uncertainty in the measurements presented herein. Averaging of the data taken on two runs performed on the same or consecutive days yields curves of average efficiency versus wavelength with an uncertainty of between ±1% and ±2.5%, depending on the data set. During the first experimental session, a change in average system efficiency of from 71% to 66% was observed; the corresponding observations during the second session were 70% to 67%. (The small optical surfaces involved in this calibration were cleaned prior to the start of the second session; the large mirrors were not, due to lack of facilities in the field.) A conservative experimental uncertainty of ±2.5% in optical system efficiency represents the worst-case contribution of this factor to the overall measurement uncertainty.

Table 5 — Comparison of Measured and Calculated Molecular Absorption for Midlatitude Summer Conditions (14.26 torr partial pressure H_2O)

Line	Line Position (cm^{-1})	Experimental Absorption (km^{-1})	Std. Dev. σ (km^{-1})	Calculated Absorption (km^{-1})	(Exp - calc)/calc (%)	σ/calc (%)
$P_3 10$	2496.721	0.0516	0.0024	0.0514	0.4	4.7
$P_3 9$	2521.769	0.0364	0.0046	0.0366	-0.5	12.5
$P_2 12$	2527.391	0.0340	0.0014	0.0346	-1.7	4.0
$P_3 8$	2546.375	0.0561	0.0048	0.0511	9.9	9.3
$P_2 11$	2553.952	0.0360	0.0058	0.0365	-1.3	16.0
$P_3 7$	2570.522	0.0701	0.0037	0.0648	8.2	5.7
$P_2 10$	2580.096	0.0736	0.0120	0.0678	8.7	17.7
$P_3 6$	2594.197	0.0364	0.0027	0.0308	18.1	8.8
$P_2 9$	2605.806	0.0554	0.0083	0.0513	8.0	16.2
$P_3 5$	2617.386	0.0221	0.0024	0.0229	-3.5	10.7
$P_2 8$	2631.067	0.0302	0.0048	0.0360	-16.0	13.3
$P_2 7$	2655.863	0.1023	0.0044	0.1004	1.8	4.4
$P_1 10$	2665.219	0.0460	0.0064	0.0381	20.5	16.7
$P_2 6$	2680.179	0.0639	0.0043	0.0600	6.6	7.2
$P_1 9$	2691.606	0.0435	0.0032	0.0463	-6.1	6.9
$P_2 5$	2703.999	0.0284	0.0036	0.0300	-5.3	12.0
$P_1 8$	2717.538	0.1456	0.0036	0.1437	1.3	2.5
$P_2 4$	2727.309	0.0437	0.0026	0.0574	-23.8	4.5
$P_1 7$	2742.997	0.0311	0.0042	0.0350	-11.1	12.3
$P_2 3$	2750.094	0.0457	0.0051	0.0425	7.6	11.9
$P_1 6$	2767.968	0.0764	0.0071	0.0876	-12.3	8.1
$P_1 5$	2792.434	0.0661	0.0068	0.0705	-6.3	9.6

Table 6 — Coefficients for Calculation of the Empirical Molecular Absorption (EMA = a + bP + cP^2) as a Function of Water-Vapor Pressure

	a	b	c
$P_3 10$	0.02647	0.001762	0.0
$P_3 9$	0.01443	0.001543	0.0
$P_2 12$	0.01371	0.001422	0.0
$P_3 8$	0.03005	0.001828	0.0
$P_2 11$	0.01774	0.001279	0.0
$P_3 7$	0.04292	0.001907	0.0
$P_2 10$	0.04852	0.001761	0.0
$P_3 6$	0.00589	0.002843	-0.0000493
$P_2 9$	0.00435	0.004861	-0.0000899
$P_3 5$	0.00208	0.001404	0.0
$P_2 8$	0.00264	0.001609	0.0000228
$P_2 7$	0.00092	0.006361	0.0000522
$P_1 10$	0.00235	0.004320	-0.0000883
$P_2 6$	0.00004	0.004481	0.0
$P_1 9$	0.00864	0.003323	-0.0000617
$P_2 5$	0.00000	0.002000	0.0
$P_1 8$	0.00014	0.009122	0.0000758
$P_2 4$	0.00012	0.003396	-0.0000237
$P_1 7$	0.00035	0.001006	0.0000805
$P_2 3$	0.00142	0.002419	0.0000480
$P_1 6$	0.00525	0.003808	0.0000828
$P_1 5$	0.00158	0.003619	0.0000633

Table 7 — Measured BDL Power Spectrum

Laser Line	Wavelength (μm)	Relative Power (%)
$P_1 6$	3.613	0.7
$P_1 7$	3.646	2.1
$P_1 8$	3.679	5.5
$P_1 9$	3.714	11.0
$P_1 10$	3.752	6.9
$P_2 6$	3.721	2.8
$P_2 7$	3.765	4.8
$P_2 8$	3.800	18.6
$P_2 9$	3.837	12.4
$P_2 10$	3.875	6.2
$P_2 11$	3.915	0.7
$P_3 6$	3.855	2.1
$P_3 7$	3.890	9.7
$P_3 8$	3.927	10.3
$P_3 9$	3.965	4.1
$P_3 10$	4.005	2.1

Table 8 — Molecular Absorption and Aerosol Extinction During the BDL Shots

Day	Time	Air Temperature (°C)	Water-Vapor Pressure (torr)	Calculated Molecular Absorption (km^{-1})	Aerosol Extinction (km^{-1})
255	1200	18.42	11.94	0.0490	0.0331
255	1420	19.00	12.47	0.0505	0.0565
255	1642	17.00	12.25	0.0501	0.0500
255	1815	16.75	12.00	0.0494	0.0500
258	1259	26.15	12.87	0.0509	0.0750
259	1233	30.73	11.16	0.0452	—
259	1820	27.25	8.50	0.0377	0.0300
260	1133	29.85	9.79	0.0413	0.0350
260	1332	29.22	12.74	0.0501	0.0350
260	1447	29.07	13.17	0.0514	0.0262
260	1650	29.50	12.25	0.0486	0.0300
260	1916	25.00	11.50	0.0469	0.0300
261	1048	26.37	13.66	0.0532	0.0272
261	1404	27.61	8.65	0.0381	0.0250
261	1542	26.21	9.02	0.0393	0.0250
262	1226	25.17	10.78	0.0447	0.0500
262	1523	25.99	12.00	0.0483	0.0500
262	1807	21.75	12.65	0.0508	0.0500

The daily variations observed in the detector relative-response (A-and-C-run) averages were ±1%. When combined with the uncertainty in the optical system efficiency and assuming ±1% uncertainty in a 5-km measurement, an overall transmission measurement uncertainty of ±4.5% results. Due to the exponential relationship between transmission and extinction coefficient, a fixed uncertainty in transmission will result in a larger uncertainty in extinction coefficient for higher transmission values. Thus the highest transmission values observed, about 79% for the $P_2 8$ or $P_3 5$ lines of DF, yielded extinction coefficients of about 0.04 km^{-1} with an uncertainty of ±18%, whereas the 30% transmissions occasionally measured for the $P_2 7$ and $P_1 8$ lines yielded extinction coefficients as large as 0.2 km^{-1} with a ±4.0% experimental uncertainty.

Experience with this experiment in Florida and California argues for better monitoring and control of the zero-path optical system efficiency. A system of air curtains is presently being installed toward this end. Uncertainties due to detector/integrator responses are currently being studied by the use of alternative geometries to that shown in Fig. 8 with the goal of reducing this factor below the 1% level.

The data acquisition and reduction procedures described in section 2.4 are based on the assumption that aerosol extinction is wavelength independent over the DF laser spectral region (3.6 to 4.1 μm) and are not sensitive to differences between weakly wavelength dependent molecular effects (H_2O and N_2 continua) and extinction due to aerosols; additional data are required to sort out these effects. Accordingly, the DAE values derived from the curve fits shown in Figs. 16a, 17a, etc. and tabulated in *Table 2 should* represent the time variation of aerosol extinction during a measurement sequence. This is readily apparent only for certain runs, in particular those taken on days 217 (Fig. 16a), 218 (Fig. 17a), 219 (Fig. 18a), and 220 (Fig. 19d). Note that the measured aerosol extinction at 1.06 μm in each case behaves in the same manner as a function of time as does the DAE curve fit for these examples. For other cases, notably days 220 (Fig. 19a), 226 (Fig. 22a), 255 (Fig. 24a), 259 (Fig. 26a), and 260 (Fig. 27d) there appears to be a repeated, small dependence of the AAE values and DAE curve fit upon time. The small quadratic dependence of the AAE values upon time evidenced in this latter group of runs could result from a residual, monotonic increase of AAE with increasing wavenumber, not completely accounted for in the analysis procedures used (see Section 2.4). The magnitude of the AAE values and fitted DAE curves for these cases is small, generally between 0.03 and 0.045 km^{-1}. Only in these cases do the repeated convex upward shapes of the DAE vs. time curves become apparent, indicating that if this shape is evidence of an error in the molecular continuum absorption model used [6], or an indication of a small wavelength dependence of aerosol extinction in the spectral region in question that such effects only become apparent for low attenuation (high transmission) conditions.

Future experiments combining laser extinction and high-resolution transmission spectroscopy will be conducted to study such questions in greater detail, particularly the magnitude and shape of the N_2 and H_2O continuum absorptions in the DF laser region.

The PMS data used independently to predict scattering at 3.8 μm worked surprisingly well in this experiment, lending confidence to this approach. In the earlier Florida experiment the agreement between the PMS-based predictions and the AAE values is not as

good. A larger variation in aerosol composition (most likely due to changes between offshore and ocean wind conditions at that site) is responsible for the differences observed in the two experiments. This is a complex problem which is currently being actively studied. The data base contained in this report should prove useful in furthering the development of techniques for modeling aerosol extinction.

Though the data from this experiment shown in plots of molecular absorption versus water-vapor pressure (Figs. 30) are not very useful in validating the predictions shown on the same plots (due to the limited range of humidities observed), the data consistently agree with the experimental curve fits derived from the Florida experiment.

The detailed information contained in this report as regards aerosol distributions, absolute humidities, wind patterns, and related optical effects on 3.8-μm propagation associated with the TRW-CTS location should prove useful as a reference for the planning and analysis of future DF laser propagation tests to be carried out using the sites described herein.

5. ACKNOWLEDGMENTS

The authors thank P. M. Livingston and P. B. Ulrich of NRL for guidance and encouragement during the execution of this work and preparation of this report. Additionally thanks is due D. Finkleman of the Naval Sea Systems Command for help in the support of this project. Several vital contributions to this work have been provided by Science Applications Inc. (SAI). Included in this category are the DF laser transmission calculations performed by R. E. Meredith, D. R. Woods, and T. W. Tuer of the SAI Ann Arbor, Michigan, office. The extensive software development and technical support provided by D. Gray, W. Furr, and W. L. Agambar of the SAI Arlington, Virginia, office are gratefully acknowledged.

The DF laser device and gas control system used in these experiments was expertly engineered by H. Bobitch, TRW Systems Group, Redondo Beach, California. The authors thank him for his valuable assistance in the initial design and operation of the fluorine gas supply system and for the operation of the DF laser system during several of the experimental measurements reported in this document.

The skillful mechanical design and construction of the apparatus used in these experiments by M. Cochran, M. Dement, and J. Cox of the NRL Chesapeake Bay Division made possible the successful execution of the experiments reported herein. Many thanks are due Mrs. J. Pinkney and Mrs. R. Reithmeyer for the dedicated typing of this manuscript. The careful editing by D. Triantos and D. H. Garcia is gratefully acknowledged.

6. REFERENCES

1. J. A. Dowling et al., "Atmospheric Laser Propagation Measurements for 0.63-, 1.06-, and 10.6-μm Wavelengths," NRL report in preparation.

2. D. R. Woods, T. W. Tuer, and R. E. Meredith, "DF Laser Propagation Analysis (1st Informal Progress Report)," SAI Report SAI-76-002-AA, Apr. 1976.

3. D. R. Woods, D. H. Leslie, and T. W. Tuer, "Application of High Resolution Spectroscopy to DF laser Propagation" paper ThD13, 1975 Annual Optical Society of America meeting, Boston, Mass., Oct. 1975.

4. W. Heath, Ph. D. Dissertation, Ohio State University, 1976.

5. 9th HEL Review Group Meeting, NASA Michaud Assembly Facility, New Orleans, La. 3-4 Dec. 1975. (Additional BDL spectral measurements have appeared in two reports: JAN Propagation Final Report-Test Series A and B (U), Contract No. N0001-75-C-0484, Oct. 1975 and JAN Propagation Program Propagation Analysis Report, Contract No. N0001-75-C-0484, July 1975, prepared by the TRW Systems Group, Redondo Beach, Calif. The BDL spectral measurements reported therein show a slight power increase ($\approx$10%) in the most prominent lines (J = 8, 9, and 10) with respect to the weaker lines (J = 5, 6, and 11) when compared to the spectrum shown in Table 7. Effective BDL molecular absorption coefficients based on the latter spectra would not differ significantly from the values presented in Table 8).

6. D. E. Burch, D. A. Gryvnak, and J. D. Pembrook, "Investigations of the Absorption of Infrared Radiation by Atmospheric Gases: Water, Nitrogen, Nitrous Oxide, Report AFCRL-71-0124 (Air Force Cambridge Research Laboratories, Hanscom AFB, Mass., 1971).